# EFFECT OF TEMPERATURE ON THE MECHANICAL BEHAVIOR OF THE CNT REINFORCED EPOXY

---

A Thesis

Presented to

The Faculty of the Graduate School

at the University of Missouri-Columbia

---

In Patrial Fulfillment

of the Requirements for the Degree

Doctorate

---

by

ALI ANVARI

Prof. Sanjeev Khanna, Thesis Supervisor

DECEMBER 2021

# Approval Page

The undersigned, appointed by the Dean of the Graduate School, have examined the dissertation entitled:

**EFFECT OF TEMPERATURE ON THE MECHANICAL BEHAVIOR OF CNT REINFORCED EPOXY**

presented by Ali Anvari,

a candidate for the degree of Doctor of Philosophy and hereby certify that, in their opinion, it is worthy of acceptance.

Professor Sanjeev Khanna

Professor Jian Lin

Professor Robert A. Winholtz

Professor Zhen Chen

Professor Qingsong Yu

# Dedication

To my family and friends whom always have given me love and support. I would like to dedicate this research to all the engineers and scientists around the globe for using the results of this research for a peaceful and friendly advancements in all the industries and applications for people to live better, safer, and easier.

Ali Anvari

# Acknowledgements

I would like to thank my family especially my brother for their help and support during my research and studies. I'm grateful for having them as my family.

I also would like to express my genuine gratitude to my academic advisor, Professor Sanjeev Khanna for his continuous guidance, training, help, and support during my research and studies in the Department of Mechanical and Aerospace Engineering at University of Missouri - Columbia. I really appreciate that very much. Thank you so much for giving me encouragement and hope to pursue my studies and research and complete my dissertation project. I will always remember him for his endless support and giving me knowledge!

Furthermore, I would like to thank to others whom collaborated with me and taught me to complete this research, especially I would like to extend my gratitude to Professor Orton from the department of civil and environmental engineering at University of Missouri - Columbia. I really appreciate for training me for using the MTS Machine.

Additionally, I would like to express my appreciation to Mr. Rupesh Devapati for helping me to use the tension test machine, and Mr. Al Bahhash for his effort preparing the specimens for the Tests. Furthermore, I would like to thank to David Stalla for providing the electron microscopy images of the fractured surfaces of the tension specimens.

I appreciate your help and support very much!

TABLE OF CONTENTS

Chapter 2



Chapter 3

Chapter 4



Chapter 5

## List of Tables Page

## List of Figures Page

# Abstract

In this thesis, the effect of temperature on the mechanical behavior of CNT reinforced epoxy has been investigated. The first step for this research will be to produce SWCNT - epoxy and MWCNT - epoxy in the lab in the forms of plates with 0.5, 1, and 1.5 wt. % of CNT concentrations. After the plates are ready, the next step was to put the plates in thermal chamber to perform thermal cycling tests. Each thermal cycle would be to heat the plates from room temperature to $0.85T_g$ which is 85% of the epoxy glass transition temperature ($T_g$). The glass transition temperature of the epoxy was determined in the lab using DSC.

For measuring the mechanical behavior of the plates, shear - beam test and tensile test were used. The process would be to measure the mechanical properties of the plates at 0 cycles (as fabricated) and after 1500 and 3000 exposure to the mentioned thermal cycles. The short beam test and tensile test can measure the interlaminar shear strength and tensile strength of the plates, respectively. Based on these data, the model for changing the interlaminar shear strength and tensile strength of the plates with increasing the thermal cycles can be developed.

Furthermore, in this research, the tensile strength, ultimate strain, and Modulus of Elasticity of epoxy, and carbon nanotube reinforced epoxy while they are exposed to different thermal cycling environments are obtained.

Thermal cycling environments can exist in many conditions such as in earth orbit for satellites which rotate around the earth and pass through the sun illumination and earth's shadow, and for airplanes which fly in different altitudes with different temperatures. Carbon nanotube reinforced epoxy is one of the nano - composite materials which have been broadly used in many applications such as aerospace, automotive, electronics, and other industries. The reason for using this material as a promising nano – composite in many industries, is its mechanical properties such as high strength, stiffness, and flexibility. The goal in this experiment is to fabricate the nano – composite and expose it to different thermal cycle numbers to monitor the changes in tensile strength, ultimate strain, modulus of elasticity, and shear strength. For this purpose, tension and short – beam tests were applied. Using the results obtained with this experiment, the mechanical behavior of nano – composites with different carbon nanotube concentrations are analyzed and discussed. Furthermore, based on this analysis, conclusions are included in the conclusions section of this research.

# Chapter 1

## Introduction

Carbon nanotubes have been introduced by Lijima in 1991 for the first time [1]. Due to the excellent properties of carbon nanotubes (CNTs), nowadays its application is broad in many industries such as aerospace and aeronautical industries. Carbon nanotubes have great mechanical and thermal properties such as high tensile strength, high Young's modulus and high aspect ratio which makes CNT one of the best martials for different applications. Furthermore, the electrical conductivity of CNT is high [2].

There are many methods to produce the CNTs such as catalyst arrays, chemical vapor deposition, electric arc discharge, sonochemistry, laser ablation, and electrolysis. It is important to know that each of these production methods will result in different CNTs with different geometries because the diameter and the length of CNTs will be different with each of these production methods. The different geometries of CNT can have effects on its reactivity, failure mechanism, surface interaction and mechanical properties. Therefore, it seems that with different production methods different CNTs with different properties can be expected [2].

Despite of the great mechanical properties of CNTs, there are a few obstacles to apply this material in many industries such as load transfer, dispersion, and alignment. For achieving higher interlaminar shear strength between the CNTs and matrix, high load transfer between them is required.

The second challenge to apply CNTs in polymer matrix is the problem of CNTs dispersion which can cause agglomeration of CNTs particles within the nanocomposite. The agglomeration of CNTs within the nanocomposite can cause stress concentration in these agglomerated areas which may result in debonding and failure. The third problem to apply CNTs is the alignment of CNTs within the polymer which doesn't seem very convenient due to the size of CNTs which is several nanometers in diameter and several micrometers in length [2].

Nevertheless, the application of CNT is still broad in many industries due to its multifunctional properties such as thermal management, enhanced stiffness and improved toughness [3]. There are several methods to disperse the CNTs within the matrix uniformly. Among these methods, the most effective one is the chemical treatment with ultrasonication process [4].

CNTs are the crystalline shape of carbon. They have high aspect ration due to the size of dimeter which is a few nanometers and the size of length of it which is about a few microns. Furthermore, they offer high flexibility and high thermal conductivity. CNTs can be in the forms of Multi-walled carbon nanotubes (MWCNTs) and Single-walled carbon nanotubes (SWCNTs). The theoretical thermal conductivities of MWCNTs and SWCNTs are 3000 W/mK and 6000 W/mk, respectively. The strength of CNTs is about 63 GPa. One of the best materials to apply as a matrix containing CNTs is epoxy which is a thermosetting resin. Epoxy has a high corrosion and chemical resistance. Furthermore, it provides high tensile strength and high dimensional stability and adhesion. It can be applied in different industries such as aeronautics, electronics, astronautics, and other applications. As a result, it seems that the CNT-epoxy can be one of the most suitable materials in different applications due to the excellent properties of both CNT and epoxy polymer.

The only problem is to develop a method to overcome the CNTs dispersion, alignment and load transfer within the epoxy. The reason that CNTs tend to agglomerate is the van der waals force between them. CNTs have high surface areas which can create high viscosity within the CNTs-epoxy. This can result in bad uniformity of CNTs within the epoxy. For enhancing the load transfer between the CNTs and epoxy and improving the uniformity of CNTs within the epoxy, method of CNTs functionalization may be applied. The TEM images of functionalized or oxidized CNTs within the epoxy have shown that not only the dispersion of CNTs within the epoxy has improved, but also interlocking between the CNTs and epoxy has increased which can result in higher load transfer between the CNTs and epoxy. This can result in higher inter-laminar shear strength in interface areas between CNTs and epoxy which is beneficial in many applications [4].

### 1.1. CNT dispersions within the epoxy

The Scanning Electron Microscopy (SEM) images of synthesized CNTs-epoxy have revealed that applying equal and more than 1 wt. % of CNTs into the CNTs-epoxy can result in higher chance of CNTs agglomeration within the epoxy which develops inhomogeneous dispersion within the epoxy. The reason is the increasing of viscosity which can inhibit the uniformity of CNTs within the epoxy or result in nonuniform dispersion. To overcome this issue, functionalized CNTs can be used. Functionalized or oxidized CNTs can be developed by using chemical treatment. The result of this chemical treatment would be, the enhancement of bonding between polymer and the CNTs which can develop network formation and interlocking [4].

The uniformity of dispersion of CNTs within the epoxy is of high significance as it can increase the flexural strength. As an instance, with the comparison of 1 wt.% pristine CNTs and 1 wt.% functionalized CNTs within the epoxy, the results can develop 77 MPa and 104 MPa flexural strength, respectively, which proves that functionalized CNTs can develop higher uniformed CNTs-epoxy nanocomposites. The reason behind this enhancement of flexural strength appears to be due to the developing covalent bonds between the functionalized CNTs and the epoxy molecules which leads to the higher strength of nanocomposite [4].

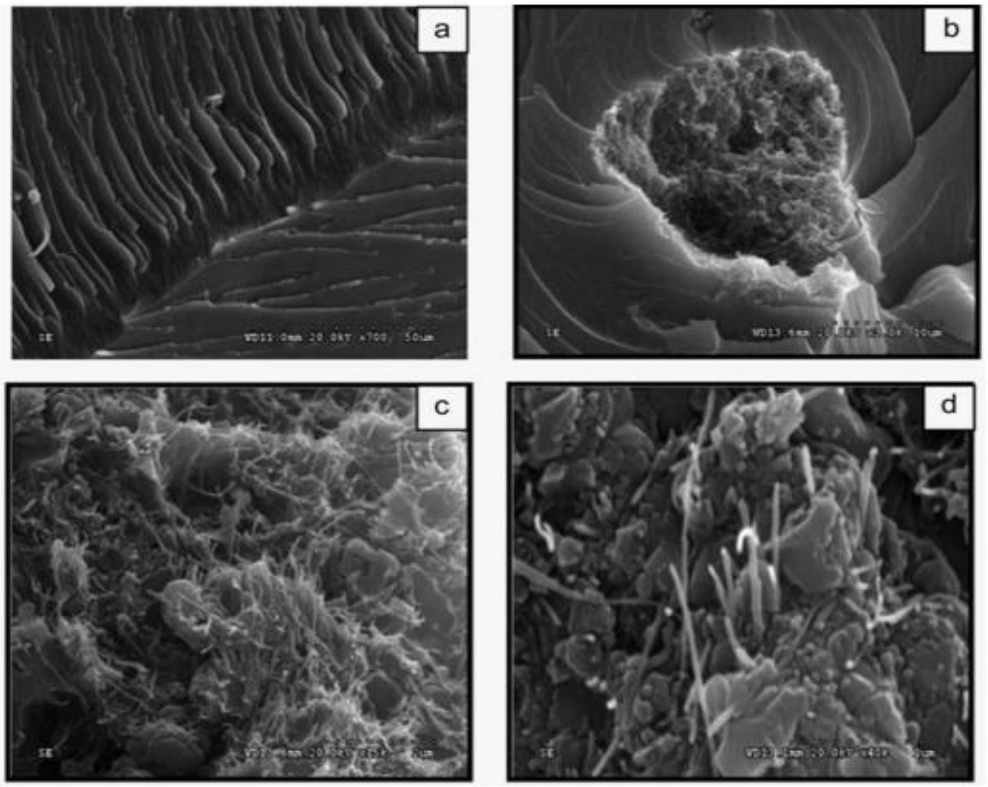


**Figure 1.1:** Fracture surface of (a-b) agglomerated CNTs within the epoxy and (c-f) CNTs/epoxy composite containing 1 wt. % CNTs [4]

In Figure 1.1, the fracture surfaces of CNTs-epoxy for both agglomerated CNTs within the epoxy (a-b) and functionalized CNTs within the epoxy is shown. In Figure 1.1 (a-b), the fracture surface shows the catastrophic failure of CNTs-epoxy due to the agglomerated CNTs and stress concentration in these agglomerated areas. The stress concentration in agglomerated CNTs results in macrocrack formation and with the continuous crack propagation, failure occurs. On the other hand, in the case of functionalized CNTs-epoxy (Figure 1.1 (c-d)), the cracks develop on the interface areas between the CNTs and epoxy and with spreading these cracks, CNTs pullout occurs which requires more energy and higher load when compared to the pristine CNTs-epoxy failure. The reason that cracks form first on the interface areas could be due to the shear stress formed around the CNTs within the production process, or due to the nonuniform dispersion [4].

In the case where CNTs-epoxy is exposed to high temperatures, application of functionalized CNTs-epoxy is beneficial because the decomposition temperature will increase with using the functionalized CNTs. Experiments have shown that the decomposition temperature for functionalized CNTs-epoxy with 1 wt. % CNTs is around 625$^{o}$C while the decomposition temperature for pristine CNTs-epoxy with 1 wt.% CNTs is around 420$^{o}$C. Therefore, for high temperature conditions above 400$^{o}$C, the application of functionalized CNTs-epoxy is highly recommended. The reason is the strong bonding between the epoxy and acid-functionalized CNTs. The modification of functionalized CNTs enable the stronger polarity of CNTs and it results in developing covalent bonds between the epoxy and CNTs molecules which results in higher thermal stability and higher decomposition temperature [4].

Furthermore, generally, the strength of pristine CNTs-epoxy compared to epoxy is 58% higher and the strength of functionalized CNTs-epoxy compared to epoxy is 100% higher with the same 1 wt.% CNTs concentration for both nanocomposites [4].

### 1.2. Mechanical Properties, Geometries and Failure Mechanism

As it has been mentioned previously, the discovery of CNTs occurred in 1991. After the discovery of CNTs, its application started to increase due to the unique and important properties such as high strength, high modulus, high stiffness, electrical conductivity, etc. Compared to steel which is one of the most popular metals in different industries, CNTs offer higher Young's Modulus and tensile strength. The Young's Modulus of steel is about 200 GPa while the Young's Modulus of CNTs is around 1TPa. The tensile strength of steel is about 505 MPa while the tensile strength of CNTs is about 1163 GPa. Moreover, CNTs can be used in other applications such as energy storage devices, hydrogen storage media, sensors, and many more [5].

CNTs are composed of graphene layers rolled to form cylinders with fullerene caps. SWCNT has only one graphene sheet while MWCNT has several graphene sheets rolled over each other. The geometries of CNTs could be in three states; 1. Armchair 2. Zig-zag and 3. Chiral. CNT's thickness is 0.34 nm which is equal to the thickness of graphene sheet, but the length and dimeter of the CNT can vary. In Figure 1.2, the three different geometries of CNTs are illustrated [5].

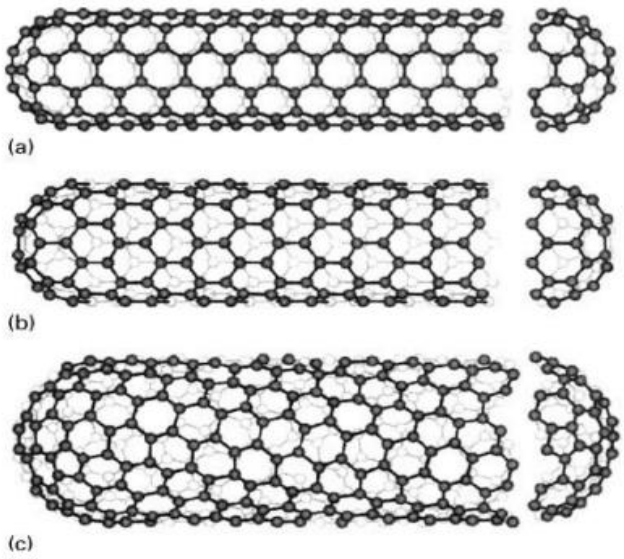


**Figure 1.2:** Different chiralities of CNTs 1. Armchair 2. Zig-zag 3. Chiral [5]

In order to investigate the failure mechanism of CNTs-epoxy in 2016 an analytical method has been introduced. This method divides the interface areas of CNTs-epoxy into three parts. First part is the area at which CNT and epoxy are fully bonded and the bonds are strong containing covalent strong bonds. The second region is the area at which the CNTs and epoxy are partially bonded. It means that some of the molecules in this area are not bonded. The third area is the surface at which no bonding exists between CNTs and epoxy. According to this analysis, the interface area close to the CNT's end cap is the most vulnerable area and stress concentration and crack initiation occurs in this region. After the failure occurs at interface area, the epoxy also cracks in the region close to the end cap of the CNT. The path of fracture is from the epoxy's crack to the failure location near the CNT's cap [5].

### 1.3. CNT Dispersions Processes

In this section, three different methods for CNTs dispersion into the epoxy will be introduced. The aim is to identify which method can result in the best dispersion of CNTs into the epoxy. As it was mentioned in the previous sections, uniformity of CNTs dispersion into the epoxy is of high significance because it can result in higher strength of CNTs-epoxy which is required in many structural applications.

In the first method of dispersion, first, CNTs are mixed with acetone and then will bath for 30 minutes. Then, the epoxy will be added to the solution of CNTs and acetone. Then, all will be heated at 60$^{o}$C and stirred with magnetic power at a speed of about 300 rpm until the full acetone evaporation. Finally, the solution will be sonicated in bath sonicator for about 30 minutes [6].

In the second method of dispersion, first, CNTs will be mixed directly with epoxy and the solution will be sonicated for 30 minutes. Then, the solution will be heated up to 60$^{o}$C. After that, it will be stirred with 300 rpm for one hour. Finally, it will be sonicated for 30 minutes for maximum dispersion [6].

In the third method, first, CNTs will be mixed with epoxy. Then, the solution will be heated up to 60$^{o}$C. After that, it will be stirred with 300 rpm for about 15 minutes. Then, will be cooled down to ambient temperature. Finally, it will be tip sonicated for 5 minutes with 50% of power and 0.5 circle [6].

In Figure 1.3 [6], the CNTs dispersion before dispersion process, and with three dispersion techniques mentioned above is shown. Contrary of what was expected, with eliminating the acetone from the solution and decreasing the sonication time, CNTs dispersion into the epoxy has become more uniform and pleasant. According to Figure 1.3, the third method is the best method to obtain the most uniform CNTs dispersion into the epoxy. Furthermore, this method is very efficient as it will save a lot of energy because the stirring process in this method will be decreased to 15 minutes. On the other hand, the sonication process will be done with only 50% of power and only for 5 minutes instead of 30 minutes final sonication in the first and second methods. Therefore, it seems that this method is highly beneficial in many aspects as it is both time and energy saving.

Furthermore, with further analyzing the Figure 1.3, it can be observed that the agglomeration of CNTs in the first method is very high. This high agglomeration could be due to the application of acetone. In the second method of dispersion, there are mainly two points of agglomeration, but the agglomeration areas are smaller than the one resulted from the first method. In the third method of dispersion, both the numbers of agglomerations and the size of those reduced. It means that the dispersion has been performed perfectly and CNTs are dispersed uniformly within the epoxy. Because the agglomerations regions have been known as the stress concentration zones which reduces the strength of CNTs-epoxy nanocomposites, it can be interpreted that the third method of CNTs dispersion into the epoxy can result into the production of highest strength CNTs-epoxy which is desirable in many structural applications.

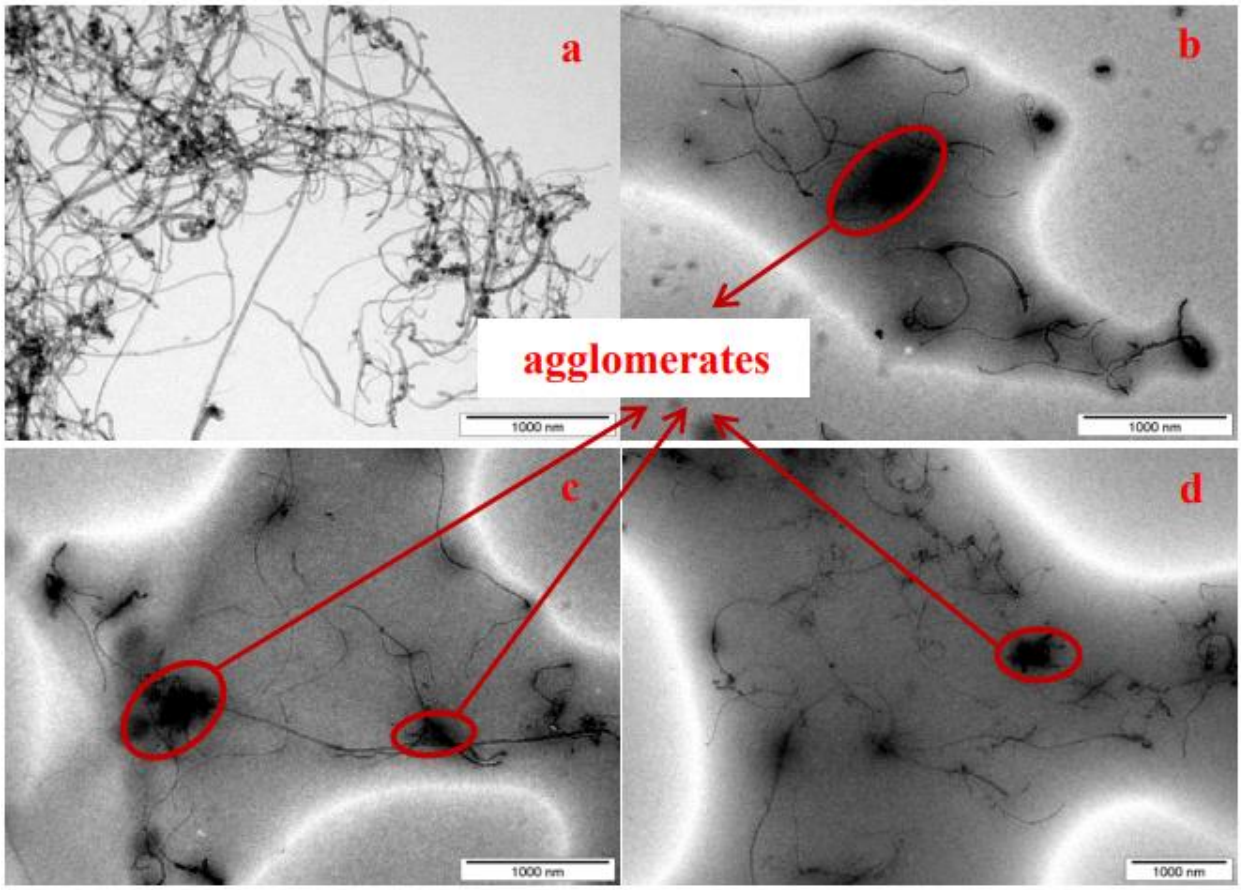


**Figure 1.3:** CNT dispersion states (TEM pictures) with different dispersion methods: a) before dispersion; b) dispersion by first method; c) dispersion by second method; d) dispersion by third method [6]

For performing the CNTs dispersion into the epoxy other methods could also be applied. The methods of high-speed dissolver and 3-roll mill are two other methods for this purpose. Furthermore, in some cases these methods are combined to perform the CNTs dispersion, but the most effective method is the ultrasonication. In Figure 1.4, CNTs dispersion into the epoxy with several methods is shown by using optical images [7].

By looking into the different sections of figure 1.4. (a-d), it doesn't seem very hard to interpret that ultrasonic horn is the best way of CNTs dispersion into the epoxy. The reason is the black spots in the figure 1.4 as they show that the quantity of these spots is higher in figure 1.4(b) which means the CNTs quantity is higher because the black spots are referred to CNTs concentrations. Furthermore, the dispersion of these spots in figure 1.4(b) is also uniform which means the ultrasonication method can perform the CNTs dispersion uniformly.

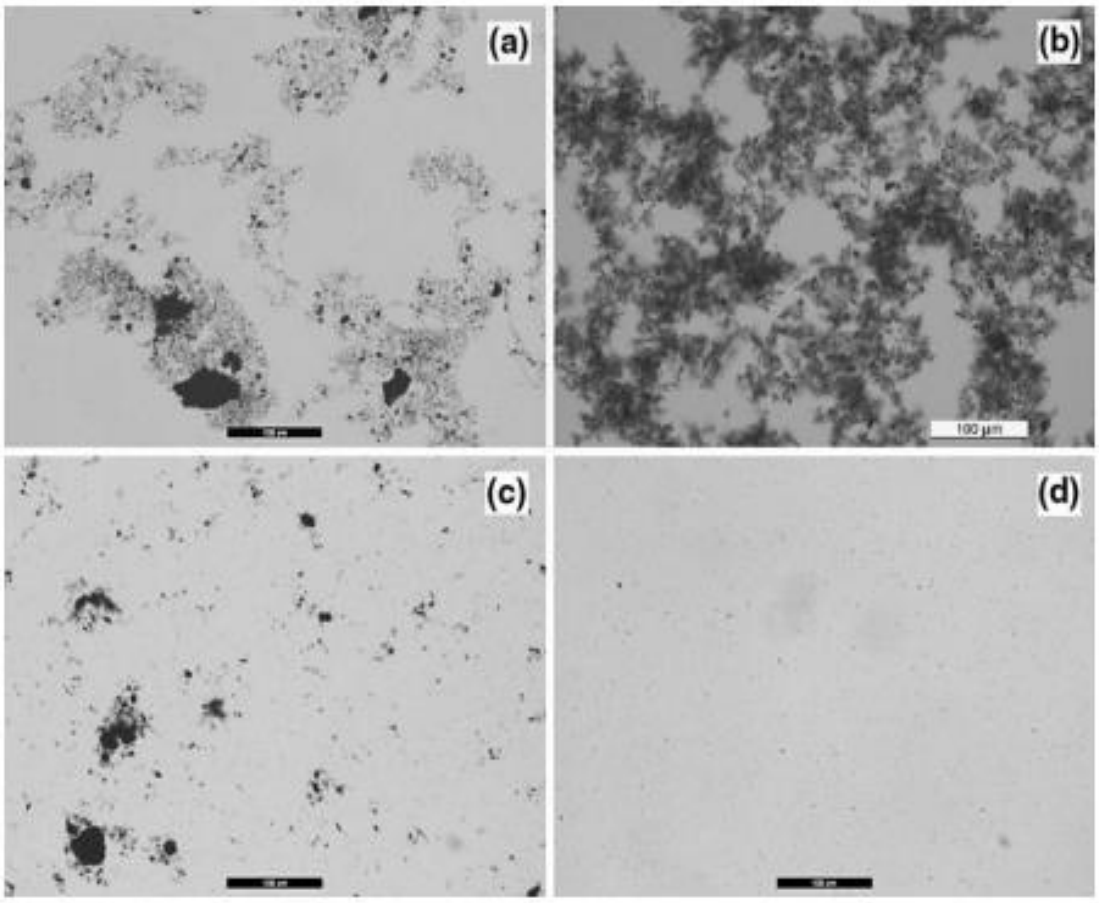


**Figure 1.4:** Optical images recorded on CNTs-dispersion in epoxy alone obtained applying a) high-speed dissolver, b) ultrasonic, c) high-speed dissolver + ultrasonic bath, d) high-speed dissolver + 3-roll mill. Scale bar is 100 µm [7]

### 1.4. Mechanical Properties of CNTs-epoxy with different CNT concentrations

In this section, Zhou et al has investigated [8] the effect of CNT concentrations on mechanical properties of CNTs-epoxy. By looking into the Table 1.1 [8], it can be observed that three mechanical properties of CNTs-epoxy with different CNT concentrations have been investigated. The first mechanical property is the Modulus of CNTs-epoxy. The Modulus of CNTs-epoxy has been increased with increasing the CNT concentrations from 0 to 0.4% CNT concentrations. The second mechanical property which has been shown in Table 1.1., is the strength of CNTs-epoxy. The strength of CNTs-epoxy has been increasing with increasing the CNT concentrations in nanocomposite from 0 to 0.3% CNT concentrations but has been decreased from 0.3 to 0.4% CNT concentrations. The third mechanical property is the failure strain. The failure strain of CNTs-epoxy also has been increasing with increasing the CNT contents up to 0.3% concentrations but has been decreasing from 0.3 to 0.4% CNT concentrations. The reason that the strength and the failure strain of CNTs-epoxy has been decreased above the 0.3% CNT contents is the nonuniformity of CNTs dispersion within the epoxy which is the cause of CNTs agglomeration.

Another mechanical property for CNTs-epoxy which has been investigated as a function CNT contents is the toughness. The toughness of a material can indicates the resistance of a material in cases dealing with fatigue. It means that the higher the toughness is, the longer time materials can stand in cases dealing with fatigue with the same loading condition.

As it is shown in Figure 1.5 [8], the toughness of CNTs-epoxy nanocomposite is increasing with increasing the CNT contents up to 0.3% CNT concentrations but is decreasing with increasing the CNT contents from 0.3% to 0.4%. This could be due to the CNTs agglomeration for the amounts more than 0.3% CNT contents within the epoxy. Therefore, according to the results that failure strain, strength and toughness of CNTs-epoxy are the maximum values at 0.3% CNT contents, it can be interpreted that the 0.3% CNT contents appears to be the optimum amount of CNT concentrations within the epoxy.

**Table 1.1:** Mechanical properties of epoxy with different CNT concentrations [8]

| | **Modulus [GPa]** | **Strength [MPa]** | **Failure strain [%]** |
|---|---|---|---|
| Neat epoxy | 2.46 | 93.5 | 4.02 |
| 0.1% CNT | 2.54 | 109 | 6.06 |
| 0.2% CNT | 2.60 | 115 | 6.80 |
| 0.3% CNT | 2.65 | 121 | 7.58 |
| 0.4% CNT | 2.75 | 113 | 5.12 |

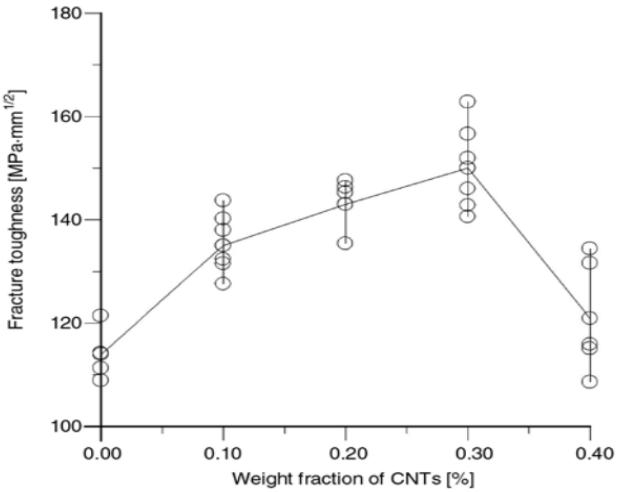


**Figure 1.5:** Toughness of CNTs-epoxy with different CNT contents [8]

### 1.4.1. The Effect of CNT Contents on the Properties of CNTs-Epoxy

CNT contents have a fundamental effect on the properties of CNTs-epoxy. As it is indicated in Figure 1.6 [9], the amount of CNT concentrations within the epoxy plays a significant role in determining the tensile strength of CNTs-epoxy. This effect is such strong that the value of the tensile strength of CNTs-epoxy with increasing the CNT contents from 1 wt. % to 4 wt. % almost doubles according to Figure 1.6 [9]. The same increment also occurs for the Young's Modulus and yield strength of the CNTs-epoxy. Furthermore, by looking into the Table 1.2, it can be perceived that the amount of Young's Modulus and yield strength of the CNTs-epoxy is increasing with increasing the CNT contents from 0 to 4% CNT contents. Application of 1 wt. % of CNT into the polymer can increase the Young's Modulus and yield strength of the CNTs-epoxy up to 100 and 200 percent, respectively, when compared to the neat epoxy. Additionally, as it is illustrated in Figure 1.7, the conductivity of CNTs-epoxy is increased with increasing the CNT contents from 0 to 4% CNT concentrations within the epoxy. Moreover, experiments have shown that the transition from insulator to conductor within CNTs-epoxy can occur between 0.5 to 1 wt. % CNT concentrations within the epoxy [9].

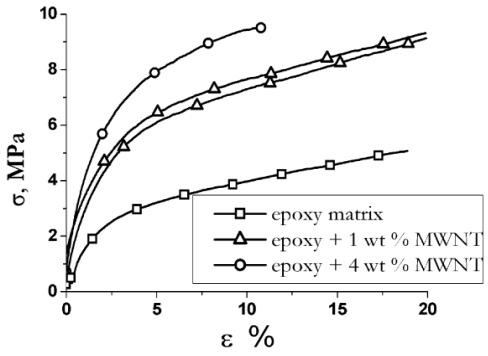


**Figure 1.6:** The effect of CNT contents on tensile strength of CNTs-epoxy [9]

**Table 1.2:** The effect of CNT contents on Young's Modulus and yield strength of CNTs-epoxy [9]

| CNTs wt.% | Young's modulus MPa | Yield strength $\sigma_{0.2\%}$MPa | $\sigma_{10\%}$Mpa |
|---|---|---|---|
| 0 | $E_0 = 118$ | 1 | 4 |
| 1 | 236($2*E_0$) | 3 | 8 |
| 4 | 465($3.9*E_0$) | 6 | 10 |

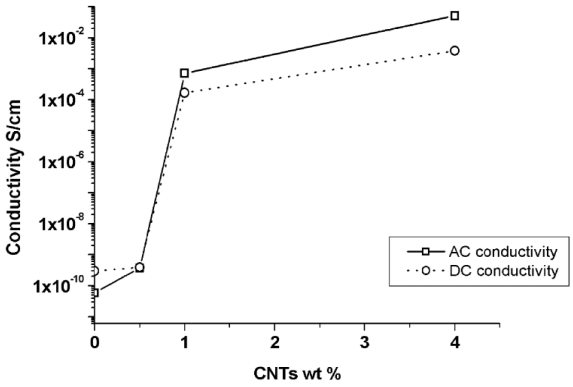


**Figure 1.7:** The effect of CNT contents on conductivity of CNTs-epoxy [9]

## 1.5. Damage Analysis of CNTs-Epoxy

One of the methods to perform a damage analysis of CNTs-epoxy is employing the continuum damage mechanics (CDM) approach with considering physical damage equation which is resulted from molecular dynamics (MD) method. This method by considering the value of bonds dissociation energy (BDE) is capable to determine the numbers of crosslinking bonds which can be break with the determined value of energy. Crosslinking is the bonding within the epoxy polymer chains. Figure 1.8 [10], indicates the effect of crosslinking degree (μ) on the yielding stress within the epoxy. It also seems important to mention that crosslinking degree is a function of time and temperature [10]. As it is illustrated in Figure 1.8, as the crosslinking degree of polymer increases, the yield stress of the polymer increases. Therefore, it appears that crosslinking has a direct effect on yield stress.

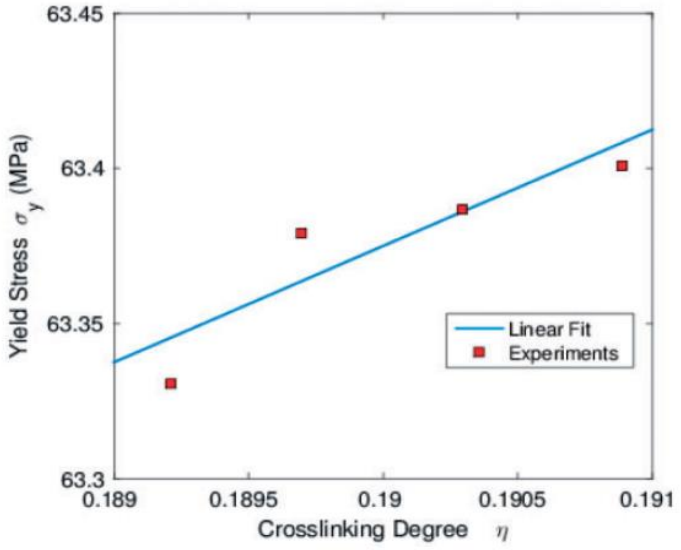


**Figure 1.8:** Yield stress as a function of crosslinking degree [10]

Nevertheless, it seems that the first zone of developing damage or the crack initiation would occur on the interface areas between the functionalized CNTs and epoxy and the damage will continue into the epoxy. The failure mechanism would be in the fiber pull-out mode for functionalized CNTs-epoxy which is called the telescope failure [11]. In the cases where pristine CNTs-epoxy has been employed, the damage might occur within the polymer chains by breaking the crosslinking bondages and the crack will spread very quickly within the polymer [3]. Therefore, it appears that the role of crosslinking degree between the polymer chains is very important for the cases dealing with pristine CNTs-epoxy due to the damage mechanism which can start from the polymer chains. Nevertheless, even with employing the functionalized CNTs-epoxy, part of the fracture area would occur in polymer chains. Hence, one way to the other, the role of crosslinking degree within the polymer chains for having a tougher and stronger CNTs-epoxy is not deniable.

### 1.6. Summary of CNTs-epoxy's important topics

The research topic related to CNTs, epoxy and CNTs-epoxy is very broad and, in this study, only the most important topics will be covered. It seems that the topics related to the mechanical properties, CNTs dispersion methods and damage mechanism are the most significant topics which in this study also it is tried to cover them as well.

The effect of various CNT dispersions methods into the epoxy, on the mechanical properties of CNTs-epoxy is one of the important topics to cover. According to a research which has been performed in 2012 by Martone et al [12], the most effective to the least effective methods of CNTs dispersion are; 1. Tip sonication 2. Mechanical stirring 3. Magnetic agitation, respectively. It means that the final CNTs-epoxy morphology which is provided by sonication method represents the most uniform texture when compared to other two methods. Furthermore, another study has been provided by Pilawka et al in 2012 [13] which confirms that the sonication of MWCNT into the polymer leads to the most uniform CNTs-epoxy nanocomposite. Additionally, in their studies [13] the investigation of the mechanical properties of CNTs-epoxy as a function of different CNT contents have been done and the results have indicated that the optimum value of CNTs into the epoxy to provide the highest mechanical strength is 0.5 wt. %. Finally, it is important to mention that for the damage initiation analysis in CNTs-epoxy a numerical method is provided by Subramanian et al [14]. This method is based on the value of the energy dissipated due to the breakage and elongation of covalent bonds within the CNTs-epoxy nanocomposite. Finally, it seems important to mention, again that the bonding between the functionalized CNTs and epoxy is stronger than the pristine CNT and epoxy. As a result, the functionalized CNTs are dispersed with higher uniformity within the epoxy which results in higher strength of the nanocomposite. On the other hand, the pristine CNTs tend to bundle within the epoxy and creating a disturbed uniformity within the epoxy with lower strength. In Figure 1.9 [15], the SEM photographs of unfunctionalized (pristine) CNTs-epoxy (a) and functionalized CNTs-epoxy (b), with 1wt% CNT contents are shown. As is obvious in Figure 1.9, the dispersion of CNTs within the epoxy in functionalized CNTs-epoxy which is illustrated in part (b) is uniform [15].

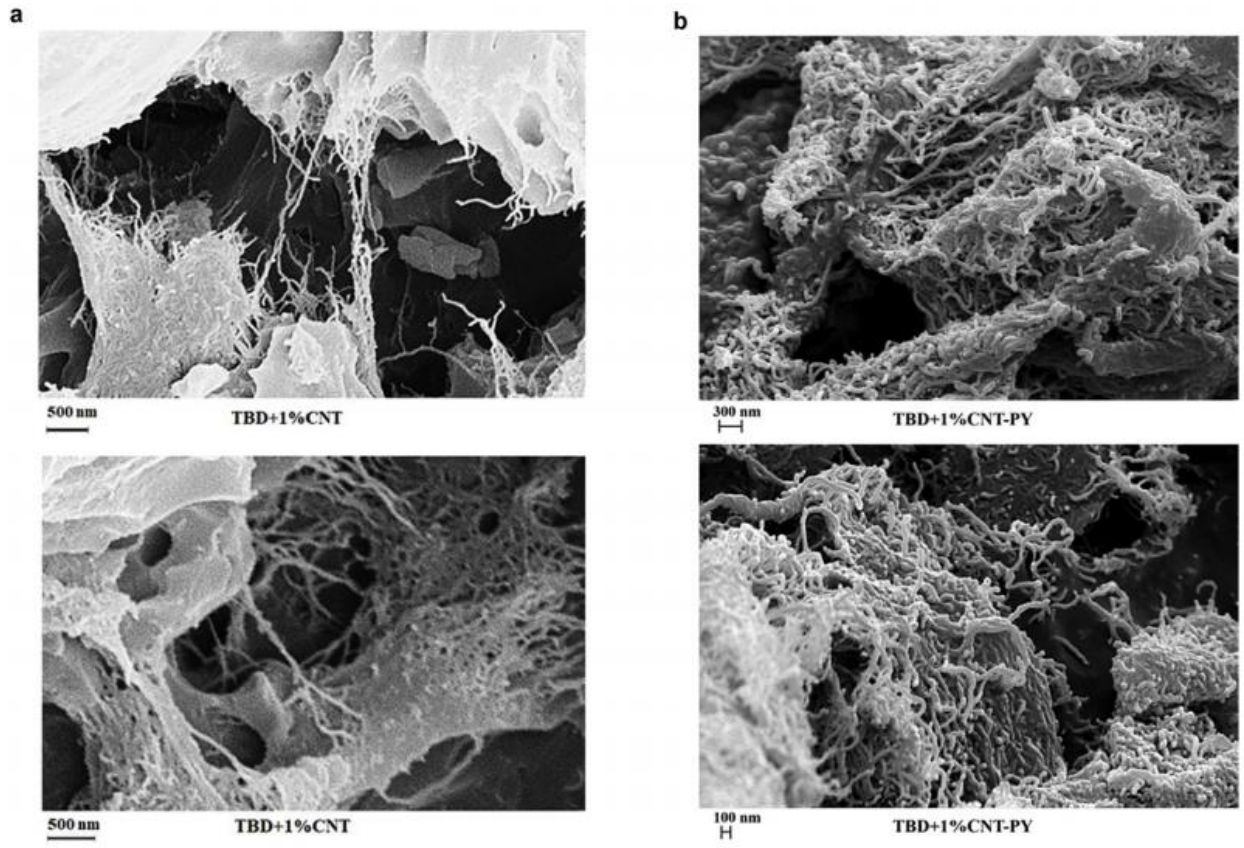


**Figure 1.9:** SEM photographs of unfunctionalized (pristine) CNTs-epoxy (a) and functionalized CNTs-epoxy (b) with 1wt. % CNT contents [15]

### 1.7. Thermal fatigue of CNT-epoxy

To the best of our knowledge, there are no previous studies related to the thermal fatigue of CNT-epoxy or the effect of thermal cycling on the mechanical properties of CNT-epoxy. The only study that has been found is the "Mechanical and Electrical Properties of MWCNT/Phenolic Composites under Moisture-Temperature Effects" which have been performed in 2007 in Switzerland by Yip et al [16]. In this study, the effect of thermal cycling on tensile strength of MWCNT/Phenolic Composites has been investigated. As is shown in Figure 1.10, the results have illustrated that with increasing number of thermal cycles, the tensile strength of MWCNT/Phenolic with 1wt% and 2wt.% MWCNT concentrations decreases while for the 0.5wt.% MWCNT concentration, the tensile strength approximately remains constant with increasing of thermal cycles. Additionally, in Figure 1.11, parts (a) and (b), the fracture surfaces produced during the tensile tests on MWCNT/Phenolic with 2wt.% MWCNT concentration after being exposed to 100 and 400 thermal cycling are shown, respectively [16].

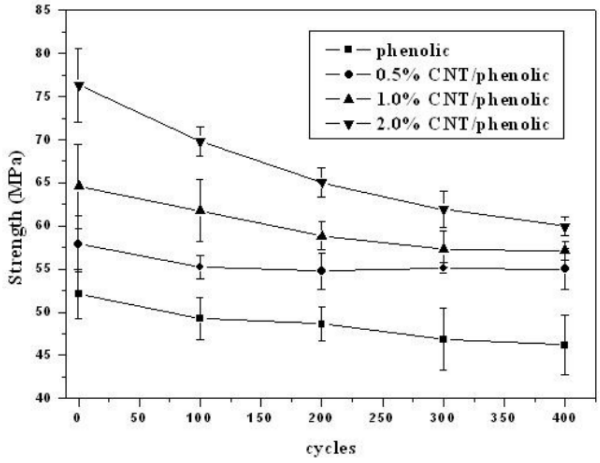


**Figure 1.10:** The effect of thermal cycling on the tensile strength of MWCNT/ Phenolic [16]

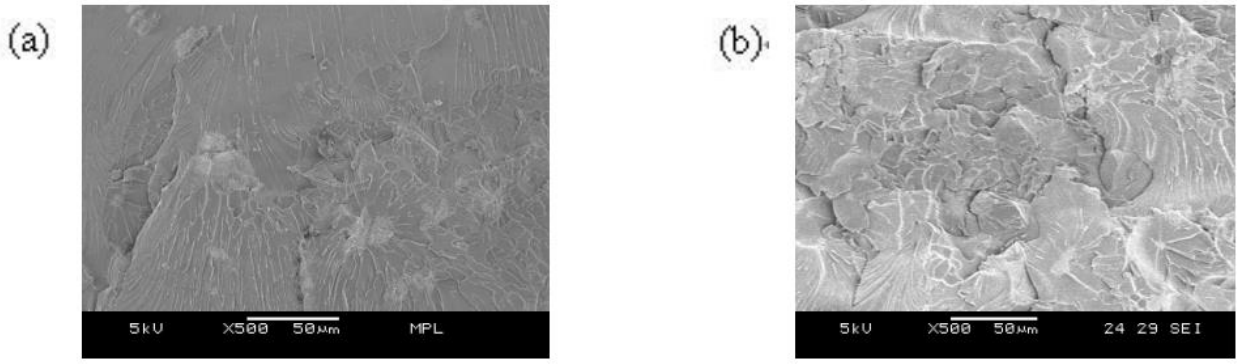


**Figure 1.11:** SEM images showing the fracture surfaces within the MWCNT/ Phenolic with 2wt% MWCNT concentrations after being exposed to 100 (a) and 400 (b) thermal cycling [16]

## 1.8. The effect of interface on mechanical properties of CNT-epoxy

CNTs may be a strong reinforcement for epoxy matrices, and the tensile strength and elastic modulus of CNT/epoxy composites may reach as high as 3600 MPa and 80 GPa, respectively. CNT/epoxy composites are promising composite materials with improved thermal and electrical conductivity, etc. because of their multi-functional properties, CNT/epoxy composites are applied as low weight structural composite materials, optical devices, thermal interface materials, electric components, electromagnetic absorption materials, etc. [17, 18].

Achieving appropriate CNT-epoxy interfacial bonding which provides enough stress transfer is a critical challenge for manufacturing CNT based epoxy composites, especially for CNT/epoxy structural composites. Three major possible mechanisms for load transfer from epoxy to a CNT exist. The first mechanism is the weak van der Waals bonding between the CNT and the epoxy, which may be the major load transfer mechanism for CNT/epoxy composites.

In this state, interfacial energies normally vary from ~50–350 mJ/m$^2$ [18]. The second method is micromechanical interlocking that may be marginal in CNT/epoxy composites if the CNTs possess atomically smooth surface. And the third is chemical bonding between CNTs and epoxy, which does not exist in many cases [18].

It is feasible to increase the load transfer from epoxy to a CNT by different techniques to enhance the mechanical performance of the nanocomposite, according to the above three major mechanisms of load transfer. Van der Waals bonding may be improved by applying small size CNT and near contact at the interface. Individual SWNTs which are well dispersed in epoxy is helpful. In the state of the micromechanical interlocking between CNTs and the epoxy's molecular chains, it appears that the ideal situation is: CNTs have high strength and inter-connected or have enough length to impede the shift of the epoxy chains [19]. The chemical attachment between CNTs and epoxy can be improved or built by surface treatments such as oxidization, physical coating and surface functionalization. The TEM images of functionalized CNTs in the epoxy resin indicated that CNTs have been completely embedded in the epoxy. Telescopic pull-outs proved the outermost layer, that has been directly attached to the epoxy, remained in the epoxy, while the innertubes transferred the crack. These results proved the evidence of enhanced interaction between CNTs and matrix [18].

Molecular dynamic results indicated that crosslinks between SWNTs and epoxy could enhance the shear strength of the SWNT-epoxy interface by more than one order of magnitude in comparison to the non-bonded interactions. From the predicted amounts of CNT axial stress and modulus, they proved that the interfacial strength of CNT/epoxy composites could be about 500 MPa.

Wagner calculated the interfacial strength of SWNT/epoxy composites applying a traditional force method improved for a hollow tube, and also tested the effect by changing some of the parameters. It was indicated that high amounts of the interfacial strength were attainable. The amounts for the interfacial strength were determined changing from 35 to 376 MPa. Results from both tests and theoretical models show that high amount of the interfacial force between CNTs and epoxy have been in principle attainable [18].

### 1.9.The effect of thermal cycles on the mechanical properties

There is a study that has compared the thermal fatigue life of Unidirectional Carbon fiber/epoxy composite (UCFEC) with CNT wire [20]. Based on this study, the materials strength of CNT wire has experienced about 10% less decrease compared to unidirectional carbon fiber/epoxy composite after they both were exposed to a large temperature variation over many thermal cycles. The temperature variation used is experienced in Low Earth Orbit (LEO) environment and measured the degradation of mechanical properties in UCFEC after being exposed to 2000 thermal cycles [21].

### 1.10. Microstructure of CNT and epoxy

#### 1.10.1. Microstructure after mixing

Figure 1.12 illustrates microstructures shown for four different concentrations of untreated CNTs dispersed within a transparent epoxy that were prepared by Ma et al. [22]. Suspensions were prepared applying a high-shear mixing approach. “For low concentration samples, a clear network of CNT can be resolved (Figures 1.12 (a) to (c)) whereas the 0.5 wt. % concentration sample (Fig. 1.12 (d)) showed domains of highly aggregated CNTs.

Confocal microscopy has been applied to identify the microstructure of CNT dispersion after mixing by sonication (Fig. 1.13). MWNTs, 0.03 wt.%, were spreaded in epoxy using a Sonicbio NR-3000 ultrasonic. The sonicator has been running with a cycle including of 30 seconds of ultrasound followed by 30 seconds of rest. Samples have been taken for imaging after 5 (Fig. 1.13 (a)) and 60 minutes (Fig. 1.13(b)) of treatment. They have been imaged applying a Leica TCS SP5 microscope. Light of 633nm wavelength has been shone at the specimen, and transmitted light and light reflected at the same wavelength have been detected. Analysis has not yet been conducted on the average size of structure for each specimen, but it is feasible to conclude that the structures after 60 minutes of sonication (Fig. 1.13 (b)) are smaller than those after 5 minutes (Fig. 1.13 (a)) [22].

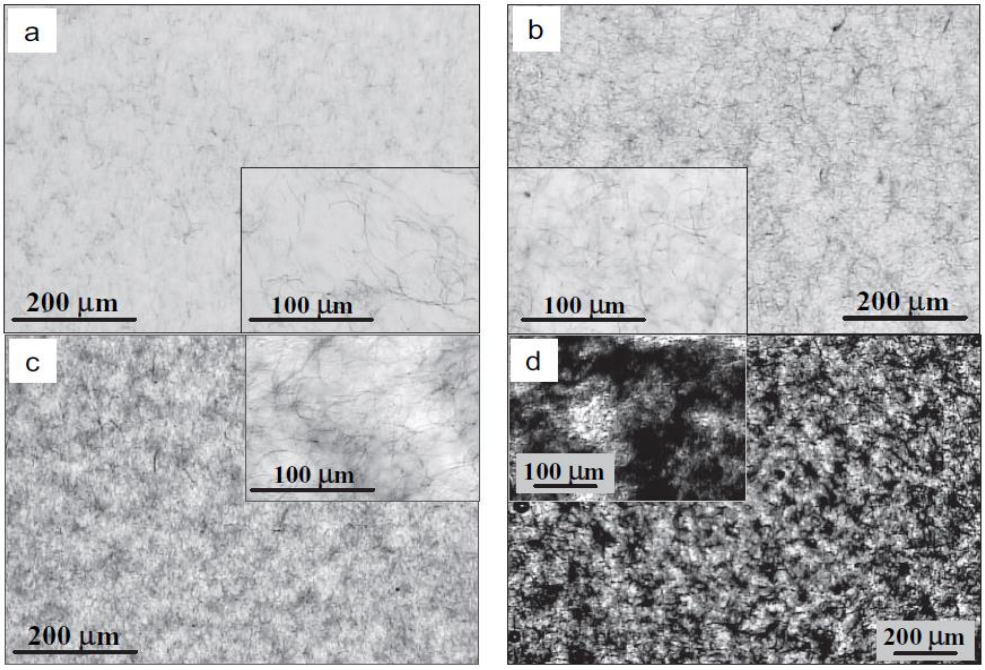


**Figure 1.12:** Optical micrographs of different concentrations of untreated MWNT suspended in epoxy: (a) 0.025 wt.%, (b) 0.05 wt.%, (c) 0.1 wt.%, and (d) 0.5 wt.%. Temperature = 25°C [22]

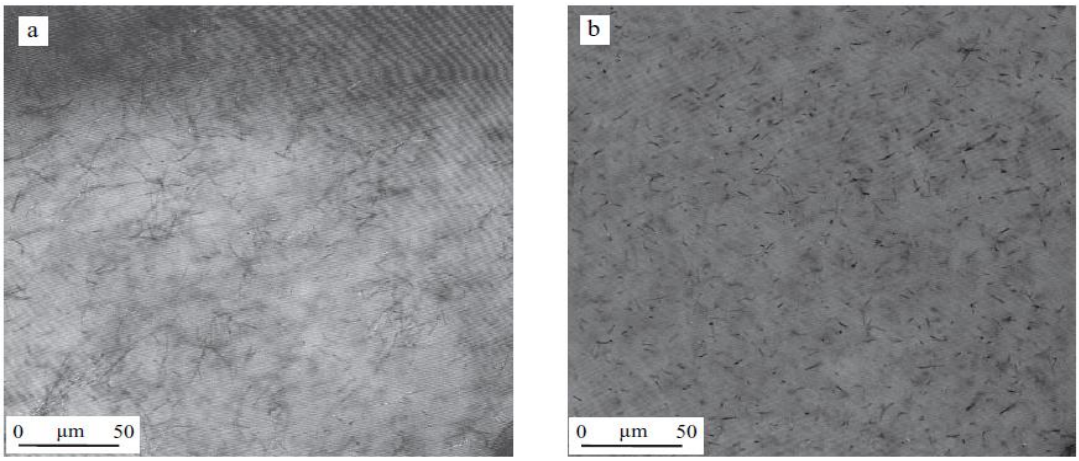


**Figure 1.13:** Confocal images of 0.03 wt.% MWNT suspended in epoxy after (a) 5 min and (b) 60 min of mixing by sonication [22]

### 1.10.2. Characterization of CNT orientation

In addition to aggregate structures, classification of CNT orientation seem desirable as the orientation of CNTs is almost closely dependent on properties like the electrical conductivity in the system. CNTs have been found to attract light and it has been recommended that some small CNTs, are still recognizable in bright-field microscopy proved that the CNT length is larger than the diffraction restriction. In a few cases, CNT orientation classification has been challenging and hence requires the application of techniques like as small-angle neutron scattering. Besides in situ classification, the CNTs orientation distribution can also be identified indirectly by conducting electron microscopy on cured samples [22].

### 1.10.3. Chemical structure of CNT-epoxy

Molecular dynamics is applied to assess the mechanical and thermal properties of creating SWNT/epoxy by adding pristine and functionalized CNTs to cross-linked epoxy. A 4601 atom DGEBA-DDS epoxy network has been built applying the 'dendrimer' growth method, where 75% of epoxy sites have been cross-linked.

The epoxy model has been approved by indicating the system is isotropic. The change in the dilatometric and mechanical properties has been studied in every orientation for both SWNT/epoxy and the full stiffness matrices and thermal expansion vectors have been obtained. As predicted, there has been an enhancement in stiffness along the CNT orientation for both the pristine and functionalized SWNT/epoxy [23].

### 1.11. Goals of this research

The objective of this research is to quantify the effects of thermal cycling on mechanical properties of CNT-reinforced epoxy. For this purpose, first step is to produce SWCNT-epoxy and MWCNT-epoxy nanocomposites in laboratory with using the epoxy cure (60 - minute epoxy cure). After the samples of SWCNT-epoxy and MWCNT-epoxy nanocomposites are produced in the lab with using the 10 * 10 * 1/8 inches mold, the next step would be to expose the specimens to about 3000 thermal cycles. Thermal cycles would be in the range of about room temperature to about 85% of the glass transition temperature of the epoxy ($0.85T_g$). After the exposure of the samples to thermal cycles mentioned, mechanical properties of the samples can be measured and compared with the mechanical properties of the samples before the cyclic thermal exposure. In this study, for measuring the mechanical properties, short beam and tensile tests would be applied to evaluate the degradation percentage of shear strength and tensile strength, respectively. The 3000 thermal cycles which is recommended in this study is based on similar experiments that have been done in 2012 by Park, et al. [21] for measuring the mechanical properties degradation after the fiber reinforced composite has been exposed to 3000 thermal cycles. The recommended study investigates the thermal fatigue of Unidirectional Carbon Fiber/epoxy in Low Earth Orbit.

If after the experiment, degradation of mechanical properties (tensile and shear strength) measured was too high, thermal cycles with the range of room temperature to $0.75T_g$ of the epoxy can be applied to the samples to measure the degradation of mechanical properties because it will be a smaller range of temperature variation in each thermal cycle. As a result, it is expected that the degradation of mechanical properties of CNT-epoxy should be reduced compared to the previous experiment. Nevertheless, it seems that the value of degradation in mechanical properties is still unknown.

After the thermal cycles have been performed on SWCNT-epoxy and MWCNT-epoxy nanocomposites, the mechanical properties of the samples can be measured with short beam and tensile tests. The results of these tests can be compared to the mechanical properties before the thermal cycles exposure. As a result, degradation percentage of mechanical properties can be measured which can show the effect of thermal cycles on mechanical properties of CNT-epoxy at high temperatures. As a result, the goals of this research would be:

- Fabricate the SWCNT-epoxy and MWCNT-epoxy nanocomposites samples. In Table 1.3, the numbers and CNT contents of the samples which will be produced for this thesis, are indicated.

**Table 1.3:** Composition of CNT-epoxy plates

| Nano composite | CNT contents (wt.%) | Number of plates |
|---|---|---|
| SWCNT-epoxy | 0.5 | 3 |
| | 1.0 | 3 |
| | 1.5 | 3 |
| MWCNT-epoxy | 0.5 | 3 |
| | 1.0 | 3 |
| | 1.5 | 3 |
| Pure epoxy | 0 | 3 |

- Expose the SWCNT-epoxy and MWCNT-epoxy nanocomposites samples to thermal cycles
- Measure the mechanical properties of SWCNT-epoxy and MWCNT-epoxy nanocomposites before and after the thermal cycling exposure using the short-beam and tensile tests. The mechanical properties could be measured after the 1000 and 2000 thermal cycles to more accurately analyze the effect of thermal cycles on mechanical properties.
- Compare the results with the mechanical properties of the samples before being exposed to the thermal cycles to evaluate the effect of thermal cycles on the SWCNT-epoxy and MWCNT-epoxy's mechanical properties.

- The mechanical properties which is going to be measured before and after the thermal fatigue experiments would include but not limited to tensile strength with using tensile test and interlaminar shear strength by using short-beam test. As it was mentioned in introduction section of this study, the damage mechanism probably could be either the initiation of damage from the interface areas of the CNTs-epoxy and failure with crack propagation mainly on the interface areas or the crack initiation and propagation occurring within the epoxy. Nevertheless, the combination of these two damage mechanisms is also possible to occur.

# Chapter 2

## 2.1 Thermal cycling effect on CNT wire

Polymer materials may be applied in many industries such as fibers, films, coatings, and sheets [24]. These forms can be used to produce carpets, clothing, reinforcements, and ropes [24]. In employment of nanomaterial and carbon, some works are provided by Saleh [25, 26, 27], Saleh et al. [28], and Gaddafi and Saleh [29]. This material may be used in many applications such as turbine blades, aerospace, etc. Other properties of these materials include lightweight and high strength [30]. Additionally, carbon fibers can be used in composite materials to produce the aileron, landing gear doors, and flaps [31]. Further assessment on composite materials characteristics are also provided by Chow et al. [32], Meszaros and Turcsan [33], and Jo and Lee [34]. Currently, unidirectional carbon fiber/epoxy composite (UCFEC) and carbon nanotube (CNT) wire have been used in several applications such as aerospace.

To make sure aerospace structure is reliable and safe, fatigue life of CNT wire and UCFEC in space is required to be predicted because thermal cycles in space can be one of the most important issues which affects the space structures. Thermal fatigue cycles occur when thermal cycles exist. A great instance for thermal fatigue cycles in space is satellite structure which rotates around the specific planets. These satellites' structures while rotating around the individual planet pass in and out of the planets' shadows that can be highly cold, and sun illumination that is very hot. As a consequence of the whole rotation around the planet, a thermal cycle creates which affects the structure. These thermal fatigue cycles can cause crack formation and propagation in space structures.

Hence, thermal fatigue assessment of aerospace structures is highly significant to prevent crack formation, propagation, and final fracture in harsh space environment. In order to estimate the very long-term stability, currently, “crack closure detection using photometrical analysis is provided by Savkin et al. [35] and “durability and integrity studies of environmentally conditioned interfaces in fibrous polymeric composite: critical concepts and comments” is submitted by Ray and Rathore [36].

### 2.2 Effect of Nano-carbon percentage on properties of composite materials

Carbon nanotubes (CNTs) represent a novel Nano scale material discovered by Lijima [1]. Important body of experimental and theoretical research is developed to this significant material. These contributions show very impressive physical characteristics such as high strength, high stiffness, low density, and thermal conductivity, recommending a role in high-strength light-weight material usage [30]. Several investigators have attempted to produce advanced CNT nanocomposite materials which contains one or more of these characteristics [38].

Among the related researches about the characteristics of nanocomposite materials, “carbon nanotube polymer composites”, is presented by Andrews and Weisenberger [39], “a review on study of composite materials in presence of cracks” is provided by Abhijeet et al [40], and “interaction of thermal loading on the damage evolution of composite materials” is submitted by Moufari and Bakkali [41]. According to both prior studies mentioned above, cracks and damage in composites are significant to predict because they can have real serious effects. It is also important to determine the value of CNT in nanocomposites which can decrease the cracks and damage in variety of loading conditions.

The value which mitigates the cracks amounts within the nanocomposite material. In this field, “crack growth as a function of temperature variation in carbon fiber/epoxy”, is currently submitted by Anvari [42]. Additionally, the role of carbon nanotubes, carbon, and other nanoparticles, in different composite materials’ characteristics is analyzed by Saleh [43], Machado et al. [44], Vallet et al. [45], Gomez et al. [46], Alswat et al. [47], Wang et al. [48], Saleh [49] and Moyo et al. [50].

### 2.3. Effect of Temperature on the Mechanical Properties of Carbon Composites

Because in this thesis the effect of temperature on the mechanical behavior of the carbon nanotube reinforced epoxy has been investigated. Therefore, in this section, similar works related to the effect of temperature on the mechanical properties of carbon composites are introduced**.**

#### 2.3.1. Ranking of Unidirectional Fibers/Matrix Composites Based on Their Interlaminar Shear Stress

The aim of this section of the study is to rank the unidirectional fibers/matrix composites based on the interlaminar shear stress existing between fibers and matrix due to thermal stress. Thermal stress induced in composites is one of the main issues in many applications such as space structures. In this section, by applying an analytical method, it is attempted to estimate the ranking of unidirectional fibers/matrix composites exposed to thermal stress based on their interlaminar shear stress between the fibers and matrix.

The application of the results of this research is very broad. These results could be very advantageous in any industry using unidirectional fibers/matrix composites exposed to thermal stress such as aerospace automotive, etc.

Thermal stress is one of the main issues in application of composites in many applications such as aerospace industry. Space structures are exposed to thermal cycles that induce thermal stress in composite structures in space. In order to investigate this effect, numbers of studies have been performed by Funk and Sykes [51], Shin et al. [52], and Unigovski et al.[53]. The objectives of the mentioned studies were to understand the damage induced due to thermal cyclic exposures.

In 2012 [54], Park et al. have conducted an experiment to simulate the thermal cycling in Low Earth Orbit (LEO) environment and estimate the effect of that on Unidirectional Carbon Fiber/Epoxy Composite (UD CF/EP). UD CF/EP material is one of the composite materials that is applied in aerospace structures such as satellites [54]. The objective of this experiment was to estimate the deterioration of UD CF/EP mechanical properties in LEO due to thermal cycling exposure.

Additionally, in 2018 [55], the experimental results achieved by Park et al. [54] have been analyzed. The analysis of the experimental results had indicated that Interlaminar Shear Strength (ILSS), Flexural Strength (FS), and Flexural Modulus (FM) of UD CF/EP were decreasing as thermal cycles were increasing in LEO simulation experiment.

Furthermore, based on the experimental results, it has been approximated that the deterioration of ILSS in UD CF/EP can be the main cause of fracture in UD CF/EP exposed to thermal stress. Nevertheless, it appears that there is no study to rank the unidirectional fibers/matrix composites (UFMCs) based on their interlaminar shear stress (ILSs). In the presented study, by applying an analytical method, the amounts of ILSs in UFMCs are calculated. Based on the assumption which has been approved in 2018 [55], the higher the ILSs is, the higher the probability to cause the fracture within the UFMC becomes. Thus, the best UFMC in terms of minimum probability of fracture or more durability when exposed to thermal cycling is the one with the minimum ILSs. As a result, this calculation would contribute to ranking the UFMCs based on their minimum ILSs (higher durability or higher thermal fatigue life).

#### 2.3.1.1. Interlaminar Shear Stress between the Fibers and Matrix Interfaces.

In 2018 [55], a relation has been proposed to estimate the ILSs within the UFMCs interfaces between the fibers and matrix. This equation is indicated as follows:

$$ILSs = (\alpha_c - \alpha_F).\Delta T.G. \quad (2.1)$$

In this part of the study, equation (2.1) [55] is employed to estimate the maximum ILSs. Based on the results obtained in 2018 [55], deterioration of ILSS in UD CF/EP seems to be the main cause of failure of this composite material which has been exposed to thermal cycling. Thus, in this section, it has been tried to establish a system to calculate the ILSs in common UFMC materials. This interpretation would verify that the risk of failure in UFMC is increased while ILSs is increased.

Therefore, in this part, ILSs in common UFMCs are calculated in order to rank them. It is important to notice that equation (2.1) is only valid in cases which fibers are impeded and constrained within the matrix. In order to calculate the maximum ILSs ($ILSs_{max}$), it is enough to replace the shear modulus with maximum shear modulus in equation (2.1). Thus, equation (2.1) becomes

$$ILSs_{max} = (\alpha_c - \alpha_F).\Delta T.G_{max}, \quad (2.2)$$

In the equation (2.2), $\alpha_c$ is the Coefficient of Thermal Expansion (CTE) of matrix in axial direction, $\alpha_F$ is the CTE of fiber in axial direction, and $\Delta T$ is the difference between the stress - free or crack - free temperature of the UFMC and the environment temperature. Furthermore, $G_{max}$ is the maximum shear modulus. It is important to notice that $G_{max}$ is determined by comparison between the shear modulus of matrix and fiber. The largest value of $G$ along the fibers' direction between the matrix and fiber needs to be identified and be substituted in equation (2.2), in order to obtain $ILSs_{max}$.

In Tables 2.1 and 2.2, there are lists of all common matrices and fibers used to develop UFMCs, respectively. In the following section, with applying equation (2.2), $ILSs_{max}$ of possible UFMCs exposed to thermal stress has been calculated.

In Table 2.3, $ILSs_{max}$ for 54 types of UFMCs are indicated as a function of $\Delta T$. In evaluation of the $ILSs_{max}$ for ranking the composite materials, the amount of $\Delta T$ is not required because it is assumed to be of the same value for all the materials and is constant for all of them. In order to use the values of $ILSs_{max}$ in Table 2.3, it is enough to have this knowledge that, based on the results obtained in 2018 [55], ILSs could be the main cause of fracture and/or de-bonding within the UFMCs. Consequently, as the value of ILSs increases, the probability of de-bonding or breaking bonds between fibers and matrix increases. This phenomenon will lead to crack initiation, propagation, and ultimately fracture within the UFMC.

Based on equation (2.2), as the difference between the CTEs of fibers and matrix increases, $ILSs_{max}$ increases. Furthermore, as the shear modulus increases, $ILSs_{max}$ increases. Thus, $ILSs_{max}$ is proportional to the difference of CTEs between fibers and matrix, and maximum shear modulus between fibers and matrix in axial direction.

It seems that the mismatch of CTEs between fibers and matrix is a great cause of failure, de-bonding, or fracture between those. The reason behind is that the axial CTE of the matrix is a positive value and the axial CTE of fiber, in most cases, is a negative value. Consequently, while UFMC is heating, the matrix is expanding in axial direction. On the other hand, fiber is contracting in axial direction. Additionally, while UFMC is cooling, matrix is contracting. On the other hand, fiber is expanding in this state in axial direction.

This reverse or mismatch behavior can cause inducing ILSs between fibers and matrix. If this process continues, it will create thermal cycles due to repeated cooling and heating. As a result of thermal cycling, due to this reverse behavior between fibers and matrix, bonds between them will start to break gradually and will create crack initiation along the axial direction of fibers within the fibers/matrix interfaces. These cracks will grow as thermal cycle numbers increase, and ultimately, will cause fracture or failure within the UFMC. In Table 2.3, unidirectional diamond fibers/CE339 epoxy matrix has the highest $ILSs_{max}$. It means that the probability of fracture due to thermal stress in this composite is the maximum. This fact is due to the high value of the axial CTE of CE339 epoxy matrix, and low axial CTE of diamond fibers. Additionally, the shear modulus of diamond is very high. Thus, $ILSs_{max}$, is highest for this UFMC material. Therefore, application of this UFMC material in low and high temperature environments with respect to crack - free temperature is not recommended. On the other hand, application of Sic fibers/borosilicate glass matrix composite is recommended because it has a minimum $ILSs_{max}$ compared to other UFMCs. Moreover, as it is indicated in Table 2.3, $ILSs_{max}$ for most of the unidirectional Sic and diamond fibers composites is very high. It means that the application of diamond and Sic fibers, in most cases, is not recommended in thermal stress condition. The reason is the high shear modulus of these fibers and the mismatch of CTEs between these fibers and the matrix.

**Table 2.1:** Axial shear modulus ($G_c$) and axial CTE ($\alpha_c$) of common matrix materials

| No. | Matrix name | $\alpha_c$ ($10^{-6}$/°C) | $G_c$ (GPa) |
|---|---|---|---|
| 1 | 934 epoxy | 43.92 [56] | 1.590 [56] |
| 2 | 5208 epoxy | 43.92 [56] | 1.590 [56] |
| 3 | 930 epoxy | 43.92 [56] | 1.590 [56] |
| 4 | CE339 epoxy | 63.36 [56] | 1.590 [56] |
| 5 | PMR15 polymide | 36.00 [56] | 1.310 [56] |
| 6 | 2024 Aluminum | 23.22 [56] | 27.58 [56] |
| 7 | Borosilicate glass | 3.240 [56] | 26.20 [56] |
| 8 | Al99.5 | 22.60 [57] | 26.00 [57] |
| 9 | 6061 Aluminum | 23.60 [58] | 26.00 [58] |
| 10 | AZ91D Mg | 28.50 [58] | 16.60 [58] |

**Table 2.2:** Axial shear modulus ($G_F$) and axial CTE ($\alpha_F$) of common fibers materials

| No. | Fiber name | $\alpha_F$ ($10^{-6}$/°C) | $G_F$ (GPa) |
|---|---|---|---|
| 1 | T300 | -0.54 [56] | 8.97 [56] |
| 2 | C6000 | -0.54 [56] | 8.97 [56] |
| 3 | HMS | -0.99 [56] | 7.59 [56] |
| 4 | P75 | -1.35 [56] | 6.90 [56] |
| 5 | P100 | -1.40 [56] | 6.90 [56] |
| 6 | Diamond | 1.05 [59] | 375 [59] |
| 7 | Sic | 2.78 [57] | 190.7 [57] |

**Table 2.3:** Ranking of UFMCs based on $ILSs_{max}$ calculated using values in Tables 2.1 and 2.2

| No. | UFMC name | $ILSs_{max}$ ($10^3$ Pa) |
|---|---|---|
| 1 | Sic Fibers/Borosilicate glass Matrix | 87.70ΔT |
| 2 | T300 Fibers/Borosilicate glass Matrix | 99.00ΔT |
| 3 | C6000 Fibers/Borosilicate glass Matrix | 99.00ΔT |
| 4 | HMS Fibers/Borosilicate glass Matrix | 110.8ΔT |
| 5 | P75 Fibers/Borosilicate glass Matrix | 120.3ΔT |
| 6 | P100 Fibers/Borosilicate glass Matrix | 121.6ΔT |
| 7 | P75 Fibers/PMR15 polymide Matrix | 257.7ΔT |
| 8 | P100 Fibers/PMR15 polymide Matrix | 258.0ΔT |
| 9 | HMS Fibers/PMR15 polymide Matrix | 280.8ΔT |
| 10 | P75 Fibers/epoxy 934 Matrix | 312.4ΔT |
| 11 | P100 Fibers/epoxy 934 Matrix | 312.7ΔT |
| 12 | T300 Fibers/PMR15 polymide Matrix | 327.8ΔT |
| 13 | C6000 Fibers/PMR15 polymide Matrix | 327.8ΔT |
| 14 | HMS Fibers/epoxy 934 Marix | 340.9ΔT |
| 15 | T300 Fibers/epoxy 934 Matrix | 398.8ΔT |
| 16 | C6000 Fibers/epoxy 934 Matrix | 398.8ΔT |
| 17 | P75 Fibers/CE339 epoxy Matrix | 446.5ΔT |
| 18 | P100 Fibers/CE339 epoxy Matrix | 446.8ΔT |
| 19 | T300 Fibers/AZ91D Mg Matrix | 482.0ΔT |
| 20 | HMS Fibers/CE339 epoxy Matrix | 488.4ΔT |
| 21 | HMS Fibers/AZ91D Mg Matrix | 489.5ΔT |
| 22 | P75 Fibers/AZ91D Mg Matrix | 495.5ΔT |
| 23 | P100 Fibers/AZ91D Mg Matrix | 496.3ΔT |
| 24 | T300 Fibers/CE339 epoxy Matrix | 573.2ΔT |
| 25 | C6000 Fibers/CE339 epoxy Matrix | 573.2ΔT |
| 26 | T300 Fibers/Al99.5 Matrix | 601.6ΔT |
| 27 | C6000 Fibers/Al99.5 Matrix | 601.6ΔT |
| 28 | HMS Fibers/Al99.5 Matrix | 613.34ΔT |
| 29 | P75 Fibers/Al99.5 Matrix | 622.7ΔT |
| 30 | P100 Fibers/Al99.5 Matrix | 624.0ΔT |
| 31 | T300 Fibers/6061 Aluminum Matrix | 627.6ΔT |
| 32 | C6000 Fibers/6061 Aluminum Matrix | 627.6ΔT |
| 33 | HMS Fibers/6061 Aluminum Matrix | 639.34ΔT |
| 34 | P75 Fibers/6061 Aluminum Matrix | 648.7ΔT |
| 35 | P100 Fibers/6061 Aluminum Matrix | 650.0ΔT |
| 36 | T300 Fibers/2024 Aluminum Matrix | 655.3ΔT |
| 37 | C6000 Fibers/2024 Aluminum Matrix | 655.3ΔT |
| 38 | HMS Fibers/2024 Aluminum Matrix | 667.7ΔT |
| 39 | P75 Fibers/2024 Aluminum Matrix | 677.6ΔT |
| 40 | P100 Fibers/2024 Aluminum Matrix | 679.0ΔT |
| 41 | Diamond Fibers/Borosilicate glass Matrix | 821.2ΔT |
| 42 | Sic Fibers/Al99.5 Matrix | 3,779.7ΔT |
| 43 | Sic Fibers/2024 Aluminum Matrix | 3,897.9ΔT |
| 44 | Sic Fibers/6061 Aluminum Matrix | 3,970ΔT |
| 45 | Sic Fibers/AZ91D Mg Matrix | 4,904.8ΔT |
| 46 | Sic Fibers/PMR15 polymide Matrix | 6,335ΔT |
| 47 | Diamond Fibers/Al99.5 Matrix | 8,081.2ΔT |
| 48 | Diamond Fibers/2024 Aluminum Matrix | 8,313.75ΔT |
| 49 | Diamond Fibers/6061 Aluminum Matrix | 8,456.2ΔT |
| 50 | Diamond Fibers/AZ91D Mg Matrix | 10,293.7ΔT |
| 51 | Sic Fibers/CE339 epoxy Matrix | 11,552.6ΔT |
| 52 | Diamond Fibers/PMR15 polymide Matrix | 13,106.2ΔT |
| 53 | Diamond Fibers/epoxy 934 Matrix | 16,076.2ΔT |
| 54 | Diamond Fibers/CE339 epoxy Matrix | 23,366.2ΔT |

## 2.4. Effect of MWCNT Diameter on Inter-Laminar Shear Stress of MWCNT/epoxy

The significant goal of this part of the study is to investigate the effect of MWCNT diameter on Inter-Laminar Shear stress (ILSs) of MWCNT/Epoxy (MWCNTE). MWCNTE is one of the nanocomposite materials that is currently being used in many applications such as aerospace industry due to its high strength and lightweight. In this section of the thesis, by applying an analytical method and using experimental data, it is attempted to evaluate the effect of MWCNT diameter on ILSs of MWCNTE.

For this assessment, two kinds of MWCNTs with different diameters are chosen. The mismatches of coefficients of thermal expansion between MWCNTs and epoxy at temperature range of -5$^{o}$C to 70$^{o}$C for both MWCNTs are calculated. Finally, with the results which are obtained by this assessment, ILSs of these two MWCNTE nanocomposites are compared. The results have shown that the nanocomposite which is contained with a MWCNT with smaller diameter could offer a lower ILSs. Because MWCNTs could be manufactured in different diameter sizes, the results of this study could be used in applications dealing with thermal cycles or thermal stress to select the suitable MWCNT with appropriate diameter within the epoxy for having the lowest ILSs.

In many industries, application of composite materials has become common such as aerospace, automobile, etc [62, 63, 64, 65]. Additionally, in current years, it has been tried to use nanocomposites in many industries [66]. In order to fabricate nanocomposites, instead of fibers, nanofibers are used. These nanofibers could be SWCNT, MWCNT, and Triple-Walled Carbon Nanotube, etc [67, 68]. Application of the mentioned nanofibers instead of fibers has the potential to enhance the strength of nanocomposites.

With the results which have been provided in 2018 [69] and applying the previous form of the thermal stress equation [70], a relation has been developed [69] to derive the maximum Inter-Laminar Shear stress ($ILSs_{max}$) within the Unidirectional Fibers/Matrix Composites (UFMC). This equation is indicated below.

$$ILSsmax = \Delta\alpha A.\max.\Delta T.Gmax. \quad (2.3)$$

It is important to notice that in equation (2.3), $\Delta\alpha_{A.max}$ is equal to the maximum value of "axial Coefficient of Thermal Expansion (CTE) of epoxy ($\alpha_{epoxy}$) minus the axial CTE of CNT ($\alpha_{CNT}$). This relation is indicated below. This equation is valid for any UFMC including SWCNTE, MWCNTE, etc.

$$\Delta\alpha A.\max = \alpha epoxy - \alpha CNT. \quad (2.4)$$

Because $\alpha_{epoxy}$ is a positive value and the $\alpha_{CNT}$ in most cases is a negative value, the amount of $\Delta\alpha$ will usually become a positive value and is indicated in Table 2.5.

It seems that by increasing the application of nanocomposites in different industries, analysis in order to obtain the mechanical properties of these nanocomposites exposed to different environments such as space environment, is required. A great instance of this application is satellite structure that rotates around the earth. As it rotates around the earth in low earth orbit, it passes through the sun illumination and earth's shadow that are extremely hot (120$^{o}$C) and cold (-175$^{o}$C), respectively [71].

Consequently, an exact thermal analysis for nanocomposites exposed to extremely hot and cold temperatures seems necessary. Thermal analysis could provide data to derive the ILSs of the nanocomposite. It appears that as the value of ILSs increases, the probability of inter-laminar deterioration within the nanocomposite increases. ILSs is highly proportional to the mismatch of CTEs between the nanofibers and epoxy matrix. There are many studies related to the research regarding the CTEs of many fiber and epoxy materials [72, 73]. Nevertheless, it seems that there is no study regarding the effect of MWCNT diameter on ILSs of MWCNTE.

In the presented part of the research, with using an analytical method with equation (2.3), and applying experimental results [67], it is attempted to investigate the effect of MWCNT diameter on the ILSs of MWCNTE. The results of this study could be very advantageous to select the best MWCNTE in cases dealing with thermal cycle or thermal stress.

### 2.4.1. Experimental procedures

"Spinnable MWCNT arrays were obtained by chemical vapor deposition using C2H2 and FeCl2 as the base material and the catalyst, respectively. The diameter of the MWCNTs was measured using a transmission electron microscope (TEM, JEOL JEM-2100F, Japan). A partially cured epoxy resin (B-stage epoxy) with a release paper was used as the starting material, where the epoxy resin comprised bisphenol-A type epoxy, novolac-type epoxy, and an aromatic diamine curing agent. The epoxy resin was then impregnated into the MWCNT monolithic sheet at 90 $^{o}$C for 3 min between the steel plates of a hot press (AS ONE AH-4015, Japan).

After peeling off the release paper from the MWCNT sheet now impregnated with the epoxy resin (prepreg sheet), the prepreg sheet was cured at 130 $^{o}$C for 1.5 h at a pressure of 1 MPa using the hot press, forming a film specimen" [67].

### 2.4.2. Problem formulation

In Table 2.4 [67], CTEs of epoxy, 25 nm diameter MWCNT (25-MWCNT) and 41 nm diameter MWCNT (41-MWCNT) within the temperature range of -5ºC to 70ºC are indicated. According to equation (2.3), variation of CTEs between the epoxy and the MWCNT within the MWCNTE is one of the reasons to raise ILSs within the nanocomposite material. Thus, in this part of the study, it is assumed that composites with less variation of CTEs between epoxy and MWCNT have higher ILSS. According to the results obtained in 2018 [69], degradation of ILSS within the UFMC could be the main cause of thermal fatigue failure in these nanocomposite materials. It seems important to note that relation (2.3) can be applied in cases where fibers are imbedded within the matrix.

In equation (2.3), $\Delta T$ is the temperature variation between the crack - free temperature of the CNT/epoxy and the ambient temperature. $G_{max}$ is the maximum shear modulus between the epoxy and CNT.

**Table 2.4:** CTEs of epoxy resin, 25-MWCNT, and 41-MWCNT at temperatures from -5 to 70 ºC [67]

| No.1 | Temperature (ºC) | CTE (1/ºC $e^{-5}$) | | |
|---|---|---|---|---|
| | | Epoxy resin | 25-MWCNT | 41-MWCNT |
| 1 | -5 | 4.60 | -1.15 | -2.00 |
| 3 | 5 | 5.30 | -0.99 | -1.60 |
| 5 | 15 | 4.00 | -0.79 | -1.30 |
| 7 | 25 | 3.50 | -0.61 | -1.02 |
| 9 | 35 | 3.80 | -0.45 | -0.85 |
| 11 | 45 | 4.30 | -0.31 | -0.76 |
| 13 | 55 | 4.70 | -0.18 | -0.75 |
| 15 | 65 | 5.00 | -0.08 | -0.82 |
| 16 | 70 | 5.20 | -0.03 | -0.90 |

In the presented section of the thesis, thermal analysis is performed to investigate the effect of MWCNT diameter on ILSs of MWCNTE. In order to evaluate this effect, variation of CTEs between epoxy and 25-MWCNT, and epoxy and 41-MWCNT at the temperature range of -5$^{o}$C to 70$^{o}$C are calculated and indicated in Table 2.6 and illustrated in Figures 2.1 and 2.2. According to the data in Table 2.5, at the temperature 5$^{o}$C, the mismatch of CTEs between epoxy and 25-MWCNT, and epoxy and 41-MWCNT, are 6.29e-5 (1/$^{o}$C) and 6.90e-5 (1/$^{o}$C), respectively. These mismatches of CTEs are highest for both MWCNTEs. It means that according to equation (2.3), at this temperature, ILSs could be the maximum value. This phenomenon could result in higher probability of crack initiation and/or de-bonding between MWCNT and epoxy.

This temperature that is representing the highest mismatch of CTEs between MWCNT and epoxy, could be named as "critical temperature," because in this temperature the probability of crack initiation and/or propagation could be the highest value. However, it is significant to pay attention that the comparison between the ILSs of two MWCNTEs here is based on the assumption that both 25-MWCNT and 41-MWCNT have the same value of shear modulus.

Furthermore, by analyzing Table 2.5, it can be concluded that mean and maximum CTE variations between 41-MWCNT and epoxy are higher than that for 25-MWCNT and epoxy. It means that ILSs between 41-MWCNT and epoxy could be higher than that between 25-MWCNT and epoxy. Due to the higher ILSs concentration within the 41-MWCNTE interface in comparison with that within the 25-MWCNTE, the risk of crack initiation and debonding increases within the nanofibers and epoxy interfaces.

**Table 2.5:** CTEs differences between 25-MWCNT and epoxy, and between 41-MWCNT and epoxy ($\Delta\alpha$) at temperature range of -5°C and 70°C

| No.1 | Temperature (°C) | $\Delta\alpha$ (1/°C $e^{-5}$) | |
|---|---|---|---|
| | | $\alpha_{epoxy} - \alpha_{25\text{-}MWCNT}$ | $\alpha_{epoxy} - \alpha_{41\text{-}MWCNT}$ |
| 1 | -5 | 5.75 | 6.60 |
| 2 | 0 | 6.05 | 6.75 |
| 3 | 5 | 6.29* | 6.90* |
| 4 | 10 | 5.49 | 6.03 |
| 5 | 15 | 4.79 | 5.30 |
| 6 | 20 | 4.40 | 4.84 |
| 7 | 25 | 4.11 | 4.52 |
| 8 | 30 | 4.06 | 4.46 |
| 9 | 35 | 4.25 | 4.65 |
| 10 | 40 | 4.52 | 4.95 |
| 11 | 45 | 4.61 | 5.06 |
| 12 | 50 | 4.74 | 5.25 |
| 13 | 55 | 4.88 | 5.45 |
| 14 | 60 | 5.03 | 5.68 |
| 15 | 65 | 5.08 | 5.82 |
| 16 | 70 | 5.23 | 6.10 |

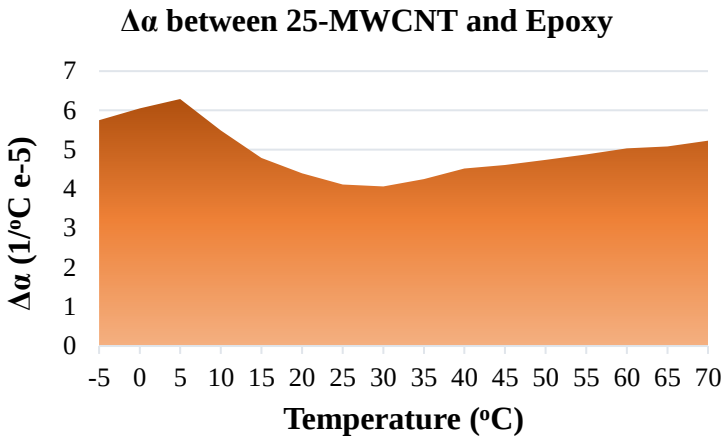


**Figure 2.1:** CTEs differences between 25-MWCNT and epoxy (Δα) at temperature range of -5°C to 70°C

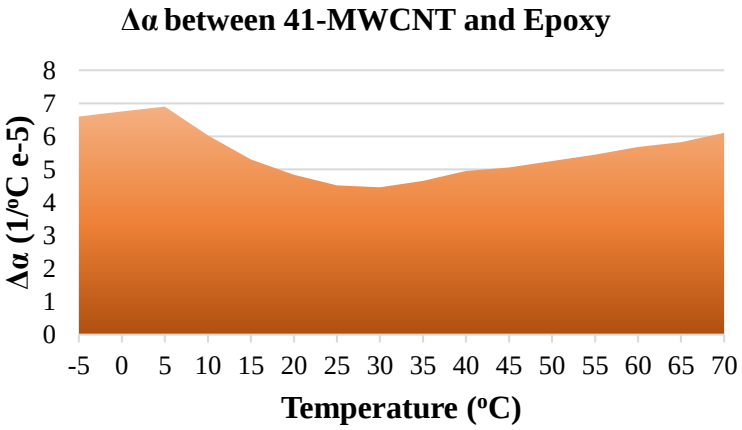


**Figure 2.2:** CTEs differences between 41-MWCNT and epoxy (Δα) at temperature range of -5°C to 70°C

### 2.5. Effect of SWCNT Diameter on Inter-Laminar Shear Stress of SWCNT/Epoxy

The fundamental aim of this part of the study is to investigate the effect of SWCNT diameter on ILSs of SWCNT/Epoxy (SWCNTE). For this purpose, three SWCNTs with three different sizes of diameters are selected. Furthermore, differences of coefficients of thermal expansion between the SWCNT and epoxy for three different diameter sizes of SWCNTs at temperature range of -5 to 85$^{o}$C are calculated. Additionally, for these three Nano-composites, ILSs at the same temperature range are derived. Finally, based on the results obtained, ILSS of three SWCNTEs are compared. The results have shown that SWCNTE contained with SWCNT which has 13.6 nm diameter, can offer higher ILSS due to minimum ILSs in comparison with other two Nanocomposites. The reason is less stress concentration on interface within the SWCNTE that would cause less crack initiation, propagation, and de-bonding on SWCNTE interface. For evaluating the ILSs within the SWCNT and Epoxy interface, the same method which has been used in the previous section has been applied in this section.

In the presented part of the research, by using analytical method and applying experimental data [67] it is attempted to compare the ILSs within three SWCNTEs that each contains SWCNT with different sizes of diameters. The results have shown that SWCNTE with SWCNT which has the largest diameter may offer higher ILSS when compared with that for other SWCNTEs.

### 2.5.1. Experimental procedures

"Spinnable SWCNT arrays were obtained by chemical vapor deposition using C2H2 and FeCl2 as the base material and the catalyst, respectively. The diameter of the SWCNTs was measured using a transmission electron microscope (TEM, JEOL JEM-2100F, Japan). A partially cured epoxy resin (B-stage epoxy) with a release paper was used as the starting material, where the epoxy resin comprised bisphenol-A type epoxy, novolac-type epoxy, and an aromatic diamine curing agent. The epoxy resin was then impregnated into the SWCNT monolithic sheet at 90 $^{o}$C for 3 min between the steel plates of a hot press (AS ONE AH-4015, Japan). After peeling off the release paper from the SWCNT sheet now impregnated with the epoxy resin (prepreg sheet), the prepreg sheet was cured at 130 $^{o}$C for 1.5 h at a pressure of 1 MPa using the hot press, forming a film specimen" [67].

### 2.5.2. Problem formulation

In this part of the research, the method which has been applied in the previous section of the thesis for evaluating the ILSS of MWCNTE has been used for SWCNTE. Therefore, equation (2.3) has been used to calculate the ILSs within the SWCNTE interface.

In Table 2.6, CTEs and shear modulus of SWCNTs with 1.4 (1.4-SWCNT), 7 (7-SWCNT), and 13.6 nm (13.6-SWCNT) diameters, and epoxy at temperature range of -5 to 85$^{o}$C are indicated. With the presented data in Table 2.6 and using equation (2.3), ILSS of SWCNTEs contained with SWCNTs with three different diameters, are compared.

**Table 2.6:** CTEs and Shear modulus of 1.4-SWCNT, 7-SWCNT, 13.6 SWCNT, and Epoxy at temperature range of -5 to 85$^{o}$C

| Temperature ($^{o}$C) | 1.4-SWCNT | | 7-SWCNT | | 13.6-SWCNT | | Epoxy | |
|---|---|---|---|---|---|---|---|---|
| | CTE (1/$^{o}$C e-5) [67] | Shear Modulus (GPa) [68] | CTE (1/$^{o}$C e-5) [67] | Shear Modulus (GPa) [68] | CTE (1/$^{o}$C e-5) [67] | Shear Modulus (GPa) [68] | CTE (1/$^{o}$C e-5) [67] | Shear Modulus (GPa) [74] |
| -5 | -1.04 | 18 | -0.74 | 5.2 | -1.5 | 3.1 | 4.60 | 1.59 |
| 0 | -1.05 | 18 | -0.75 | 5.2 | -1.5 | 3.1 | 4.95 | 1.59 |
| 5 | -1.06 | 18 | -0.76 | 5.2 | -1.5 | 3.1 | 5.30 | 1.59 |
| 10 | -1.07 | 18 | -0.76 | 5.2 | -1.6 | 3.1 | 4.60 | 1.59 |
| 15 | -1.08 | 18 | -0.77 | 5.2 | -1.6 | 3.1 | 4.00 | 1.59 |
| 20 | -1.10 | 18 | -0.78 | 5.2 | -1.6 | 3.1 | 3.70 | 1.59 |
| 25 | -1.11 | 18 | -0.78 | 5.2 | -1.6 | 3.1 | 3.50 | 1.59 |
| 30 | -1.12 | 18 | -0.79 | 5.2 | -1.7 | 3.1 | 3.53 | 1.59 |
| 35 | -1.12 | 18 | -0.79 | 5.2 | -1.7 | 3.1 | 3.80 | 1.59 |
| 40 | -1.13 | 18 | -0.79 | 5.2 | -1.7 | 3.1 | 4.15 | 1.59 |
| 45 | -1.14 | 18 | -0.80 | 5.2 | -1.7 | 3.1 | 4.30 | 1.59 |
| 50 | -1.15 | 18 | -0.80 | 5.2 | -1.7 | 3.1 | 4.50 | 1.59 |
| 55 | -1.16 | 18 | -0.80 | 5.2 | -1.7 | 3.1 | 4.70 | 1.59 |
| 60 | -1.16 | 18 | -0.80 | 5.2 | -1.7 | 3.1 | 4.90 | 1.59 |
| 65 | -1.17 | 18 | -0.80 | 5.2 | -1.8 | 3.1 | 5.00 | 1.59 |
| 70 | -1.18 | 18 | -0.80 | 5.2 | -1.8 | 3.1 | 5.20 | 1.59 |
| 75 | -1.18 | 18 | -0.80 | 5.2 | -1.8 | 3.1 | 5.40 | 1.59 |
| 80 | -1.19 | 18 | -0.80 | 5.2 | -1.8 | 3.1 | 5.60 | 1.59 |
| 85 | -1.19 | 18 | -0.80 | 5.2 | -1.8 | 3.1 | 5.70 | 1.59 |

In Tables 2.7, 2.8, and 2.9, all the results from the thermal analysis (equation (2.3)) of three SWCNTEs are indicated. Furthermore, in Figures 2.3, 2.4, 2.5, 2.6, 2.7, and 2.8, all the results obtained by employing equation (2.3) and data in Table 2.3, are shown.

According to the following results, average and maximum differences of CTEs between 13.6-SWCNT and epoxy is higher than that for between 1.4-SWCNT and epoxy, and between 7-SWCNT and epoxy. On the other hand, maximum and average ILSs within 1.4-SWCNTE is higher than that within 7-SWCNTE and 13.6-SWCNTE. According to these results, because as ILSs increases, the ILSS decreases, it appears that ILSS of 13.6-SWCNTE and 1.4-SWCNTE are highest and lowest, respectively. Thus, it seems that thermal cycle numbers to failure of 7-SWCNTE is between the thermal cycle numbers to failure of 13.6-SWCNTE and 1.4-SWCNTE. As a result, it appears that as the diameter size of SWCNT increases, ILSS increases. These results can contribute to select the best SWCNTE in case of having maximum thermal fatigue life in environments dealing with thermal cycles.

Although the CTEs mismatches between 13.6-SWCNT and epoxy is higher than that for between 1.4-SWCNT and epoxy, but ILSs is higher for 1.4-SWCNTE. The reason is due to the higher shear modulus of 1.4-SWCNT (18 GPa) [68] in comparison with that for 13.6-SWCNT (3.1 GPa) [68]. Because according to equation (2.3), for determining ILSs, $\Delta\alpha$ is multiplied by $\Delta T$ and G. Thus, because G is very higher for 1.4-SWCNT in comparison with that for 13.6-SWCNT, ILSs is higher for 1.4-SWCNTE, although it has a lower $\Delta\alpha$ between 1.4-SWCNT and epoxy.

It seems important to mention that deterioration and de-bonding within the nanofiber and matrix interface is due to the reverse behavior between the nanofiber and epoxy. This reverse behavior is the result of opposite values of CTEs between the SWCNT and epoxy, or MWCNT and epoxy. Due to the opposite values of CTEs between the nanofibers and matrix, while the MWCNTE or SWCNTE is cooling with respect to crack - free temperature, epoxy is contracting while MWCNT or SWCNT is expanding in the axial direction. On the other hand, while MWCNTE or SWCNTE is heating, epoxy is expanding, while MWCNT or SWCNT is contacting. This reverse behavior has the potential to induce deterioration and de-bonding within the SWCNTE or MWCNTE interfaces between the nanofibers and matrix.

The deterioration within the SWCNTE and MWCNTE interface could cause crack initiation and/or propagation within these areas. In the cases dealing with thermal cycles, this reverse behavior between the epoxy and MWCNT or SWCNT repeats over and over. Therefore, higher degradation on interface between the nanofiber and matrix can be expected.

For the effect of shear modulus on ILSs, it should be mentioned here that within -5$^{o}$C to 85$^{o}$C, the shear modulus would have a constant value or approximately a constant value. Therefore, it is not expected to have variational effect on ILSs.

As it is mentioned before, it appears that, the higher the ILSs, the lower the thermal fatigue life becomes. The reason is because higher ILSs can cause stress concentration on fibers and matrix interfaces. Consequently, it has a potential to induce crack initiation, propagation, and de-bonding within the fibers and matrix interfaces.

**Table 2.7:** Mismatches between the CTEs of 1.4-SWCNT and Epoxy (Δα), and ILSs at temperature range of -5 to 85°C within the 1.4-SWCNTE

| **Temperature (°C)** | **1.4-SWCNTEC** | |
|---|---|---|
| | **Δα (1/°C e-5)** | **ILSs (MPa)** |
| -5 | 5.6 | 28.4 |
| 0 | 6.0 | 24.8 |
| 5 | 6.4 | 20.6 |
| 10 | 5.7 | 13.3 |
| 15 | 5.1 | 7.30 |
| 20 | 4.8 | 2.60 |
| 25 | 4.6 | 1.70 |
| 30 | 4.6 | 5.90 |
| 35 | 4.9 | 10.6 |
| 40 | 5.3 | 16.2 |
| 45 | 5.4 | 21.5 |
| 50 | 5.6 | 27.5 |
| 55 | 5.9 | 33.8 |
| 60 | 6.1 | 40.4 |
| 65 | 6.2 | 46.6 |
| 70 | 6.4 | 54.0 |
| 75 | 6.6 | 61.6 |
| 80 | 6.8 | 69.7 |
| 85 | 6.9 | 76.9 |
| **Average** | 5.7 | 29.7 |

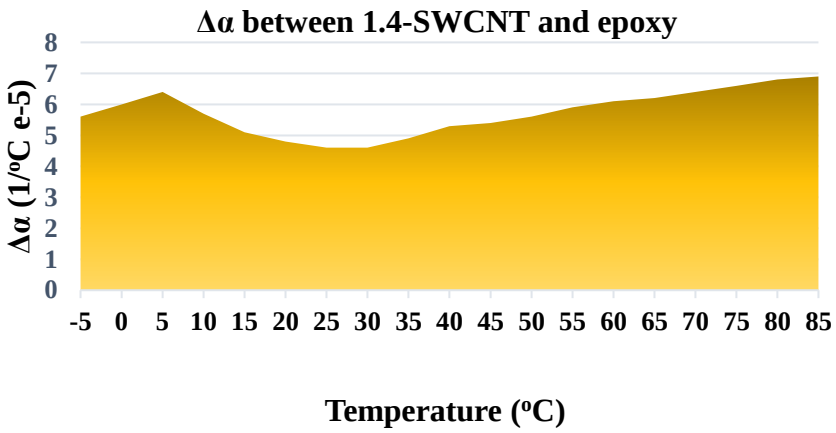


**Figure 2.3:** Mismatches between the CTEs of 1.4-SWCNT and Epoxy (Δα) at the temperature range of -5 to 85ºC within the 1.4-SWCNTE

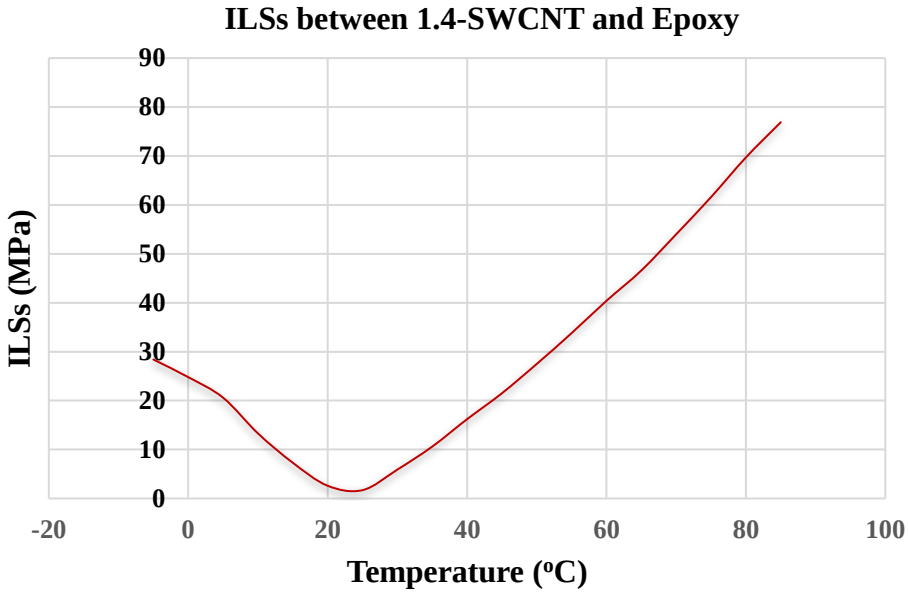


**Figure 2.4:** ILSs within the interface of 1.4-SWCNT and Epoxy at the temperature range of -5 to 85ºC within the 1.4-SWCNTE

**Table 2.8:** Mismatches between the CTEs of 7-SWCNT and Epoxy (Δα), and ILSs at the temperature range of -5 to 85°C within the 7-SWCNTE

| Temperature (°C) | 7-SWCNTEC | |
|---|---|---|
| | Δα (1/°C e-5) | ILSs (MPa) |
| -5 | 5.3 | 7.80 |
| 0 | 5.7 | 6.80 |
| 5 | 6.1 | 5.70 |
| 10 | 5.4 | 3.60 |
| 15 | 4.8 | 2.00 |
| 20 | 4.5 | 0.70 |
| 25 | 4.3 | 0.50 |
| 30 | 4.3 | 1.60 |
| 35 | 4.6 | 2.90 |
| 40 | 4.9 | 4.40 |
| 45 | 5.1 | 5.80 |
| 50 | 5.3 | 7.40 |
| 55 | 5.5 | 9.20 |
| 60 | 5.7 | 11.0 |
| 65 | 5.8 | 12.7 |
| 70 | 6.0 | 14.7 |
| 75 | 6.2 | 16.8 |
| 80 | 6.4 | 19.0 |
| 85 | 6.5 | 21.0 |
| **Average** | 5.4 | 8.10 |

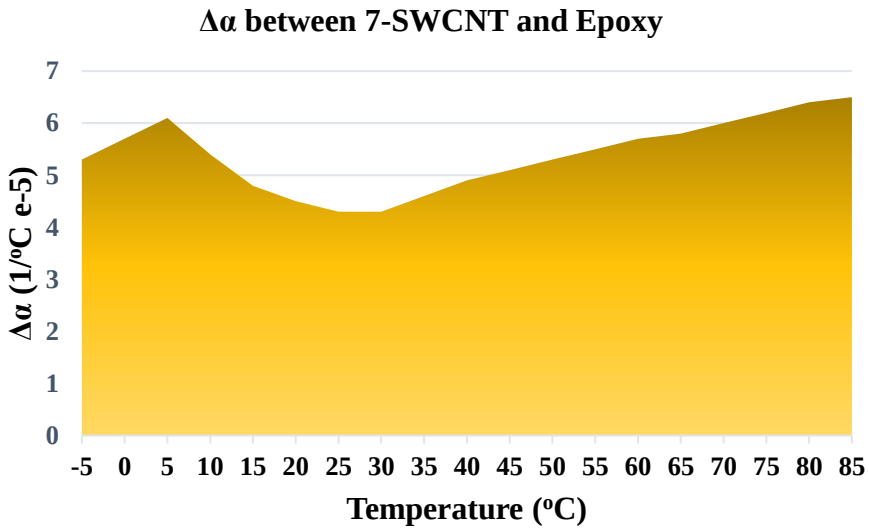


**Figure 2.5:** Mismatches between the CTEs of 7-SWCNT and Epoxy (Δα) at the temperature range of -5 to 85ºC within the 7-SWCNTE

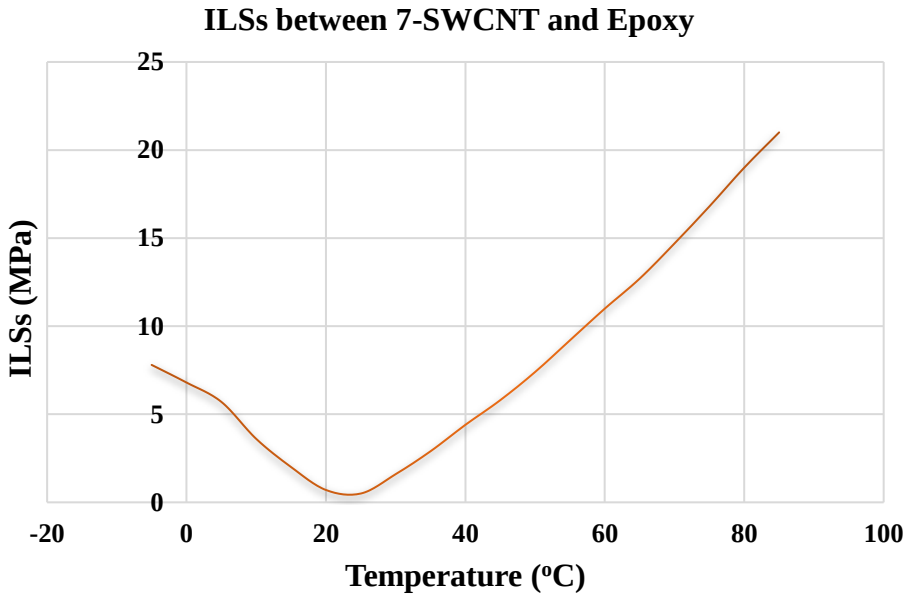


**Figure 2.6:** ILSs within the interface between the 7-SWCNT and Epoxy at the temperature range of -5 to 85ºC within the 7-SWCNTE

**Table 2.9:** Mismatches between the CTEs of 13.6-SWCNT and Epoxy (Δα), and ILSs at the temperature range of -5 to 85ºC within the 13.6-SWCNTE

| **Temperature (ºC)** | **13.6-SWCNTE** | |
|---|---|---|
| | **Δα (1/ºC e-5)** | **ILSs (MPa)** |
| -5 | 6.1 | 5.30 |
| 0 | 6.4 | 4.60 |
| 5 | 6.8 | 3.80 |
| 10 | 6.2 | 2.50 |
| 15 | 5.6 | 1.40 |
| 20 | 5.3 | 0.50 |
| 25 | 5.1 | 0.30 |
| 30 | 5.2 | 1.10 |
| 35 | 5.5 | 2.00 |
| 40 | 5.8 | 3.10 |
| 45 | 6.0 | 4.10 |
| 50 | 6.2 | 5.20 |
| 55 | 6.4 | 6.30 |
| 60 | 6.6 | 7.60 |
| 65 | 6.8 | 8.90 |
| 70 | 7.0 | 10.2 |
| 75 | 7.2 | 11.6 |
| 80 | 7.4 | 13.1 |
| 85 | 7.5 | 14.4 |
| **Average** | 6.3 | 5.60 |

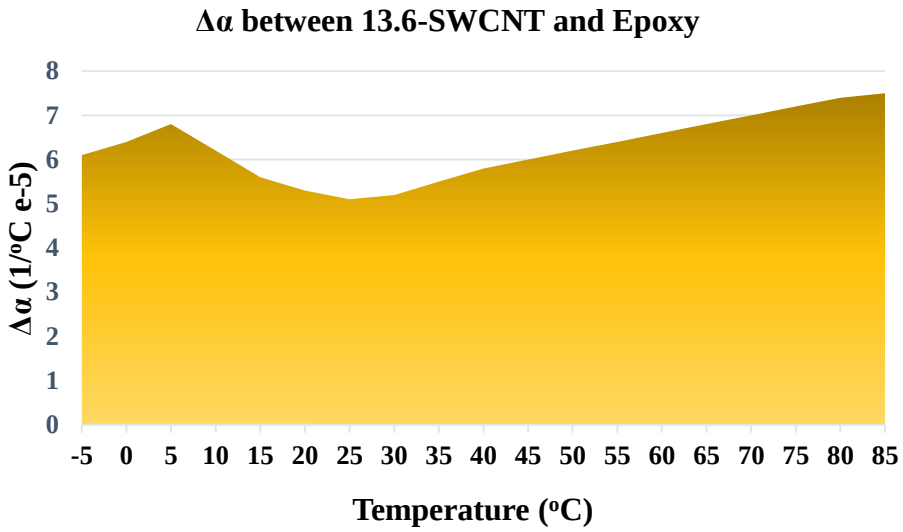


**Figure 2.7:** Mismatches between the CTEs of 13.6-SWCNT and Epoxy (Δα) at the temperature range of -5 to 85°C within the 13.6-SWCNTE

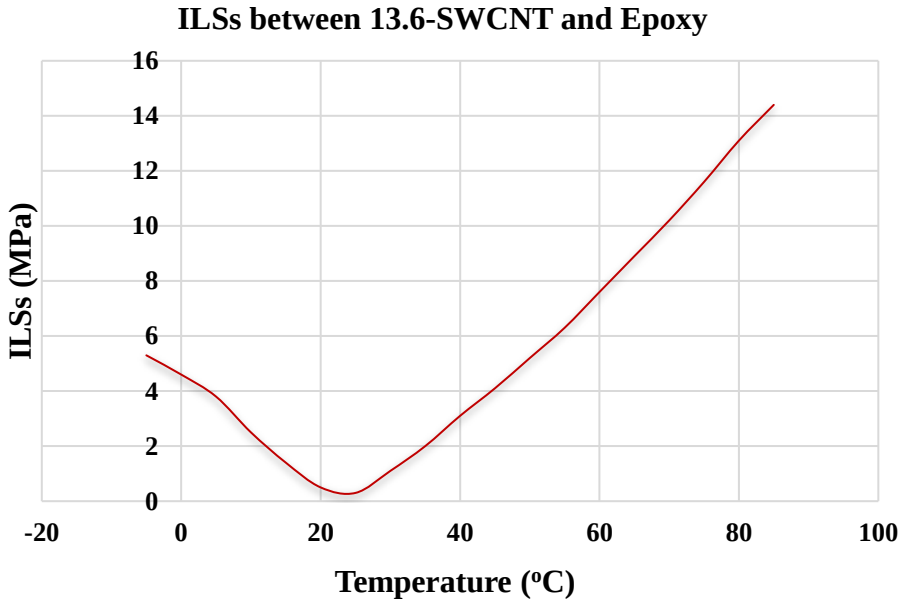


**Figure 2.8:** ILSs within the interface between the 13.6-SWCNT and Epoxy at the temperature range of -5 to 85°C within the 13.6-SWCNTE

In the presented part of the research, by applying analytical method and employing experimental data [67], the effect of SWCNT diameter on ILSs of SWCNTE is investigated. For this purpose, three SWCNTs with three size of diameters were selected; SWCNTs with 1.4, 7, and 13.6 nm diameters. After analyzing the values of ILSs for these Nano-composites with Nano-fibers with different diameters, it has been determined that 1.4-SWCNTE and 13.6-SWCNTE have the highest and lowest ILSs, respectively. It means that due to the less ILSs and consequently, less stress concentration and crack propagation within the 13.6-SWCNTE, ILSS within this Nano-composite can be higher in comparison with the other two Nano-composites. Based on the results obtained by this procedure, it appears that, the larger the diameter of SWCNT, the higher the ILSS and thermal fatigue life becomes.

## 2.6. The Effect of Structural Parameters on the Properties of Zig-zag and Armchair Carbon Nanotubes

Chirality is one of the structural parameters which has the potential to affect on the CNT properties. Within zigzag SWCNT, chiral angle ($\theta$) is equal to zero, while within armchair SWCNT, $\theta$ is equal to $30^o$. If $0^o < \theta < 30^o$, SWCNT is a chiral nanotube. Chirality of CNT can't influence its strain-stress characteristics within the elastic zone, but can influence its characteristics within the plastic zone. The distance between the carbon atoms within the CNT structure is 0.142 nm. Based on the reported results which are obtained from the experiments, zigzag CNT is capable to withstand higher tensile stress along its tube axis when is compared to armchair and chiral CNTs [75].

Zigzag, armchair, and chiral CNTs have about 1.0 TPa Young's modulus. Additionally, the maximum tensile strength of all CNTs are equal to 0.10 TPa. Furthermore, all CNTs can elongate in the axial direction with a strain higher than 0.2 [75].

When SWCNTs are exposed to mechanical loading, the failure mode could be in the form of brittle fracture. Furthermore, while SWCNTs are subjected to high temperatures, their fracture resistance decreases, significantly. Nevertheless, at low temperatures, SWCNTs can fail in the form of brittle fracture. In the case of applying zigzag SWCNT, the chance of failure in the form of brittle fracture at low temperatures is higher. Further analyses have shown that brittle fracture in zigzag SWCNT is the consequence of breaking atomic bonds between the carbon atoms in a short period of time. However, longer nanotubes could exhibit higher fracture resistance when they are compared to shorter tubes [76].

Investigations have shown that structural defects within the CNT could exist in the shape of pentagon-heptagon carbon atoms cell. Additionally, zigzag SWCNTs are inclined to fracture at high strain and low temperatures. Furthermore, zigzag SWCNTs are more likely to fracture under the compressive strain rather the tensile strain. High compressive strain along the zigzag SWCNT axis could cause permanent deformation in the tube axial direction. In cases dealing with compressive fatigue, these permanent deformations could result in significant loss of strength and consequently, buckling along the nanotube structure axis [77].

SWCNT diameter is normally within the range of a few nanometers and its length is typically larger than a micrometer. SWCNTs are identified by employing a chiral vector. The chiral vector contains two integers (n, m) which could describe the SWCNT chirality. For armchair nanotubes, n is equal to m, and for zig-zag nanotubes, m is equal to zero. All other combinations of n and m would describe a chiral SWCNT [78].

Density Functional Theory (DFT) and atomistic approach could be used to calculate the Young's modulus of SWCNTs. SWCNTs are made from carbon atoms which are bonded with hexagonal pattern. In SWCNT structure, each carbon atom is bonded to three carbon atoms [79].

Continuum Mechanics and Molecular Dynamics (MD) numerical approaches could be used to simulate the CNT structure. Non-linear spring modeling could be applied to simulate the C-C bond stretch in CNT structure. CNT geometry represents a frame-like structure in which carbon atoms are connected with covalent bonds.

Covalent bonds between carbon atoms could be simulated as load-bearing beams. CNT structure could determine its Young's modulus value. Shear modulus of CNT would increase with increasing its chiral angel. Furthermore, the increment of chiral angel increases the CNT tensile and bending rigidity [80].

The size of diameter and length of CNT could influence the value of its elastic moduli. The distance between the SWCNTs cylinders within the MWCNT is equal to 0.34 nm. The interaction between the SWCNTs within the MWCNT is through the Vander Waals forces. The main cause of failure in CNTs could be due to buckling under compressive force. The value of Young's modulus along the CNT axis is very high, while this value is low across the CNT radial direction. The diameter of CNT could vary from 1 to 100 nm. CNT is among the good thermal conductors along its axial axis. CNT is stable up to 750$^{o}$C in air and 2800$^{o}$C in vacuum conditions. Due to the high stiffness of CNT, it could be used to make bullet-proof clothing [81].

### 2.6.1. Inter-laminar shear stress as a function of temperature

In the previous sections, it has been proved that ILSs within the SWCNTE interface can change as the temperature changes. At temperatures around the ambient temperature, this variation is low because it can't have an effect on the value of shear modulus and the change is due to the alteration of the temperature and CTEs values of SWCNT and epoxy. These effects are indicated in equation (2.3). However, at extreme low and high temperatures, the influence of temperature on the value of ILSs can be high. The reason is at very high and low temperatures the value of shear modulus could change.

Furthermore, the values of CTEs for both CNT and epoxy can undergo a large amount of alterations. Therefore, a high fluctuation within the value of ILSs can be expected.

According to the results which have been obtained by Kahaly and Waghmare in 2008 [27], the value of CTE for (7, 0) zig-zag SWCNT can increase up to 900% from room temperature to 1800 K. These results can contribute to calculate the ILSs as a function of temperature within the zig-zag SWCNTE interface. The extremely high temperature exists in the propulsion systems and on the exterior surface of spacecrafts during the re-entry to earth. As a result of this thermal analysis [27], the CTE of (7, 0) zig-zag SWCNT in axial direction as a function of temperature ($\alpha(T)_{SWCNT}$), between 0 and 400 Kelvin, can be expressed with the following relation:

For $0\ K \leq T < 400\ K$,

$$\alpha(T)SWCNT = (3.75e-12) * T2 - (1.25e-9) * T, \quad (2.5)$$

Furthermore, the $\alpha(T)_{SWCNT}$ for temperatures between 400 and 1800 Kelvin can be expressed with the following relation:

For $400\ K \leq T \leq 1800\ K$,

$$\alpha(T)SWCNT = (-6.2e-13) * T2 + (2.006e-9) * T - (6.032e-7), \quad (2.6)$$

Consequently, with the substitution of relations (2.5) and (2.6) into the equation (2.3), equations (2.7) and (2.8) for ILSs are developed and shown below. The equations (2.7) and (2.8) can express the ILSs for the temperature range between 0 and 400 Kelvin, and 400 and 1800 Kelvin, respectively.

$$ILSs(T) = G(T)SWCNT.|(T - 296.15)|.|(\alpha(T)epoxy - (3.75e-12) * T2 + (1.25e-9) * T)|, \quad (2.7)$$

$$ILSs(T) = G(T)SWCNT.|(T - 296.15)|.|(\alpha(T)epoxy + (6.2e-13) * T2 - (2.006e-9) * T + (6.032e-7))|, \quad (2.8)$$

As it is indicated in equations (2.7) and (2.8), ILSs is a function of temperature because the huge temperature fluctuation can change the values of CTEs of the (7, 0) zig-zag SWCNT and epoxy. Furthermore, with the large alteration in the temperature, the value of SWCNT shear modulus, $G(T)_{SWCNT}$, would change. Therefore, all the parameters in the equations (2.7) and (2.8) are temperature dependent. Please note that the temperature T in equations (2.7) and (2.8) is according to the Kelvin unit, and the temperature 296.15 in equations (2.7) and (2.8), is the ambient temperature based on the Kelvin unit. Additionally, $\alpha(T)_{epoxy}$, is the epoxy CTE as a function of temperature.

# Chapter 3

## Experimental Procedures

In this section of the thesis all of the experimental procedures from the carbon nanotube reinforced epoxy fabrication to tension and shear tests have been included and explained.

### 3.1. CNT - epoxy composite fabrication and exposure to thermal cycling

MWCNTs has been provided from the "US Research Nanomaterials, Inc." The outer diameter of the purchased MWCNTs have been 20 – 30 nm. The SWCNTs have been provided from the OCSiAl company. The outer dimeter of the purchased SWCNTs have been 2 nm. Furthermore, the epoxy 2020 has been provided from the Fibreglast company.

For fabricating CNT - epoxy, the first step would be to take 200 grams epoxy in beaker and put in vacuum for 2 minutes. The second step would be to add 0.5, 1 and 1.5 wt.% of MWCNT or SWCNT to epoxy with mixing them into the epoxy with glass rod. The third step would be to use ultrasonicator to disperse the MWCNT or SWCNT into the epoxy, uniformly. The ultrasonicator equipment which has been used to mix the CNTs with epoxy, is shown in Figure 3.1.

After the CNT - epoxy mixture is provided either with SWCNT or MWCNT followed by the procedure mentioned, it's time to pour the mixture into a mold and let it cure with "60 - minute epoxy cure" at 90$^{o}$F for 22 hours. The dimensions of the aluminum mold are 10 * 10 * 1/8 inches. After the CNT - epoxy nanocomposite is fabricated, it's time to expose it to thermal cycling. Thermal cycling which is going to be applied in this experiment would be from room temperature

(25$^{o}$C) to 0.85$T_g$ of the epoxy (65$^{o}$C). The glass transition temperature has been determined by applying the Differential Scanning Calorimetry (DSC) Experiment.

Thermal cycles would be repeated for 3000 times. After the SWCNT - epoxy and MWCNT - epoxy samples have been exposed to these thermal cycles, tensile strength of the exposed sample has been measured by applying tensile tests and is compared to the strength of the sample before 3000 thermal cycles. The results will help to evaluate the strength degradation percentage of the CNT - epoxy after being exposed to 3000 thermal cycles. In the Figure 3.2, control section of the oven which has been used to cure the Nano – composite plates and conduct the thermal cycling experiment, is shown.

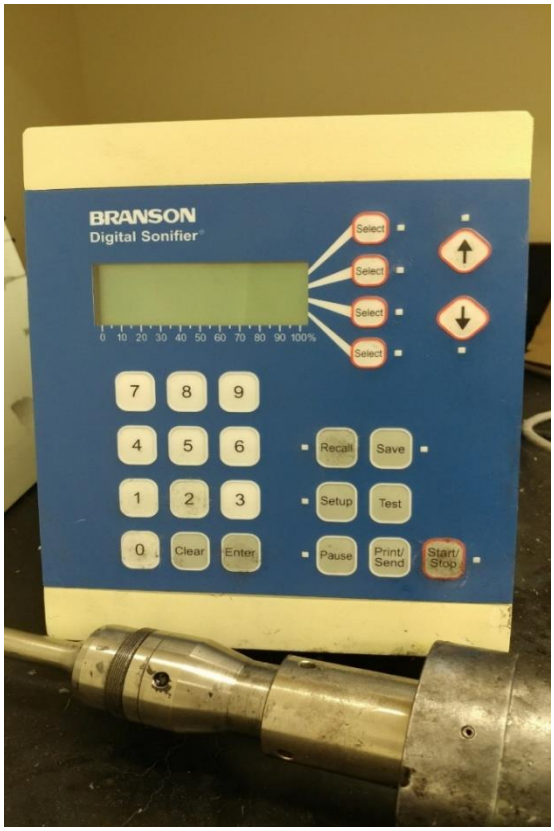


**Figure 3.1:** Ultrasonicator equipment which has been used to mix the CNTs with epoxy

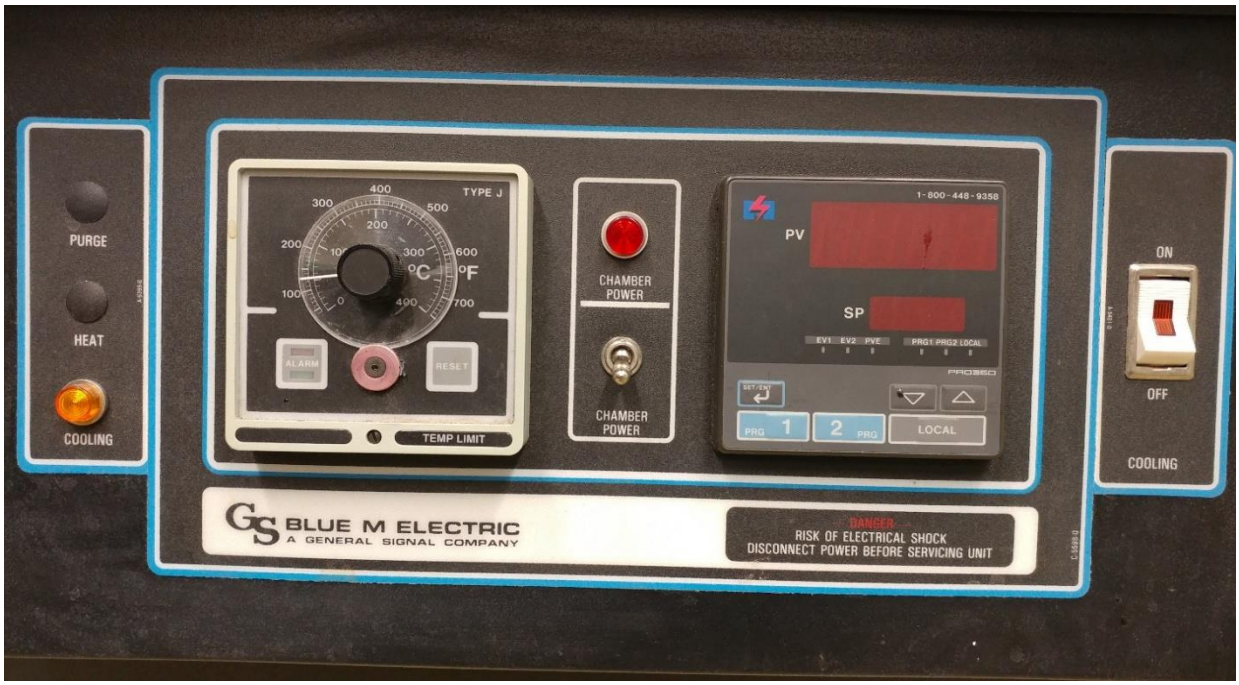


**Figure 3.2:** The control section of the oven which has been used to cure the Nano – composite plates and conduct the thermal cycling experiment

### 3.2.Short-Beam Test

ASTM #D2344 or three-point bending test of a high modulus fiber matrix composites is applied to estimate the Interlaminar shear strength (ILSS) of fiber-matrix composites. Interlaminar shear strength can be used to control the quality or to compare the shear strength of different composite materials.

### 3.2.1. Experimental procedures

At least five specimens per test condition should be tested. Test at standard laboratory atmosphere (23 ± 3° C (73 ± 5° F) and 50 ± 10% relative humidity). This test is conducted by centering the composite sample symmetrically over the fixture of the support which is loaded in with either an electromechanical or servo-hydraulic testing equipment. The applied load to the sample will continue at mid-span of the specimen until the sample fails into two parts or the applying load drops down 30% or the loading grip shift exceeds the sample thickness. The loading grip which is applied to deform the sample operates at a 0.05 inches/minute or 1.0 mm/min constant velocity until the breakage occurs. The specimen which is used in this test should be flat. The shear strength will be defined as 75% of the breaking load.

This experiment method indicates the short-beam strength of fiber reinforced composite materials. Sample is a short beam machined obtained from a flat or curved laminate up to 6 mm thick. The beam has been loaded in three-point bending tests according to ASTM # D2344 [83].

Application of this experiment method is restricted to discontinuous or continuous-fiber-reinforced epoxy composites, because the elastic properties have been balanced and symmetric with respect to the beam longitudinal axis [83].

The short-beam experiment samples are center loaded as shown in Figures 3.3 and 3.4. The samples ends are placed on two supports which allow lateral movement, the load being used by means of a loading instrument centered on the midpoint of the experiment sample [83].

In Figures 3.3 and 3.4, the specimen dimensions are shown in SI and Inch-Pound unites, respectively. Furthermore, in Figure 3.5, the horizontal shear load diagram has been illustrated. Finally, in Figure 3.6, failure modes in the short-beam test has been shown.

### 3.2.2. Data analysis

Short-beam strength can be calculated using the following equation [83]

$$F = \frac{0.75P}{b*h} \quad (3.1)$$

F = Short-beam strength, MPa (psi);

P = maximum load observed during the test, N (lbf);

b = measured specimen width, mm (in.), and

h = measured specimen thickness, mm (in.).

For each series of test methods, calculate the average value, standard deviation, and coefficient of variation (in percent) for each property determined as follows:

$$\bar{x} = (\sum_{i=1}^{n} x_i)/n \quad (3.2)$$

$$s_{n-1} = \sqrt{(\sum_{i=1}^{n} x_i^2 - n(\bar{x})^2)/(n-1)} \quad (3.3)$$

$$CV = 100 \times s_{n-1}/\bar{x} \quad (3.4)$$

Where:

$\bar{x}$ = Sample mean (average);

$S_{n-1}$ = Sample standard deviation;

CV = Sample coefficient of variation, %;

n = number of specimens; and

$x_i$ = measured or derived property.

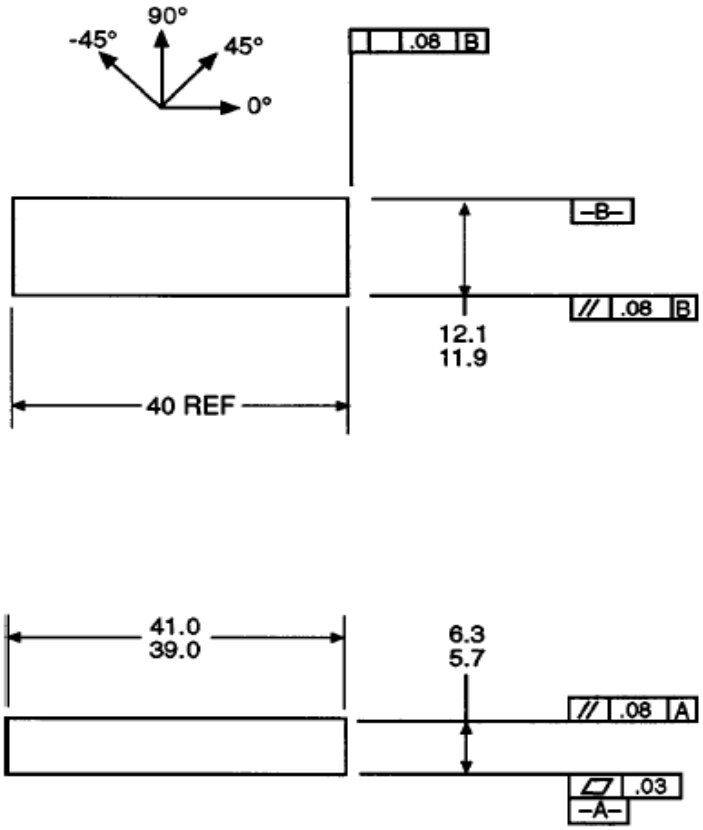


NOTE 1—Drawing interpretation per ANSI Y14.5-1982 and ANSI/ ASM B46.1-1986.
NOTE 2—Ply orientation tolerance ±0.5° relative to –B–.

**Figure 3.3:** Flat Specimen Configuration (SI) [83]

### 3.2.3. Specimen dimensions

Notation numbers at the right of the figure is the number allowed for the specimen to have misalignment between the two parallel edges of the sample. As an instance, 0.08 mm indicates that misalignment between the two parallel edges of the sample should be less than 0.08 mm. These numbers can be defined as tolerances [1]. In Figure 2, these numbers are defined in Inch Pound unit. Specimen dimensions should be 40*12 mm and the thickness could be up to 6 mm. Furthermore, it is recommended that [83]:

Specimen length = thickness * 6

Specimen width, b = thickness * 2

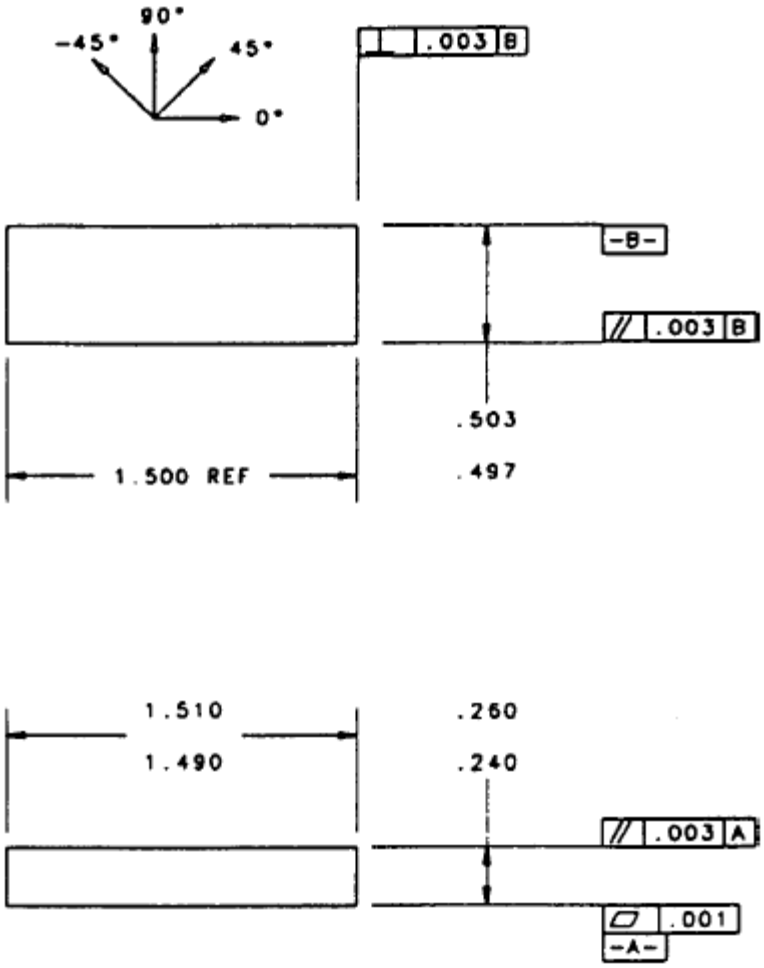


NOTE 1—Drawing interpretation per ANSI Y14.5-1982 and ANSI/ ASME B46.1-1986.

NOTE 2—Ply orientation tolerance ±0.5° relative to –B–.

**Figure 3.4:** Flat Specimen Configuration (Inch Pound) [83]

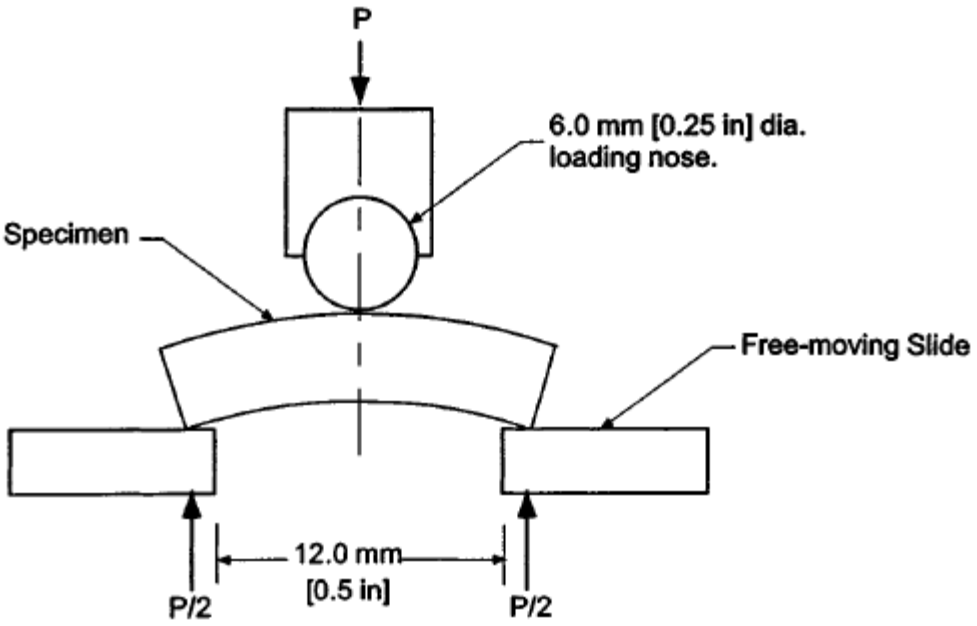


FIG. 5 Horizontal Shear Load Diagram (Curved Beam)

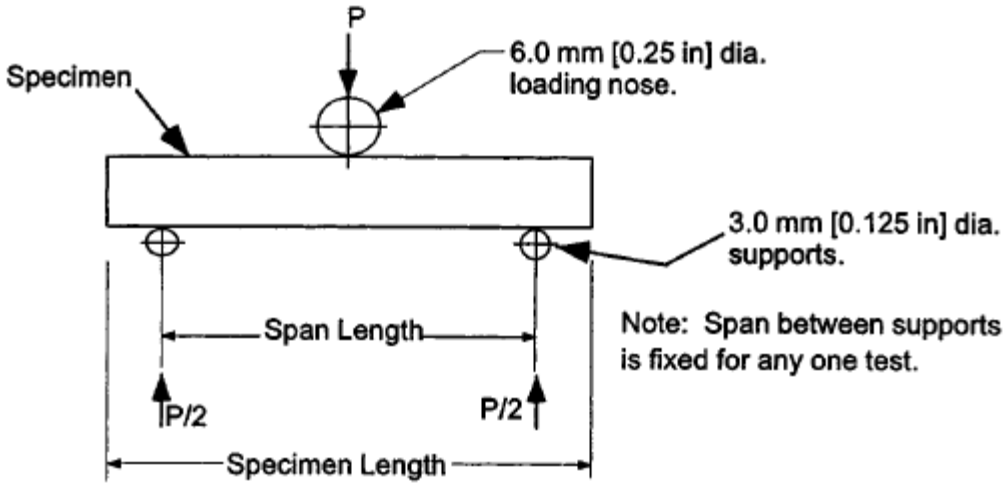


**Figure 3.5:** Horizontal Shear Load Diagram (Flat Laminate) [83]

1. Interlaminar Shear

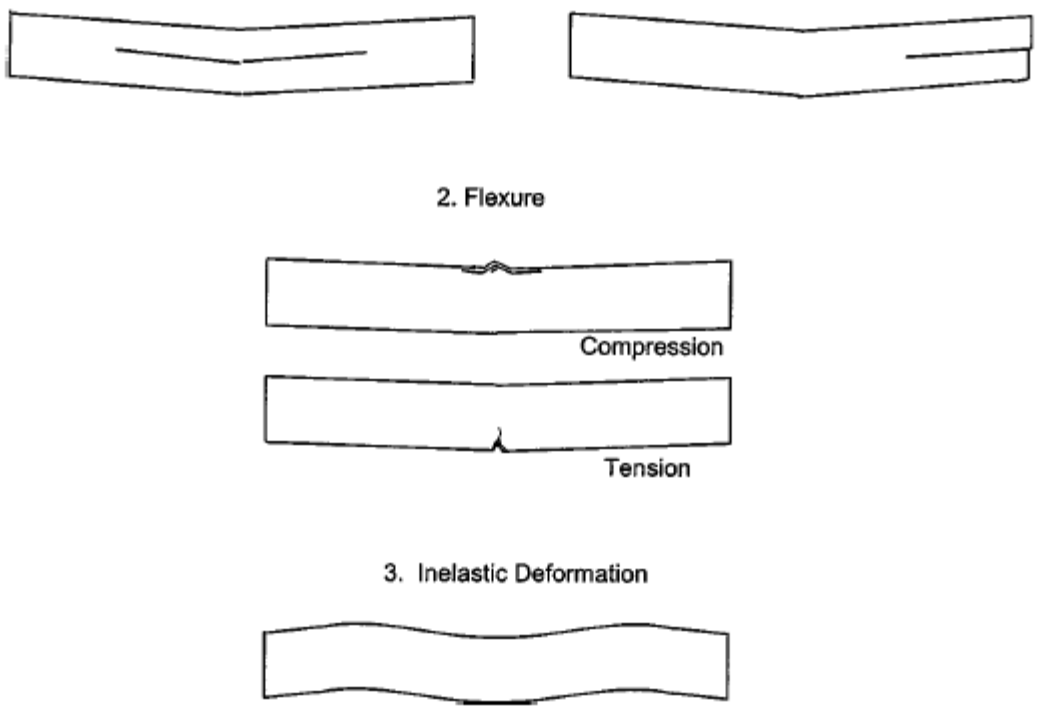


**Figure 3.6:** Typical Failure Modes in the Short Beam Test [83]

In the Figure 3.6, the failure modes of composite after being loaded with short-beam test have been illustrated. In part 1 of Figure 3.6, the failure occurs at the interface of laminates. It means that the interface area which is located between the composite laminates has the lowest strength. In part 2, the failure occurs in the matrix region at the exterior sides due to compression and tension at these zones. It means that the matrix has less strength when compares to the fiber's strength. In part 3, failure is related to the inelastic deformation which occurs within the whole specimen [83]. In Figures 3.7, 3.8, and 3.9, the ILSS specimen dimension, the ILSS testing fixture, and ILSS testing machine are shown, respectively.

**Figure 3.7:** ILSS specimen dimension

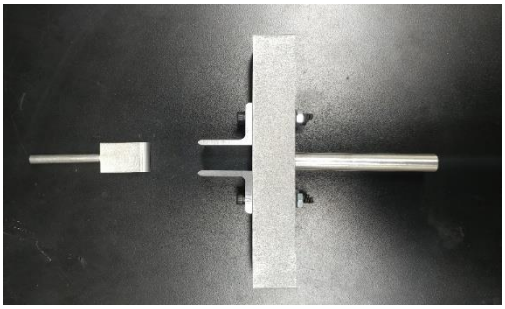

**Figure 3.8:** ILSS testing fixture


**Figure 3.9:** ILSS testing machine

### 3.2.4. Fracture surfaces analysis

In the following Figure [84], the fracture mechanism of pristine (unfunctionalized) CNTs-epoxy which is being exposed to shear beam test is illustrated. For taking these photographs in Figure 3.10 [84], SEM and optical imaging techniques have been applied. With the investigation of Figure 3.10, it can be observed that the failure occurs within the CNTs-epoxy interface area with the propagation of transverse cracks and delamination phenomenon. This kind of failure is called interlaminar failure and it occurs by CNTs ropes bridging mechanism [84].

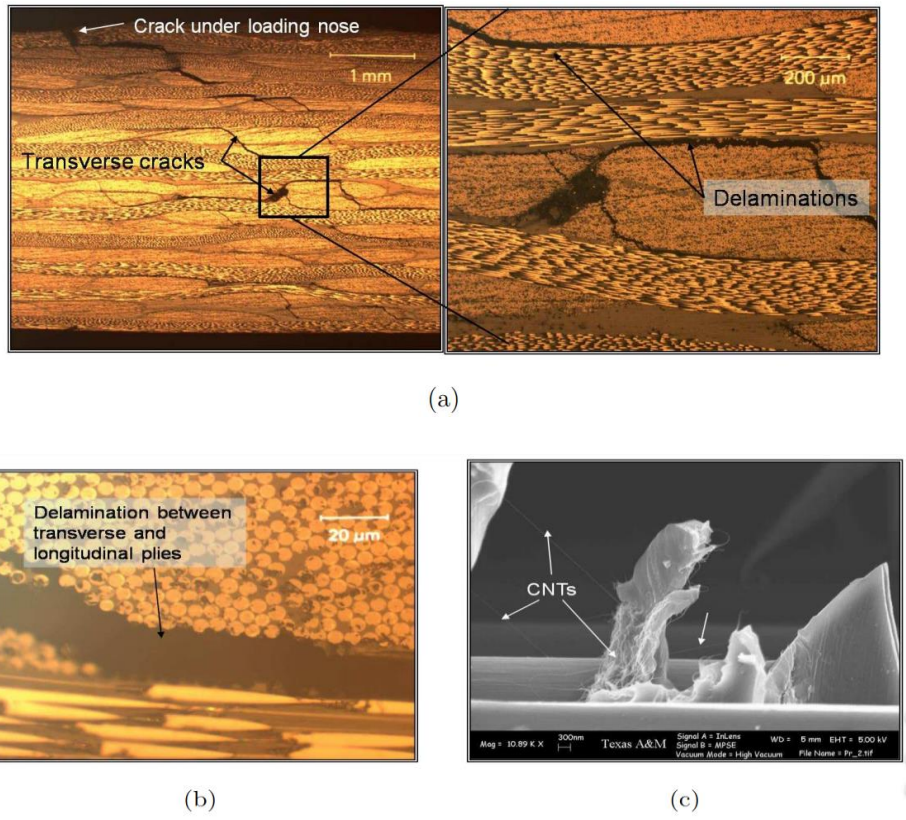


**Figure 3.10:** Optical and SEM of Short Beam Test specimen by pristine CNTs. (a) Specimen edge showing all the laminae and failure mechanisms. Mid-plane illustrates transverse cracking and

delamination process. (b) Zoomed-in image illustrates transverse crack causing the interlaminar failure. (c) SEM image of delamination plane shows CNTs ropes bridging mechanism [84]

### 3.3.Tensile test

The other name of tensile testing is tension testing which is a basic engineering and materials science. In this test, the specimen is subjected to tension stress until it fails under the ultimate tensile stress. Many properties can be measured via the application of tensile testing such as breaking length, ultimate tensile strength, reduction in area and maximum elongation. After these properties have been measured with the application of tensile testing, other properties such as yield strength, Young's modulus, and Poisson's ratio may also be obtained. The most applicable tensile testing for measuring the isotropic materials mechanical characteristics is the uniaxial tensile testing. However, for some of the materials biaxial tensile testing should be used. In the following Figure, tensile testing machine is shown.


**Figure 3.11:** Tensile Testing Machine

Tensile tests may be performed for several reasons. Result of this test could be applied in selecting materials for variety of applications. Tensile properties mainly are included in material characteristics to ensure appropriate material's qualification. These properties often can be measured within making of new processes and materials, so that variety of processes and materials may be compared. Ultimately, tensile characteristics often can be used to estimate the material behavior under loading [85].

Consider the normal tensile sample shown in Figure 3.12. It includes enlarged ends or shoulders for gripping. Important section of the sample is the gage part. The cross-sectional surface of the gage part is decreased relative to that of the remainder of the sample hence that deflection and failure can be localized in that area. Gage length is the part over which evaluations have been made and is centered within the decreased part. Distances between the ends of the gage section and the shoulders should be wide enough so that the larger ends do not impede deflection within the gage part, and the gage length should be wide relative to its diameter. Otherwise, the stress state can be more complicated than the simple tension [85]. However, the loading may continue until the fracture occurs and a stress-strain curve could be developed.

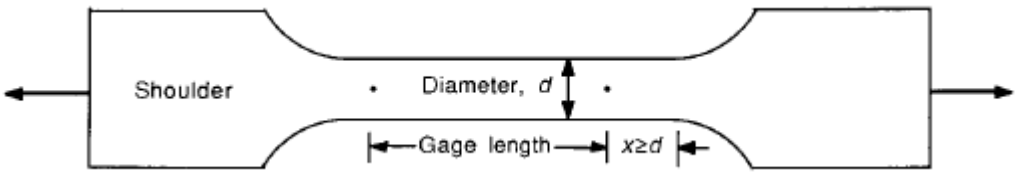


**Figure 3.12:** Typical tensile specimen, showing a reduced gage section and enlarged shoulders. To avoid end effects from the shoulders, the length of the transition region should be at least as great as the diameter, and the total length of the reduced section should be at least four times the diameter [85]

Calculating the stress and strain in tensile test is simple. For these purposes, the following relations could be used [85].

$$S = F/A \quad (3.5)$$

S = Stress in MPa or psi

F = Force in N or Ib

A = Sample's cross-sectional area in $m^2$ or $in^2$

For measuring the strain, the following equation can be used.

$$\varepsilon = \frac{\Delta l}{l} \quad (3.6)$$

ε = Strain is specimen

Δl = Change in specimen's length

L = Initial specimen's length

### 3.3.1. Experimental procedures

At least five specimens per test condition should be tested. Test at standard laboratory atmosphere (23 ± 3° C (73 ± 5° F) and 50 ± 10% relative humidity). A flat piece of nanocomposite material having a determined rectangular cross section should be placed in the grips which is attached to a testing machine and constantly loaded in tension when recording load. The final strength of the nanocomposite material could be specified from the highest load imposed before fracture. If the strain is recorded with displacement or strain transducers, then the figure of stress-strain curve of the nanocomposite material could be specified, from where the final tensile modulus, tensile strain of elasticity, transition strain, and Poisson's ratio could be derived [85].

In this test, strain rate should be selected to induce fracture within 1 to 10 min. The standard strain rate of 0.01 $min^{-1}$ should be applied to the specimen. Furthermore, a standard head displacement rate of 2 mm/min (0.05 in./min) is required [85].

### 3.3.2. Required data

This approach is designed to introduce tensile property data for nanocomposite material characteristics, quality assurance, structural design and analysis, and research and development. Parameters that affect the tensile test and should hence be reported involves the following: nanomaterial, methods of nanocomposite material production and lay-up, sample stacking sequence, sample preparation, sample conditioning, test environment, sample gripping and alignment, test speed, void content, time at temperature, and percentage of volume reinforcement. Properties, which could be obtained from this test procedure involve the following [85]:

1. Ultimate tensile strength,
2. Ultimate tensile strain,
3. Tensile chord modulus of elasticity,
4. Poisson's ratio, and
5. Transition strain.

### 3.3.3. Specimen dimensions

In the following Table, the specimen dimensions for the tensile testing is indicated. Since, in this experiment, CNT Reinforced epoxy is tested, the balanced and symmetric geometry should be chosen because the specimen is homogeneous.

The reason is, within the preparation process of the CNT Reinforced epoxy, mechanical and ultrasonication mixers have been applied to spread the CNT particles within the specimen, uniformly. Therefore, it is expected that the specimen would be balanced and symmetric [85].

**Table 3.1:** The specimen dimensions for the tensile test according to the ASTM D 3039 [85]

| Fiber Orientation | Width, mm [in.] | Overall Length, mm [in.] | Thickness, mm [in.] | Tab Length, mm [in.] | Tab Thickness, mm [in.] | Tab Bevel Angle,° |
|---|---|---|---|---|---|---|
| 0° unidirectional | 15 [0.5] | 250 [10.0] | 1.0 [0.040] | 56 [2.25] | 1.5 [0.062] | 7 or 90 |
| 90° unidirectional | 25 [1.0] | 175 [ 7.0] | 2.0 [0.080] | 25 [1.0] | 1.5 [0.062] | 90 |
| balanced and symmetric | 25 [1.0] | 250 [10.0] | 2.5 [0.100] | emery cloth | — | — |
| random-discontinuous | 25 [1.0] | 250 [10.0] | 2.5 [0.100] | emery cloth | — | — |

### 3.3.4. Data analysis

For each series of test methods, calculate the average value, standard deviation, and coefficient of variation (in percent) for each property determined as follows [85]:

$$\bar{x} = (\sum_{i-1}^{n} x_i)/n \tag{3.7}$$

$$s_{n-1} = \sqrt{(\sum_{i=1}^{n} x_i^2 - n(\bar{x})^2)/(n-1)} \tag{3.8}$$

$$CV = 100 \times s_{n-1}/\bar{x} \tag{3.9}$$

Where:

$\bar{x}$ = sample mean (average);

$S_{n-1}$ = sample standard deviation;

CV = sample coefficient of variation, %;

n = number of specimens; and

$x_i$ = measured or derived property.

derive the ultimate tensile strength applying Eq 3.10 and report the results to three significant figures. If the tensile modulus is to be calculated, determine the tensile stress at each required data point using Eq 3.11 [85]

$$F^{tu} = P^{max}/A \tag{3.10}$$

$$\sigma_i = P_i/A \tag{3.11}$$

where:

$F^{tu}$ = ultimate tensile strength, MPa [psi];

$P^{max}$ = maximum load before failure, N [lbf];

σi = tensile stress at *i*th data point, MPa [psi];

$P_i$ = load at *i*th data point, N [lbf]; and

*A* = average cross-sectional area, $mm^2$

If tensile modulus or ultimate tensile strain is to be calculated, and nanomaterial response is being specified by an extensometer, calculate the tensile strain from the presented displacement at each needed data point applying Eq 3.12 and report the results to three significant figures [85].

$$\epsilon_i = \delta_i / L_g \tag{3.12}$$

where:

$\epsilon_i$ = tensile strain at *i*th data point, με;

$\delta i$ = extensometer displacement at *i*th data point, mm [in.];

and

$L_g$ = extensometer gage length, mm [in.].

The tabulated strain ranges should just be applied for nanomaterials that do not exhibit a transition region (a significant change in the slope of the stress-strain curve) within the given strain range. If a transition zone happens within the suggested strain range, then a higher suitable strain range shall be employed and reported [85].

$$E^{\text{chord}} = \Delta\sigma / \Delta\epsilon \tag{3.13}$$

where:

$E^{\text{chord}}$ = tensile chord modulus of elasticity, GPa [psi];

$\Delta\sigma$ = difference in applied tensile stress between the

two strain points of Table 3.2, MPa [psi]; and

$\Delta\epsilon$ = difference between the two strain points

(nominally 0.002).

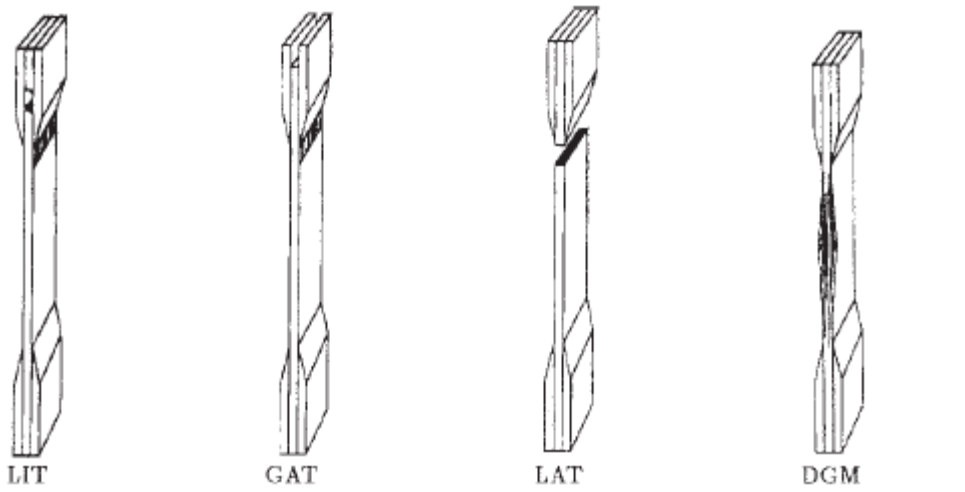


First Character

| Failure Type | Code |
|---|---|
| Angled | A |
| edge Delamination | D |
| Grip/tab | G |
| Lateral | L |
| Multi-mode | M(xyz) |
| long. Splitting | S |
| eXplosive | X |
| Other | O |

Second Character

| Failure Area | Code |
|---|---|
| Inside grip/tab | I |
| At grip/tab | A |
| <1W from grip/tab | W |
| Gage | G |
| Multiple areas | M |
| Various | V |
| Unknown | U |

Third Character

| Failure Location | Code |
|---|---|
| Bottom | B |
| Top | T |
| Left | L |
| Right | R |
| Middle | M |
| Various | V |
| Unknown | U |

**Figure 3.13:** Tensile Test Failure Codes/Typical Modes [85]

**Table 3.2:** Specimen Alignment and Chord Modulus Calculation Strain Ranges [85]

| Tensile Chord Modulus Calculation Longitudinal Strain Range | | Longitudinal Strain Checkpoint for Bending |
|---|---|---|
| Start Point με[A] | End Point με | με |
| 1000[B] | 3000 | 2000 |

[A] 1000 με = 0.001 absolute strain.
[B] This strain range is to be contained in the lower half of the stress/strain curve. For materials that fail below 6000 με, a strain range of 25 to 50 % of ultimate is recommended.

Choose the suitable chord modulus longitudinal strain range from Table 3.2. Calculate (by plotting or otherwise) the transverse strain (measured perpendicular to the used load), $\varepsilon_t$, at each of the two longitudinal strains (measured parallel to the applied load), $\varepsilon_l$, strain range end points. If data is not available at the exact strain range end points (as often happens with digital data), apply the closest data point. Determine Poisson's ratio by Eq 3.14 and report to three significant figures. Furthermore, report the strain range applied.

$$\nu = -\Delta\epsilon_t/\Delta\epsilon_l \tag{3.14}$$

where:

$\nu$ = Poisson's ratio;

$\Delta\varepsilon_t$ = difference in lateral strain between the two longitudinal strain points of Table 3.2, με; and

$\Delta\varepsilon_l$ = difference between the two longitudinal strain points

of Table 2 (nominally either 0.001, 0.002, or 0.005).

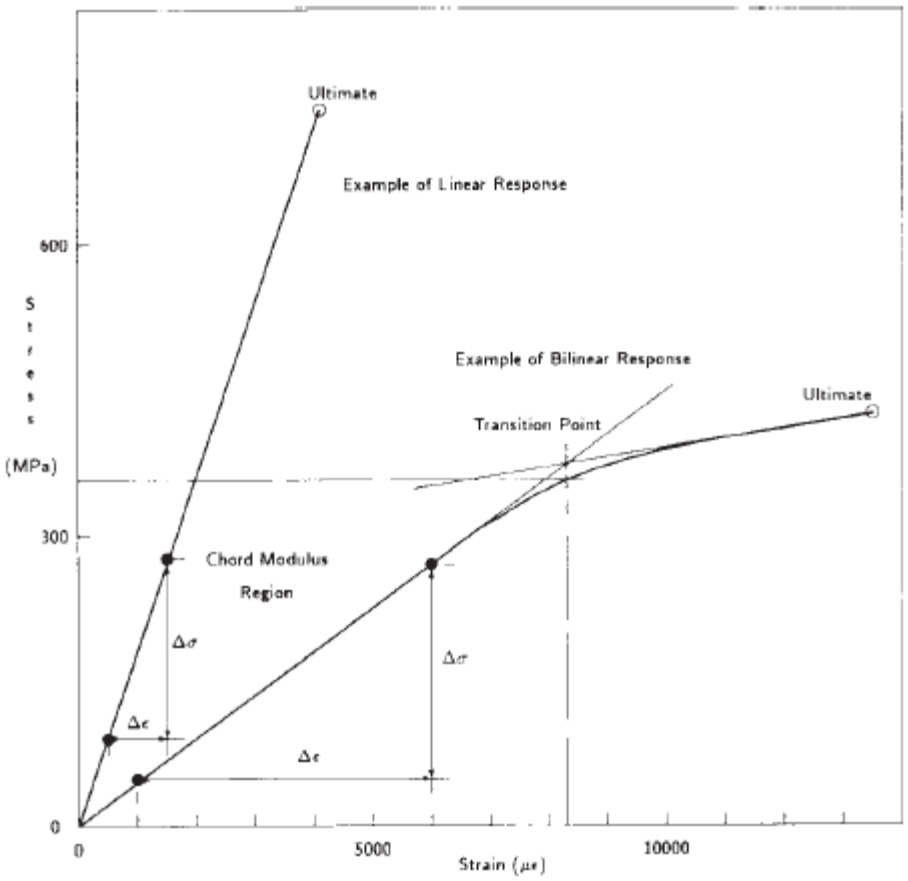


**Figure 3.14:** Typical Tensile Stress-Strain Curves [85]

Nevertheless, due to the homogeneity of CNT-epoxy in this experiment, the following dog – bone specimen dimensions for the tension – test, have been used. This geometry has been selected based on the ASTM D638 – 14 [86].

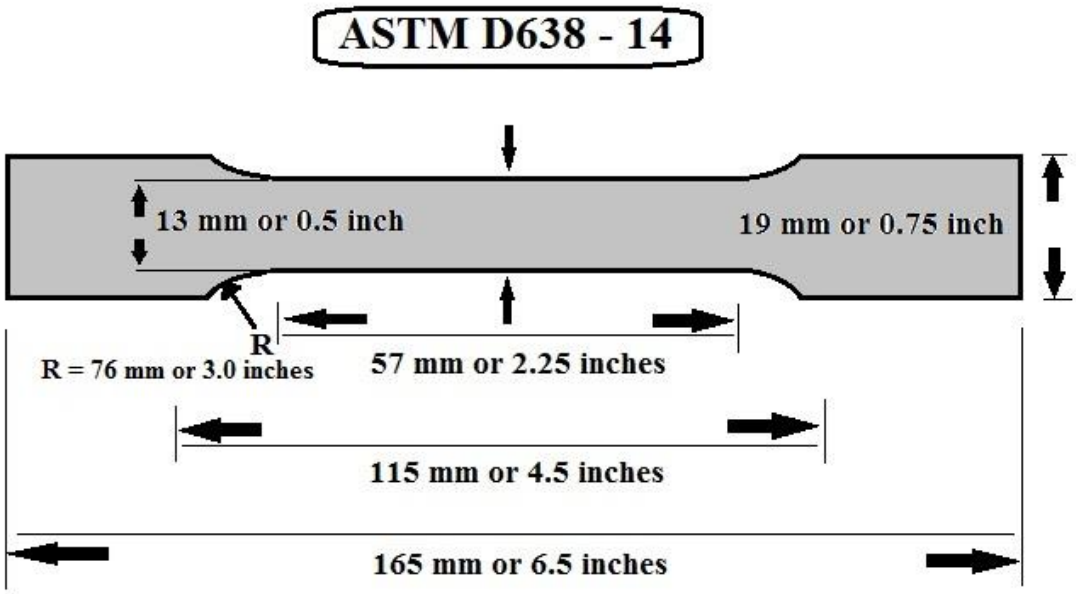


**Figure 3.15:** Geometry and Dimensions of the Dog – Bone Specimens which has been used in Tension – Test based on the ASTM D638 – 14 [86]

In the Figure 3.16, the real dog – bone specimens which have been fabricated for the tension test, are shown.

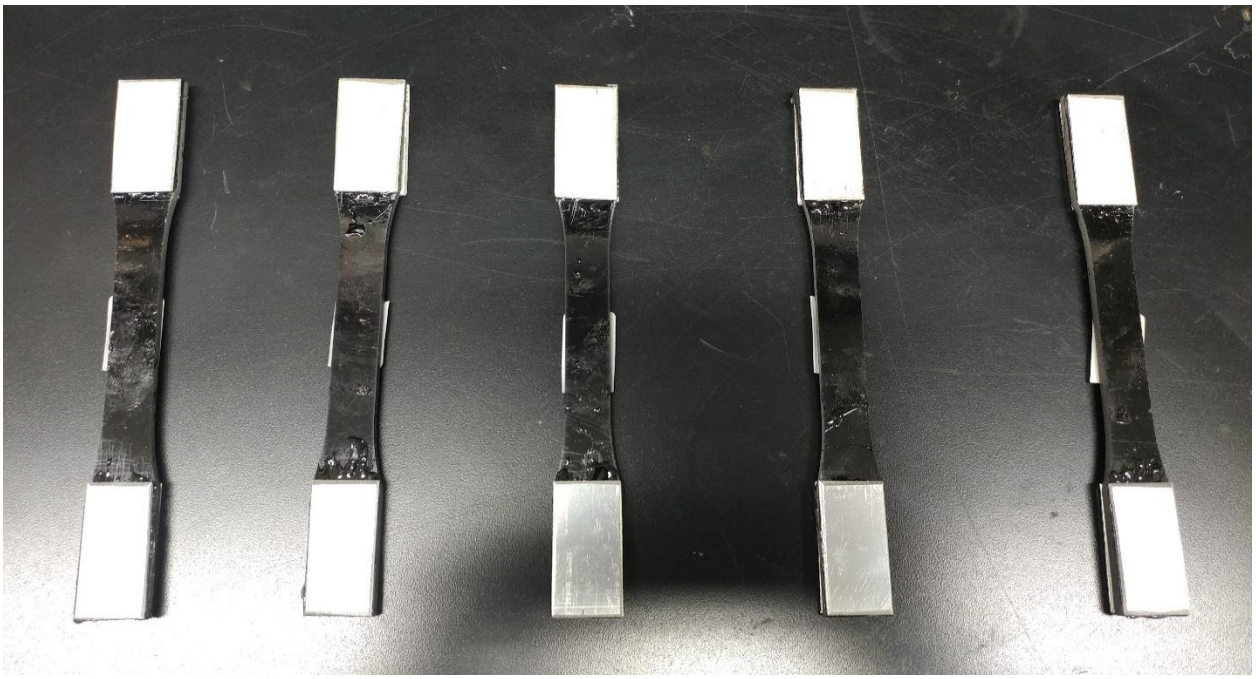

**Figure 3.16:** Dog – bone specimens which have been fabricated for the tension test in this experiment

### 3.4. Previous study on carbon fiber reinforced epoxy composite subjected to thermal cycling

This section focuses to explain about the similar experiment which has been done for property evaluations of composites after being exposed to thermal cycles. For evidence of the morphological alterations in composite materials, planar and cross-sectional images of the specimens were captured by applying a S-2400 scanning electron microscope (SEM) equipment (Hitachi High-Technologies Co., Japan). The layers' densities ($g/cm^3$) were investigated before and after thermal fatigue cycling exposures based on the ASTM. The amount of volume percentage for fiber ($V_f$) and void ($V_v$) in every composite material were evaluated by weighing a 25 $cm^2$ square of layer specimen and by solution of the epoxy matrix in 70 wt.% nitric acid, according to the ASTM standards of D 3171 and D 2734, respectively. Furthermore, the glass transition.

temperature mentioned as Tg was evaluated by differential scanning calorimetry (DSC) applying a DSC 50 equipment (Shimazdu Co., Japan) according to the ASTM E 1269 standard. The Tg temperature is a significant material property, determined as the individual temperature at which a material's characteristics are drastically altered. For DSC tests, the glass transition temperature is determined as an alteration in the heat capacity as epoxy of matrix is transferred from a glassy hard state to a rubbery soft state [21].

The alterations in the mechanical characteristics of composite layers subjected to thermal fatigue cycling environment condition were evaluated based on the suitable ASTM standards: (1)

Inter-laminar shear strength (ILSS, ASTM D 2344), (2) flexure strength/modulus (ASTM D 790 procedure A and B), (3) longitudinal tensile strength/modulus (ASTM D 3039) and (4) longitudinal compressive strength/modulus (ASTD D 3410).

All of the mechanical experiments were performed with a servo-hydraulic 100 kN MTS 810 experimental machine (MTS Systems Co., USA) at a constant displacement rate up to the ultimate failure. The specimen dimensions and their standards are illustrated in Figure 3.17. A minimum of eighteen specimen were prepared at every environmental condition (i.e., thermal cycles) to convenient statistically samplings [21].

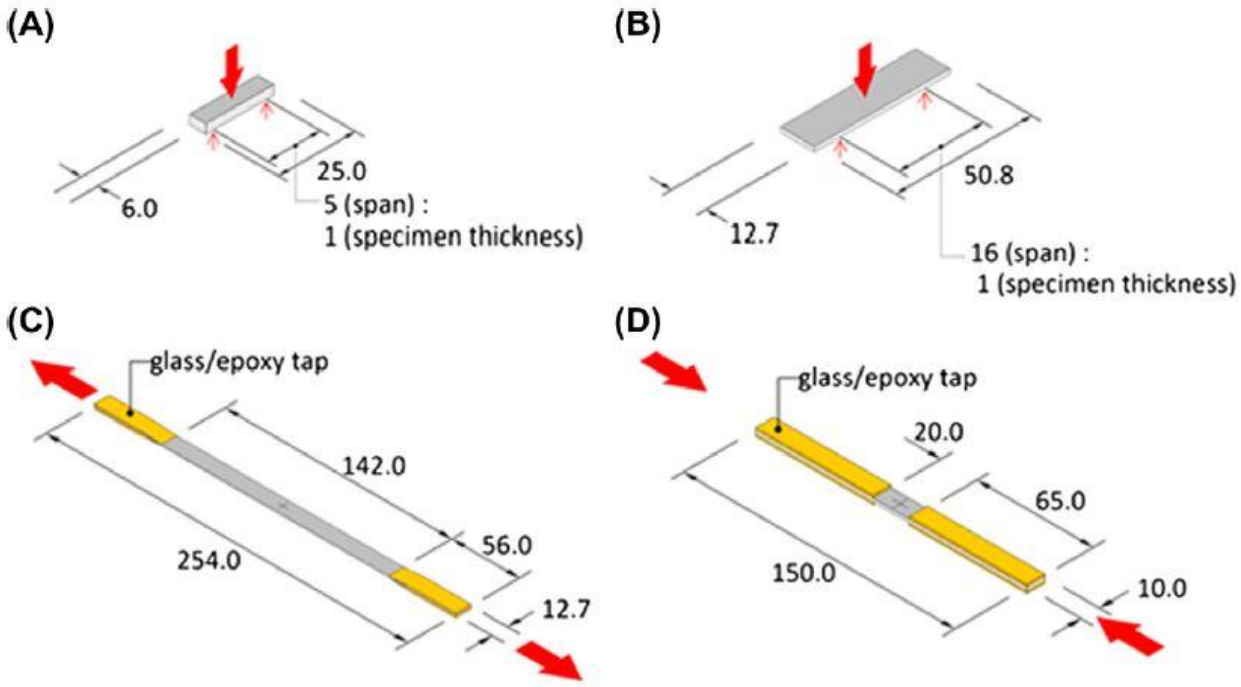


**Figure 3.17:** Specimen dimensions (units: mm) used for static mechanical experiments: (A) ILSS, ASTM D 2344; (B) flexure strength/modulus, ASTM D 790; (C) longitudinal tensile strength/modulus, ASTM D 3039; and (D) longitudinal compressive strength/modulus, ASTM D 3410 [21]

In Figure 3.17, mechanical properties evaluation tests on samples have been illustrated. However, in our thesis experiments only the short-beam tests and tensile tests will be conducted.

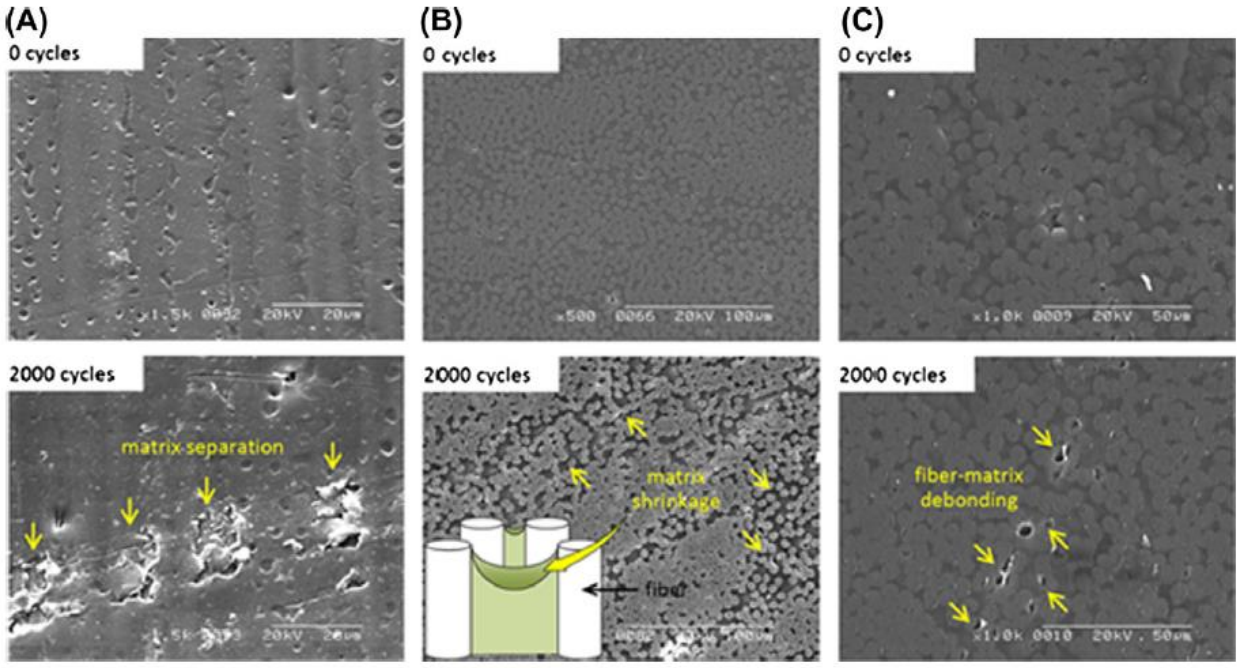


**Figure 3.18:** Electron micrographs illustrating different kinds of damage in states before and after thermal fatigue cycling: (A) composite laminate surface at 1500 × magnification illustrating matrix separation; (B) a cross-sectional image at 500 × magnification illustrating matrix shrinkage; and (C) a cross-sectional image at 1000 × magnification illustrating fiber–epoxy of matrix de-bonding [21]

As it is illustrated in Figure 3.18, electron micrographs showing different kinds of damage in states before and after thermal cycling exposure for UCFEC is indicated. The same process can be performed for CNT-epoxy showing different kinds of damage before and after being exposed to thermal cycling exposure.

### 3.4.1. Inter-laminar shear strength and flexure strength/modulus

Flexure and ILSS characteristics have been basically defined for quality control operation and material characterization, where comparative rather than absolute amounts is needed. The ILSS numerical values for specimens subjected to cyclic vacuum thermal fatigue conditions were explicitly lower than those derived from the baseline, also the corresponding reduction in the presented rates right after 2000 cycles were 14.7% for M40 J composite and 12.2% for M60 J material. In contrast, the alteration in the M55 J composite was normal at 5.8%. The most occurred failure state observed was inter-laminar yielding fracture, although many specimens corresponded nearly to the local deterioration state such as cross-ply cracking (i.e., flexure compression and flexure tension) [5]. The mentioned data explained about the thermal cycling effect on UCFEC which is similar of what is going to be done in this research. The following paragraphs also explain about the effect of thermal cycling on mechanical properties of UCFEC.

For the flexure characteristics, severe deterioration in the flexure strength was also reported due to the aging influence. It is important to mention that the flexure strength represents the numerical value of the stress at fracture on the specimen surface, and its failure state is commonly obtained by the rupture of fibers rather than inter-laminar shear. Hence, it is very less sensitive to the environmental condition than the ILSS. For the material of M55 J composite, it was reported that little strengthening was obtained in the closely stage of fatigue cycling: the statistical strength ranges available overlap. The researches by Gao et al. and Papanicolaou et al. observed that higher cross-linking in the epoxy of matrix, which was produced by some additional chemical reaction materials among unreacted groups, enhanced the flexure tolerance in the early mode of fatigue cycling.

Moreover, a comparison between the flexure tolerance and the DSC outputs cannot be enough due to the Tg of the M55 J composite was obtained to reduce significantly. With Comparing among different composite materials showed that the reduction in the flexure tolerance at 2000 cycles was 10.1% (M40 J), 13.3% (M55 J) and 0.8% (M60 J). It seems it is due to the failure state of flexure specimens that many failures of M40 J and M55 J composites presented inter-laminar shear fracture or ply-level buckling that was initiated by delamination in the outer lamina. On the other hands, M60 J composites exhibited that the sample failure happens on both sides of its exterior surfaces (i.e., fiber micro-buckling). The decrease for the flexure modulus happened in the following arrangement after 2000 thermal cycles: 22.1% (M40 J) > 13.8% (M60 J) > 0.4% (M55 J) [21].

### 3.4.2. Longitudinal tensile strength/modulus

The tensile characteristics of composite materials are basically thought to be independent to the environment due to the carbon fibers' inertness. Adverse environments, furthermore, could affect the epoxy matrix and the region of fiber/matrix interface, that directly help to the tensile tolerance and fracture toughness [21].

The longitudinal tensile tolerance showed an intermediate reduction ranging from 6.7% to 11.1%, whereas the reduction of the amount for tensile modulus happened gradually due to the normalized reduction fell between 1.8% and 6.9%. With comparing different composites, the largest reduction in the tolerance and for the modulus were observed for M60 J layers. This might be due to the large value for the tensile modulus (588 GPa) of the M60 J carbon fiber itself, that is along with an enhancement in the crystallinity and orientation for the crystallographic planes are parallel with the fiber length, as shown in Figure 3.19A.

An approximately linear relationship exists between the CTE and fiber modulus, and with the increase in longitudinal modulus of the carbon fibers, the axial CTE decreases. The incompatibility between the largest modulus M60 J fiber with the smallest CTE (most negative) may result in further extreme behavior within transient thermal loads due to the increased mismatch between the CTEs in the composite material constituents [21].

In Figure 3.19, UCFEC is illustrated. The difference between UCFEC and CNT-epoxy is the diameter size of carbon fiber which is in the range of micrometers and the diameter size of CNT which is in the range of nanometers. On the other hand, in this research CNTs orientation within the epoxy is random and is not unidirectional as carbon fiber is within epoxy in UCFEC.

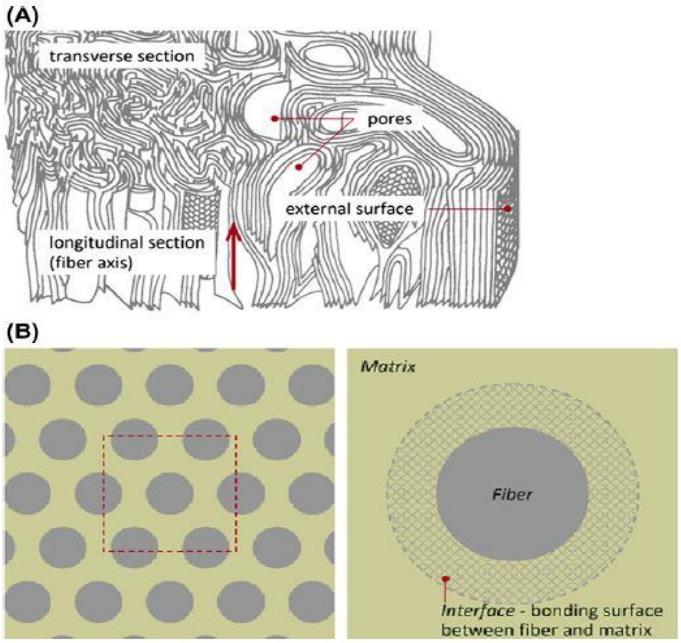


**Figure 3.19:** (A) Three-dimensional model for PAN-based, large-modulus carbon fibers; and (B) the carbon fiber–matrix interface structural model [21]

Additionally, it is reported that fiber–matrix interfacial bonding controls the stress transit between the matrix and the fiber, the stress mechanism and relaxation of damage and propagation. A schematic image of the fiber–matrix interface is provided in Figure 3.19B. The failure mechanism for the fiber–matrix bond significantly affects the fracture tolerance and the toughness of composite layers. Normal tensile stress–strain figures of the M55 J composites are shown in Figure 3.19A. It is obvious in Figure 3.19B that the value of toughness for the M55 J composite reduced after being subjected to 2000 cycles: the final strain was decreased by 44.5%. This reported observation may be explained with the presence of disjoining loads of molecular interactions between sand adjacent phases and polymer molecule. The total modulus and strength of such composite materials were affected by the mechanical robustness within the interfacial zone due to the occupies a high-volume fraction in the composite microstructure [21].

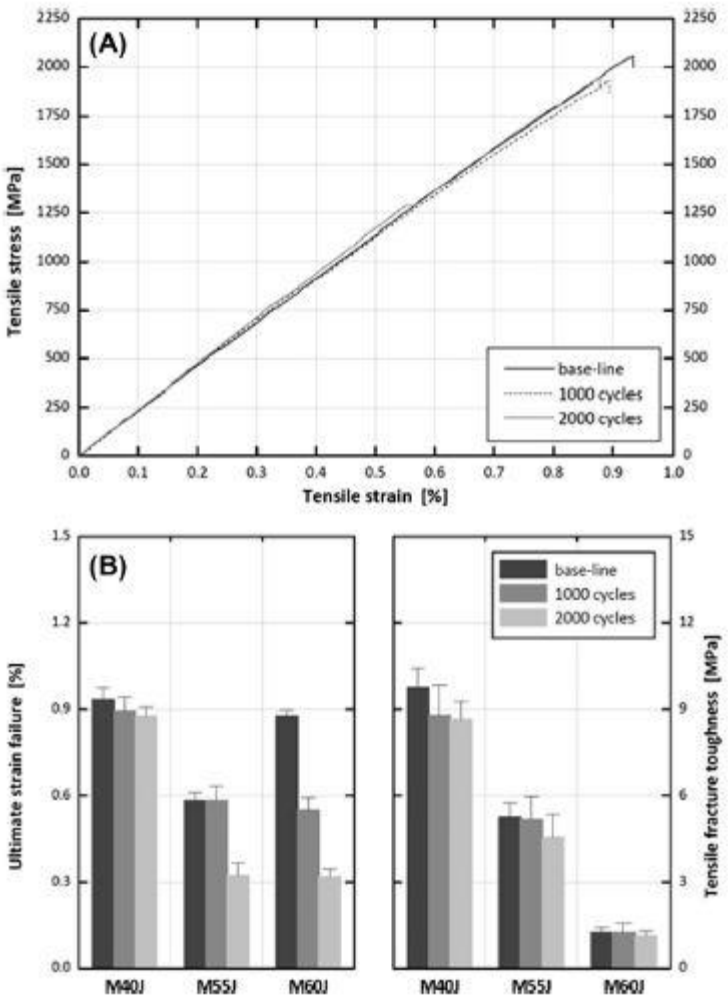


**Figure 3.20:** Comparisons for tensile characteristics of the M55 J composite as a function of vacuum thermal fatigue cycling: (A) tensile stress–strain figures; and (B) the final strain at fracture and the tensile fracture toughness [21]

A figure similar to Figure 3.20 can be developed for CNT-epoxy's tensile strength after the tensile tests have been done on the samples.

### 3.4.3. Fractography observation by microscopy

As mentioned earlier, thermal loads are highly a result of different CTEs between the matrix and fiber in an axial laminate. Thus, the fiber–matrix area plays a significant role in controlling the total characteristics of the composite material, such as off-axis tolerance, the fracture toughness along with the environmental stability. Representative fracture morphologies shown after being subjected to ILSS, longitudinal, and flexure experiments are illustrated in Figure 3.21. Fractographic schematic because of the vacuum thermal fatigue cycle conditions was reported with interfacial separations and fiber pull-outs within the fiber–matrix interface areas. As a result, it may be comprehended that the predominant reason of thermal cycling deterioration is interfacial separation and sliding along the interface areas. As it was mentioned in the introduction chapter in the section of damage mechanism, damage initiation and propagation within the CNTs-epoxy interface areas is very probable especially in the cases which functionalized CNTs are used to fabricate the CNTs-epoxy. As a result, it seems significant to mention that despite the dimensions difference between the carbon fiber and CNT, the failure mechanism of CNTs-epoxy nanocomposite could be very similar to the failure mechanism of carbon fiber/epoxy composite. And this is the reason that the similar procedures which has been done to study the thermal fatigue effect on carbon fiber/epoxy could be done to perform the study of thermal fatigue effect on CNTs-epoxy. Therefore, the weak interfacial adhesion and the existence of micro-voids, and possible microcracking, may naturally facilitate the initiation of frictional sliding within the thermal cycling [21].

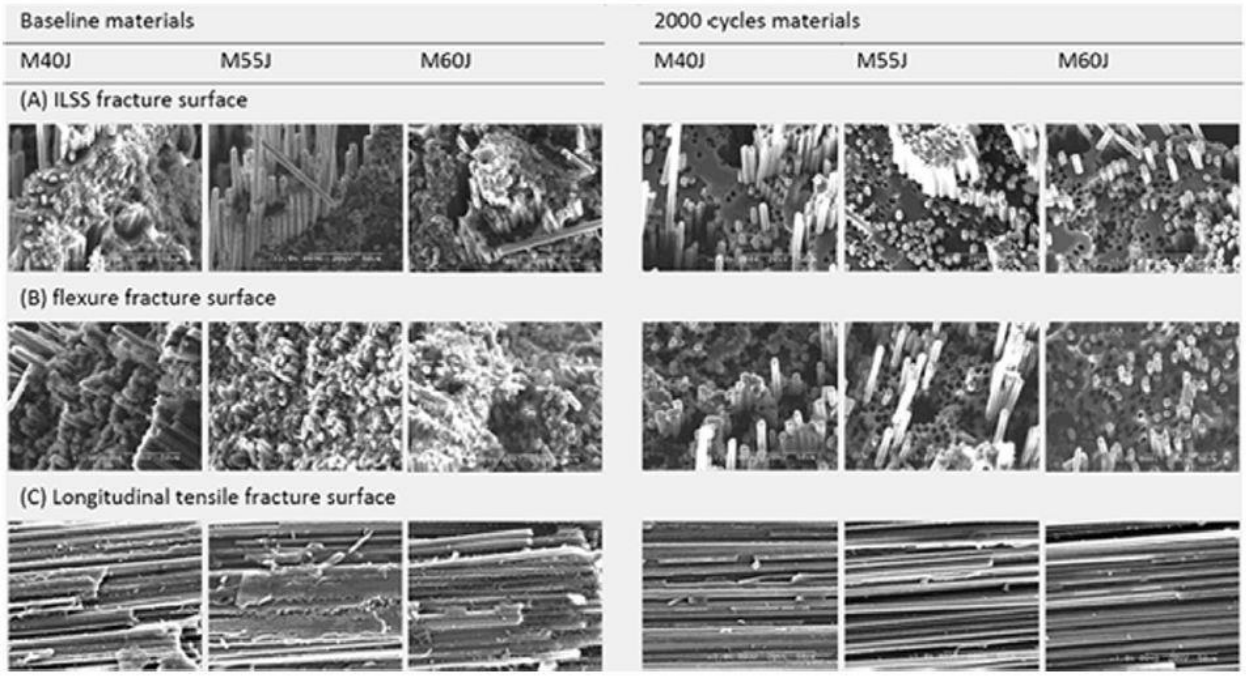


**Figure 3.21:** Typical fracture surface morphologies after being subjected to ILSS, flexure and axial tensile experiments: the electron micrographs obtained with 1000 × magnification [21]

The same procedure as it has been performed for UCFEC as it is shown in Figure 3.21, can be conducted to show the fractured or damage surfaces within the CNT-epoxy and then can be illustrated similar to Figure 3.21 in the thesis to show the fracture surfaces caused by short-beam and tensile tests in CNT-epoxy before and after the thermal cycling exposure.

# Chapter 4

## Results and Discussions

All the results which have been obtained from the tension test of dog – bone specimens and short – beam shear test specimens, are illustrated below. As discussed in the previous sections, these are the results for seven different materials, which are listed below.

1. Epoxy
2. 0.5 wt.% MWCNT - epoxy
3. 1.0 wt.% MWCNT - epoxy
4. 1.5 wt.% MWCNT - epoxy
5. 0.5 wt.% SWCNT - epoxy
6. 1.0 wt.% SWCNT - epoxy
7. 1.5 wt.% SWCNT – epoxy

### 4.1. Tension test results

Table 4.1 provides a summary of the tension test results for epoxy specimens with different CNT reinforcements and number of thermal cycles.

**Table 4.1: Tension test results for CNT – Epoxy composite specimens**

| Materials | Number of Thermal Cycles | 0 | 1500 | 3000 |
|---|---|---|---|---|
| Epoxy | Tensile Strength (psi) | 5,350 | 5,938 | 6,245 |
| | Modulus of Elasticity (psi) | 319,799 | 412,201 | 606,310 |
| | Ultimate Strain | 0.0264 | 0.01445 | 0.0103 |
| 0.5 wt.% MWCNT - epoxy | Tensile Strength (psi) | 4,145 | 5,279 | 4,120 |
| | Modulus of Elasticity (psi) | 373,423 | 437,568 | 388,679 |
| | Ultimate Strain | 0.0111 | 0.0121 | 0.0106 |
| 1.0 wt.% MWCNT - epoxy | Tensile Strength (psi) | 5,433 | 5,137 | 4,193 |
| | Modulus of Elasticity (psi) | 471,076 | 430,355 | 461,784 |
| | Ultimate Strain | 0.0109 | 0.01188 | 0.00908 |
| 1.5 wt.% MWCNT - epoxy | Tensile Strength (psi) | 4,539 | 5,345 | 4,974 |
| | Modulus of Elasticity (psi) | 492,488 | 431,473 | 578,372 |
| | Ultimate Strain | 0.00922 | 0.01242 | 0.0086 |
| 0.5 wt.% SWCNT - epoxy | Tensile Strength (psi) | 3,055 | 3,007 | 3,662 |
| | Modulus of Elasticity (psi) | 500,706 | 450,503 | 452,098 |
| | Ultimate Strain | 0.0061 | 0.007 | 0.0081 |
| 1.0 wt.% SWCNT - epoxy | Tensile Strength (psi) | 3,185 | 3,322 | 3,192 |
| | Modulus of Elasticity (psi) | 510,773 | 460,668 | 470,699 |
| | Ultimate Strain | 0.0064 | 0.0072 | 0.007 |
| 1.5 wt.% SWCNT – epoxy | Tensile Strength (psi) | 3,029 | 3,560 | 2,506 |
| | Modulus of Elasticity (psi) | 517,351 | 465,777 | 464,074 |
| | Ultimate Strain | 0.0059 | 0.008 | 0.0054 |

The pure epoxy material specimens display increasing tensile strength and elastic modulus with increasing thermal cycles. Consequently, the ultimate tensile strain to failure decreases as the epoxy becomes more brittle with increasing thermal cycles.

The mechanical properties of the MWCNT reinforced epoxy at room temperature (zero thermal cycles) and due to thermal cycling are always lower than the unreinforced epoxy. However, for each concentration of MWCNT the tensile properties improve at 1500 thermal cycles but degrade as the number of thermal cycles increases to 3000. It is postulated that the higher number of thermal cycles produce micro-cracking in the matrix and CNT agglomerates, and partial debonding of the CNTs from the epoxy matrix due to relation of the compressive stress on the MWCNT due to epoxy shrinkage during cure. With single wall CNT (SWCNT) reinforcement the mechanical properties are lower than both the unreinforced epoxy and the MWCNT reinforced epoxy composite. The trend in property changes with respect to SWCNT concentration and thermal cycles is similar to that with MWCNT specimens. With MWCNT composites the best properties are obtained with 1.5 wt% reinforcement, while for SWCNT composites the best properties are obtained with 1 wt% reinforcement.

Apparently with SWCNT reinforcement the best properties are obtained for smaller CNT concentration of 0.5 wt% for 3000 thermal cycles. However, in the case of SWCNT the best properties at 3000 thermal cycles is obtained for the highest concentration of 1.5 wt%.

### 4.2. Shear test results

The shear properties of composite material under transverse loading in the three-point bend loading configuration are shown in Table 2. The shear properties are significantly lower with both types of CNT reinforcements and the number of thermal cycles as compared to pure epoxy. The SWCNT reinforcement produces the lowest shear properties for all thermal cycles.

**Table 4.2: Short – beam test results for CNT – Epoxy composite specimens**

| Materials | Number of Thermal Cycles | 0 | 1500 | 3000 |
|---|---|---|---|---|
| Epoxy | Shear Strength (psi) | 2,949 | 2,237 | 2,634 |
| | Displacement (Inch) | 0.0230 | 0.0196 | 0.0172 |
| 0.5 wt.% MWCNT – epoxy | Shear Strength (psi) | 1,277 | 1,540 | 2,086 |
| | Displacement (Inch) | 0.013 | 0.0145 | 0.0094 |
| 1.0 wt.% MWCNT - epoxy | Shear Strength (psi) | 2,635 | 1,757 | 1,119 |
| | Displacement (Inch) | 0.0206 | 0.0120 | 0.0098 |
| 1.5 wt.% MWCNT - epoxy | Shear Strength (psi) | 1,161 | 2,210 | 1,406 |
| | Displacement (Inch) | 0.0093 | 0.0091 | 0.0090 |
| 0.5 wt.% SWCNT - epoxy | Shear Strength (psi) | 1,046 | 1,235 | 1093 |
| | Displacement (Inch) | 0.0077 | 0.0089 | 0.0099 |
| 1.0 wt.% SWCNT - epoxy | Shear Strength (psi) | 1,164 | 667 | 870 |
| | Displacement (Inch) | 0.0090 | 0.0079 | 0.0083 |
| 1.5 wt.% SWCNT – epoxy | Shear Strength (psi) | 1,082 | 931 | 901 |
| | Displacement (Inch) | 0.0077 | 0.0078 | 0.0087 |

## 4.3. Statistics data from the tensile and shear tests

In the tables below, the statistics data that are obtained from the tensile and shear tests are indicated. These statistic data in the table below show the range and standard deviation of both tensile and shear strengths for each material that was tested.

**Table 4.3: Statistical data analysis of tensile strength obtained from all CNT – epoxy specimens**

| Materials | Number of Thermal Cycles | 0<br>Range;<br>Standard Deviation | 1500<br>Range;<br>Standard Deviation | 3000<br>Range;<br>Standard Deviation |
|---|---|---|---|---|
| Epoxy | Tensile Strength (psi) | 5300 – 5400;<br>50 | 4979 – 6849;<br>617.1 | 4130 – 7904;<br>1437.1 |
| 0.5 wt.% MWCNT - epoxy | Tensile Strength (psi) | 2185 – 5467;<br>1326.8 | 4283 – 5954;<br>592.4 | 2734 – 5018;<br>942.5 |
| 1.0 wt.% MWCNT - epoxy | Tensile Strength (psi) | 4534 – 6310;<br>628 | 4325 – 5817;<br>539.6 | 3130 – 4979;<br>670 |
| 1.5 wt.% MWCNT - epoxy | Tensile Strength (psi) | 3644 – 5075;<br>478 | 4654 – 6151;<br>535.2 | 3638 – 6132;<br>1025.9 |
| 0.5 wt.% SWCNT - epoxy | Tensile Strength (psi) | 2627 – 3546;<br>355.4 | 2664 – 3395;<br>294.1 | 3235 – 4161;<br>349.1 |
| 1.0 wt.% SWCNT - epoxy | Tensile Strength (psi) | 2877 – 3412;<br>201.7 | 2810 – 3798;<br>334.8 | 2441 – 3915;<br>578.8 |
| 1.5 wt.% SWCNT – epoxy | Tensile Strength (psi) | 2785 – 3414;<br>226.2 | 3251 – 4059;<br>288.6 | 2128 – 2891;<br>336.1 |

Variations in the strength values is significant and ranges from a low of about 500 psi to a high of about 3000 psi for CNT reinforced specimens. This variation is even higher in unreinforced epoxy specimens. The variations are lowest in SWCNT reinforced specimens. These trends are noted for both tensile strength in Table 3 and shear strength tests in Table 4. In this preliminary study, it is unclear what are the reasons for the relatively large variations, and more detailed investigation on the effect thermal cycles on the matrix and the matrix-CNT interface effects is needed and will be subject of future effort.

**Table 4.4: Statistical data analysis of shear strength obtained from all CNT – epoxyspecimens**

| Materials | Number of Thermal Cycles | 0<br>Range;<br>Standard Deviation | 1500<br>Range;<br>Standard Deviation | 3000<br>Range;<br>Standard Deviation |
|---|---|---|---|---|
| **Epoxy** | **Shear Strength (psi)** | 2737 – 3085;<br>145.8 | 1071 – 3420;<br>815 | 2255 – 3535;<br>528.5 |
| **0.5 wt.% MWCNT - epoxy** | **Shear Strength (psi)** | 1011 – 1450;<br>165.3 | 1055 – 2056;<br>399.9 | 1387 – 2685;<br>534.6 |
| **1.0 wt.% MWCNT - epoxy** | **Shear Strength (psi)** | 2179 – 3089;<br>378.9 | 1522 – 2149;<br>278.8 | 959 – 1443;<br>190.4 |
| **1.5 wt.% MWCNT - epoxy** | **Shear Strength (psi)** | 929 – 1397;<br>153.3 | 1041 – 3387;<br>976.3 | 1054 – 2223;<br>476.6 |
| **0.5 wt.% SWCNT - epoxy** | **Shear Strength (psi)** | 808 – 1300;<br>181 | 1043 – 1493;<br>169.1 | 882 – 1324;<br>207.9 |
| **1.0 wt.% SWCNT - epoxy** | **Shear Strength (psi)** | 963 – 1673;<br>295.7 | 520 – 847;<br>120.3 | 645 – 1109;<br>167.7 |
| **1.5 wt.% SWCNT – epoxy** | **Shear Strength (psi)** | 971 – 1268;<br>115.2 | 784 – 1137;<br>147.7 | 748 – 977;<br>82.2 |

### 4.4. Fracture surface analysis using electron microscopy for various tensile test specimens

**(a) Monolithic epoxy:**

At **room temperature (RT)**, fractured paths and surfaces were rough and wavy as seen in Figure 4.1. The surface has smooth surface regions spread among the rough regions and also small through surface cracks along with spallation is visible at higher magnification of 1000X. A rough fracture surface indicates the potential for larger fracture energy in epoxy at room temperature.

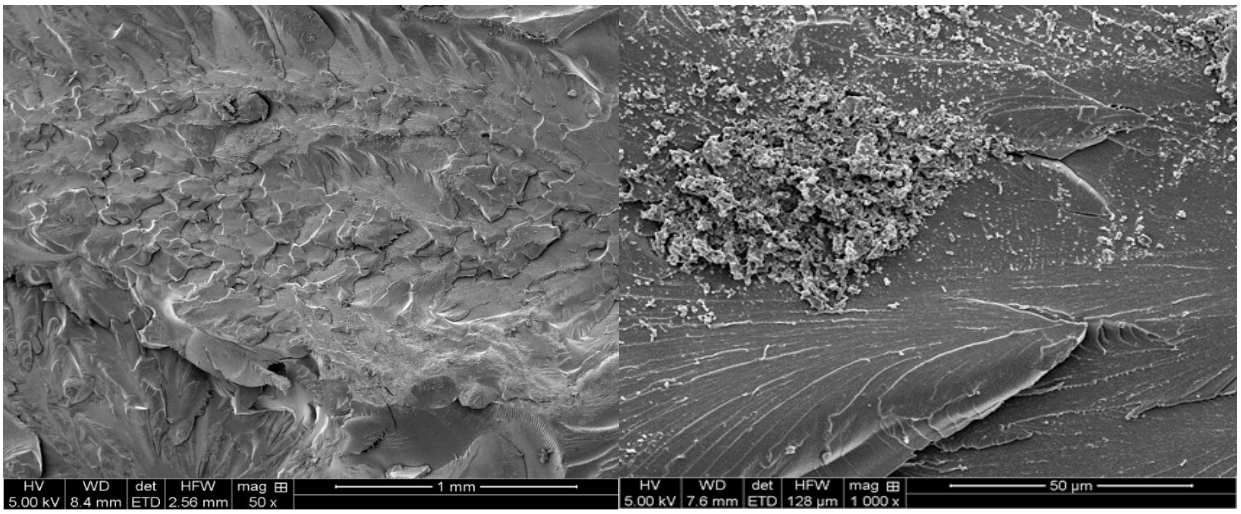


**Figure 4.1:** Fracture surfaces due to tensile failure in Epoxy at room temperature

Fracture surfaces of specimens subjected to **1500 thermal cycles** had smoother surfaces and consequently smaller regions that were rough as compared to the room temperature specimens, as shown in Figure 4.2. Smoother fracture surfaces indicate that the thermally cycled epoxy is more brittle with higher tensile strength as compared to the room temperature epoxy.

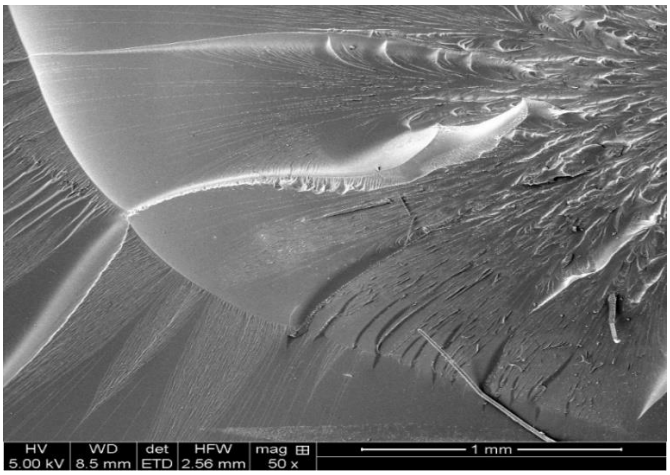


**Figure 4.2:** Fracture surfaces due to tensile failure in Epoxy subjected to 1500 thermal cycles

**(b) 0.5 wt. % MWCNT – epoxy composite:**

At room temperature, fracture surfaces were rough and wavy (at 50X magnification) interspersed with smooth surfaces (at 1000X magnification), as shown in Figure 4.3. MWCNTs were found to have been dispersed fairly uniformly within the epoxy with small regions of agglomeration. The addition of multiwall CNTs decreased the tensile strength as compared to the room temperature strength of nascent epoxy potentially due to the stress concentration caused by lack of covalent bonding between the epoxy and the CNT.

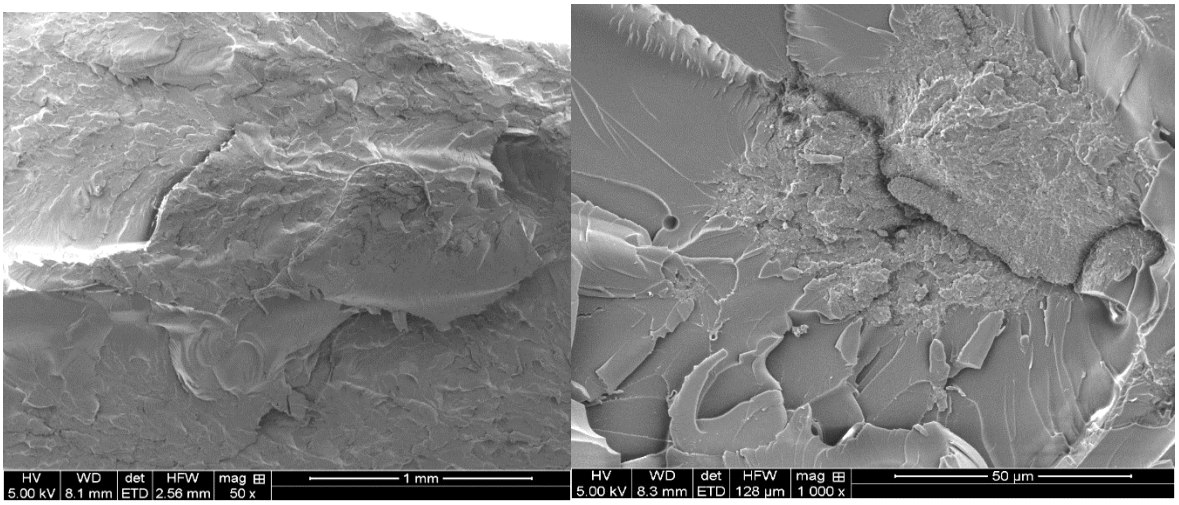


**Figure 4.3:** Fracture surfaces due to tensile failure in a 0.5 wt. % MWCNT reinforced epoxy composite at room temperature

At **1500 Thermal Cycles**, the tensile strength increased by over 20% compared to the room temperature specimens. No major changes in the fracture surface characteristics were noted compared to the room temperature fracture specimens except that the surface is wavier with larger peaks and valleys (as in 1000X image of Figure 4.4) that could cause an increase in the tensile strength. Another potential reason for increase could be the relaxation in residual stresses due to the thermal cycling.

In Figure 4.4 a CNT bundle can also be seen that has been pulled out and its surface is clean indicating no atomic bonding between the epoxy matrix and the CNT. After 3000 thermal cycles, however, the tensile strength dropped by about 20% compared to the 1500 thermal cycled specimens. It is postulated that after 3000 thermal cycles there were increased cracks in the matrix in and around the CNT agglomerates, as seen in Figure 4.4.

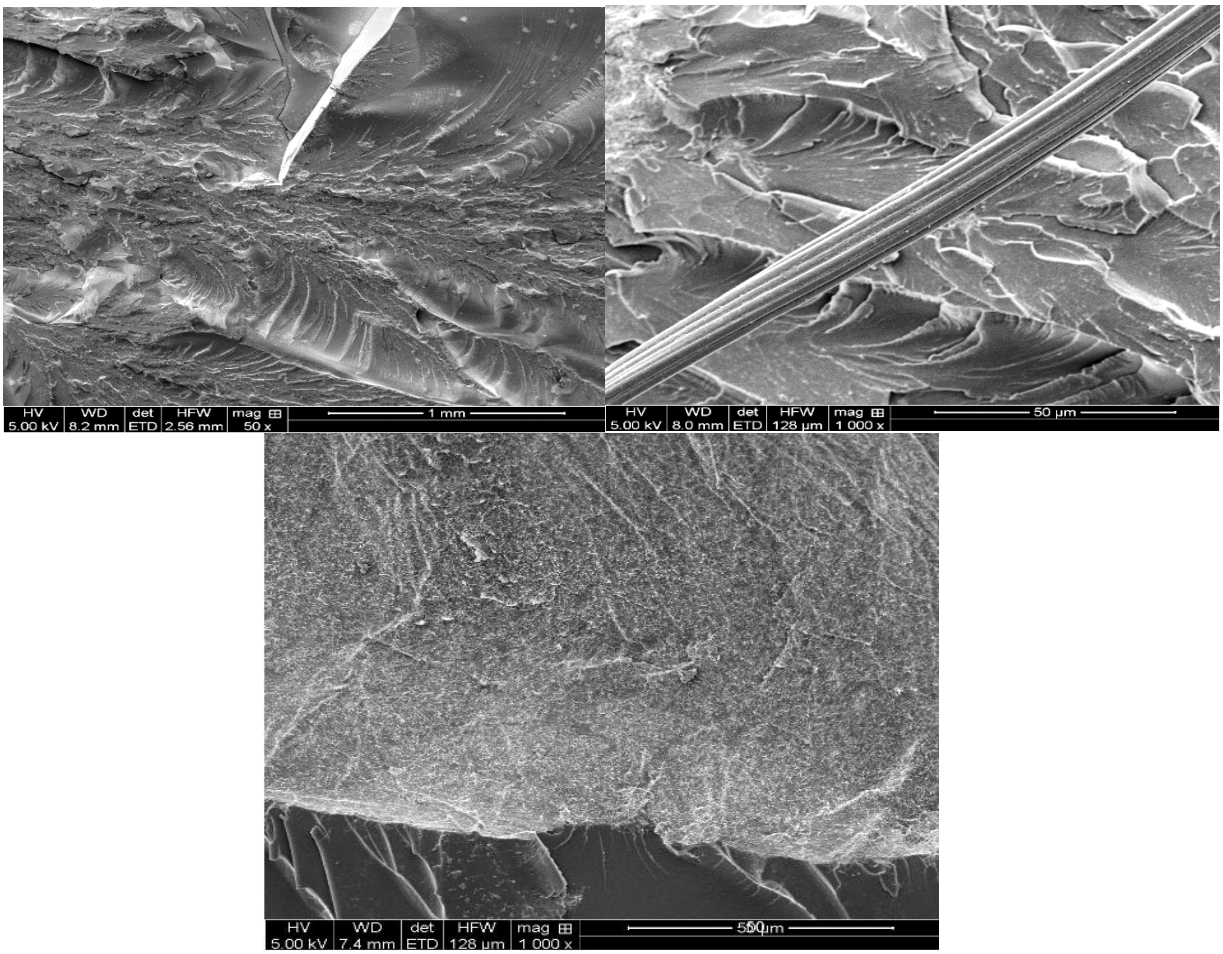


**Figure 4.4:** Fracture surfaces due to tensile failure in a 0.5 wt.% MWCNT reinforced epoxy composite subjected to 1500 thermal cycles

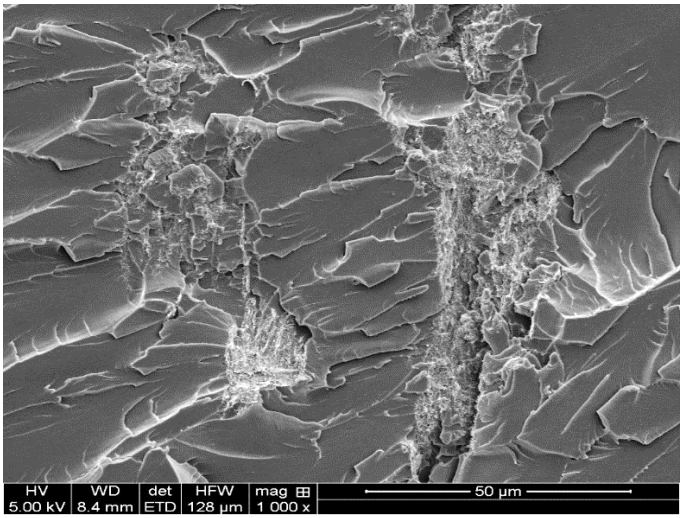


**Figure 4.5:** Fracture surfaces due to tensile failure in a 0.5 wt. % MWCNT reinforced epoxy composite subjected to 3000 thermal cycles

**(c) 1.0 wt. % MWCNT – epoxy:**

For all thermally cycled specimens, namely RT, 1500 and 3000 thermal cycles, fracture characteristics were very similar to that observed for the 0.5 wt. % MWCNT specimens. Also, the tensile strength values are very similar for both the 0.5 wt. % and 1.0 wt. % MWCNT specimens.

**(d) 1.5 wt. % MWCNT – epoxy:**

**At RT,** fracture surfaces are somewhat rough with many interspersed smooth and relatively flatter regions, as shown in Figure 4.6. No other specific cracks are observed.

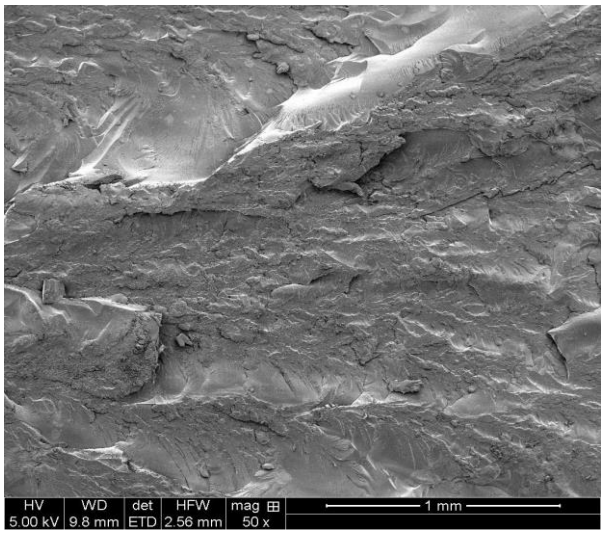


**Figure 4.6:** Fracture surfaces due to tensile failure in a 1.5 wt. % MWCNT reinforced epoxy composite at room temperature

At **1500 Thermal Cycles**, fracture surfaces have increased in roughness compared to the room temperature specimens, as shown in Figure 4.7. Furthermore, the CNT agglomeration regions display minor and small length cracks (at 1000X) as compared to lower CNT concentration specimens.

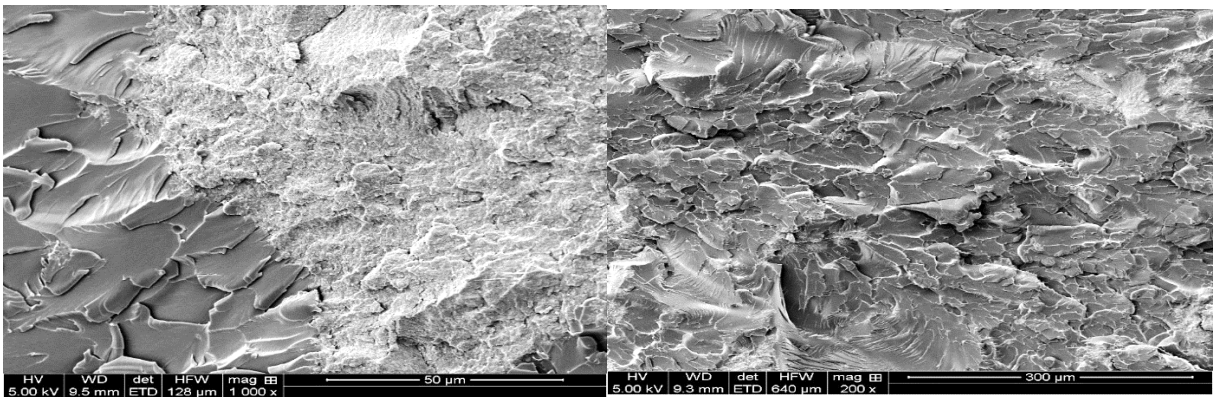


**Figure 4.7:** Fracture surfaces due to tensile failure in a 1.5 wt. % MWCNT reinforced epoxy composite subjected to 1500 thermal cycles

At **3000 Thermal Cycles**, more agglomerated areas have been observed on the fracture surfaces. Furthermore, fracture surfaces are in a complex non – uniform shapes. Additionally, needle – like MWCNTs can be observed on the fractured surfaces, as shown in Figure 4.8. In the CNT agglomerated regions, the cracking has increased compared to the 1500 thermal cycled specimens.

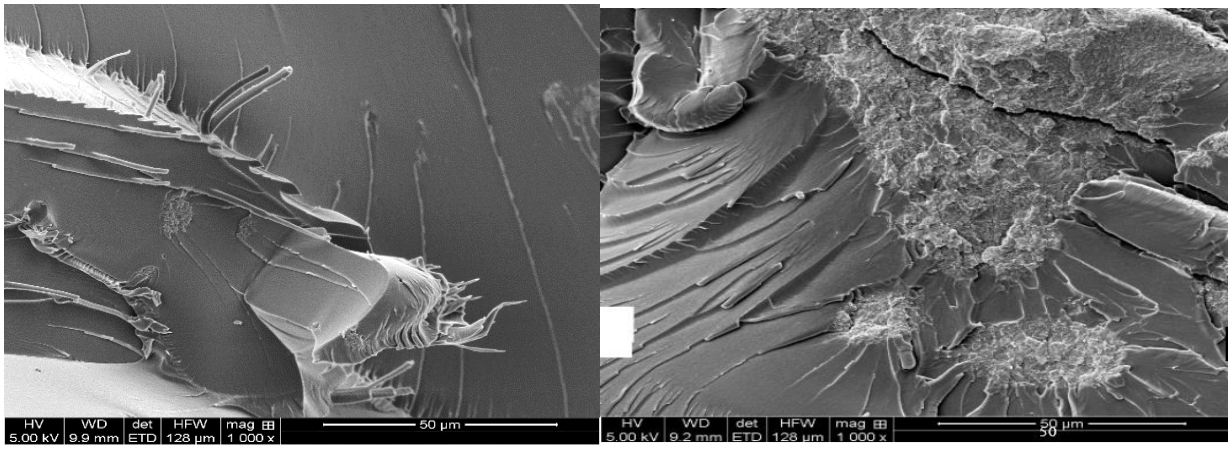


**Figure 4.8:** Fracture surfaces due to tensile failure in a 1.5 wt. % MWCNT reinforced epoxy composite subjected to 3000 thermal cycles

**(e) SWCNT – epoxy composites:**

Single wall CNT reinforcement of epoxy produces composites whose mechanical properties are lower than both the unreinforced epoxy and the MWCNT reinforced composites. Their properties are 40-60% lower than the epoxy matrix material and also compared to the MWCNT composites. We do not provide scanning microscope pictures for each CNT concentration and thermal cycles but rather provide evidence that potentially explains the reason for the degradation in properties of SWCNT composites. The greater stiffness of the single walled CNTs and greater level of agglomeration of CNTs compared to multi walled CNTs along with greater damage and cracking in the fracture regions leads to lower mechanical properties.

As can be seen in Figure 4.9 (50X and 200X magnification) for 1.5 wt.% SWCNT after 1500 thermal cycles there is extensive cracking and furthermore there is evidence of significant cracking in the regions where CNTs have agglomerated (5,000X and 20,000Xmagnification).

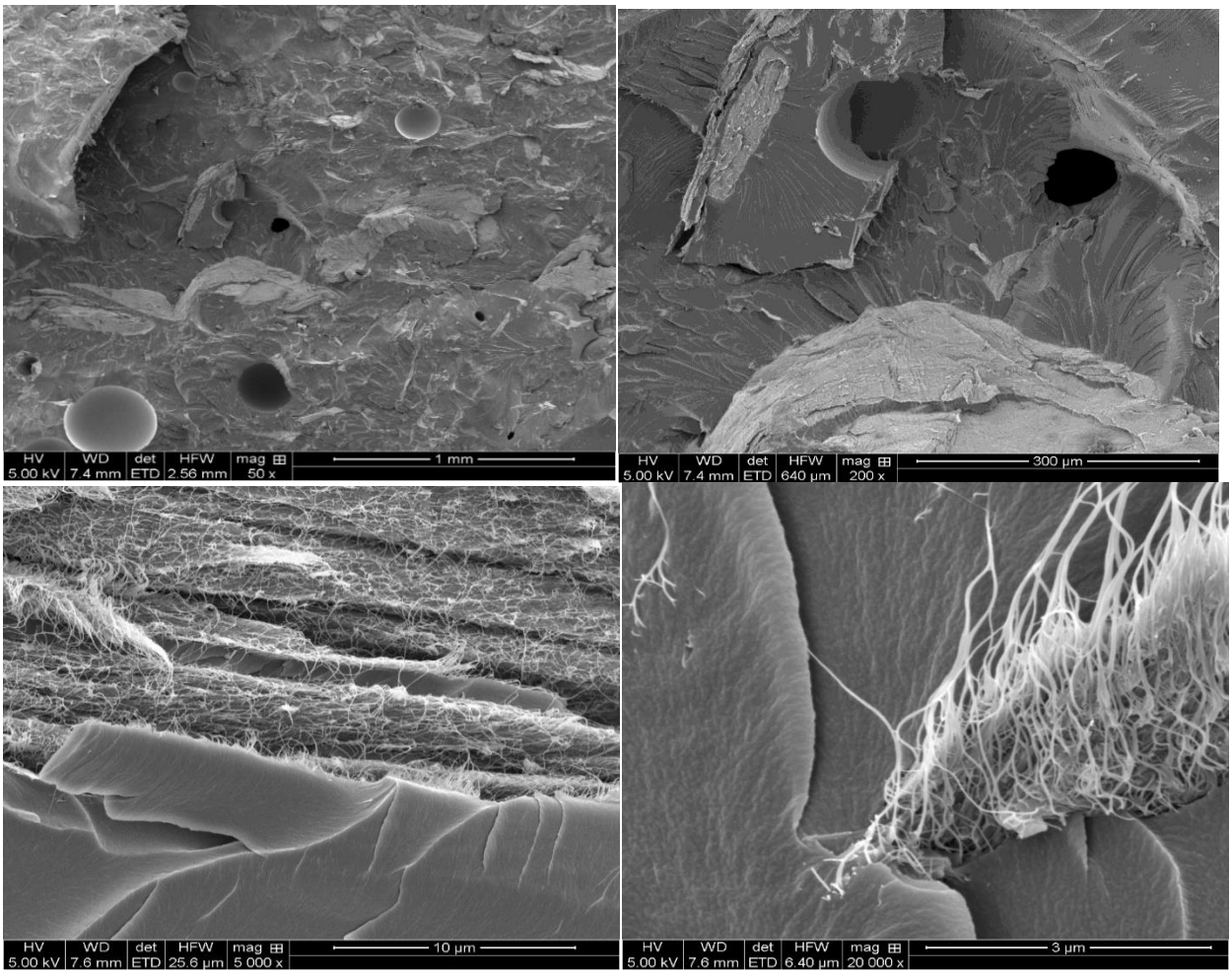


**Figure 4.9:** Fracture surfaces in a 1.5 wt. % SWCNT reinforced epoxy composite subjected to 1500 thermal cycles

Similar trends are noted with potentially greater damage and cracking at 3000 thermal cycles in 1.5 wt. % SWCNT composites, as shown in Figure 4.10.

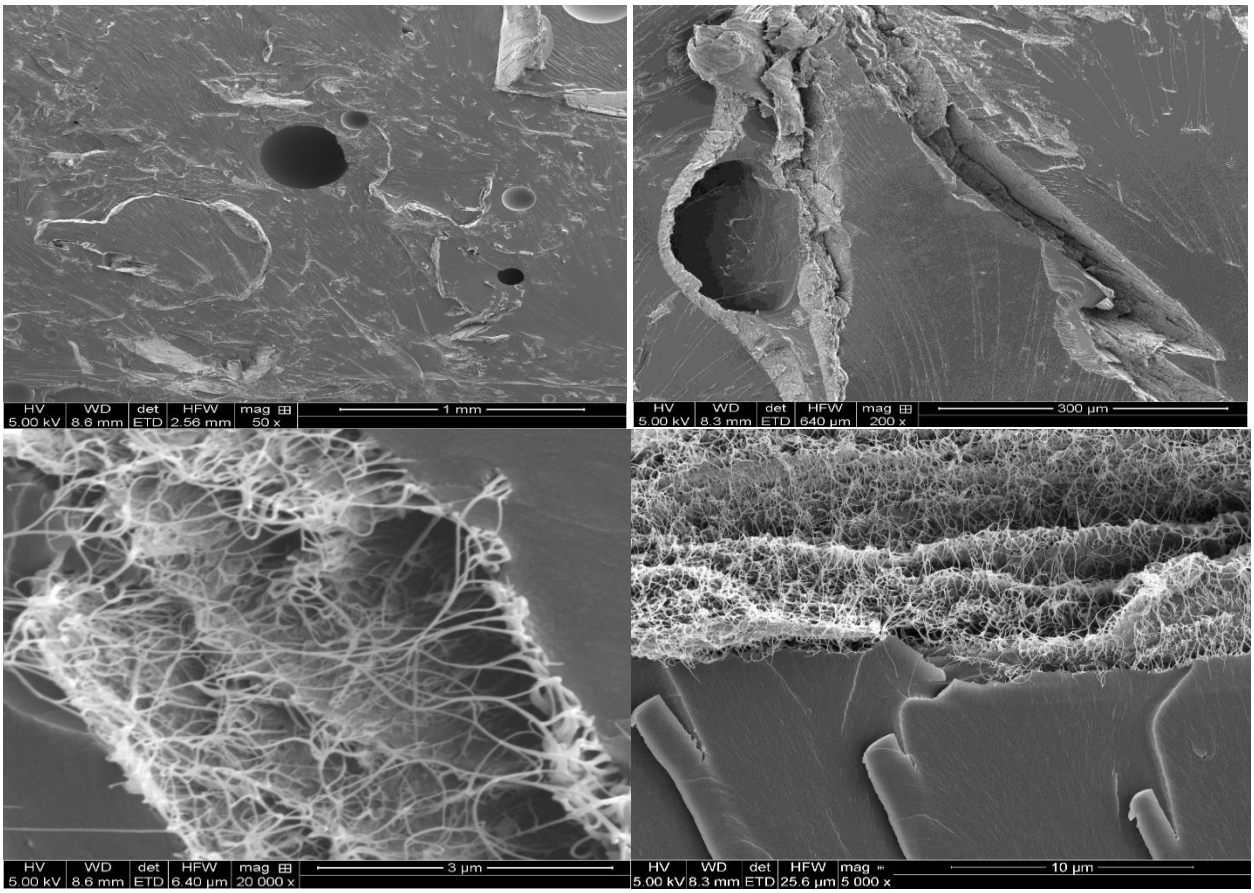


**Figure 4.10:** Fracture surfaces in a 1.5 wt. % SWCNT reinforced epoxy composite subjected to 3000 thermal cycles

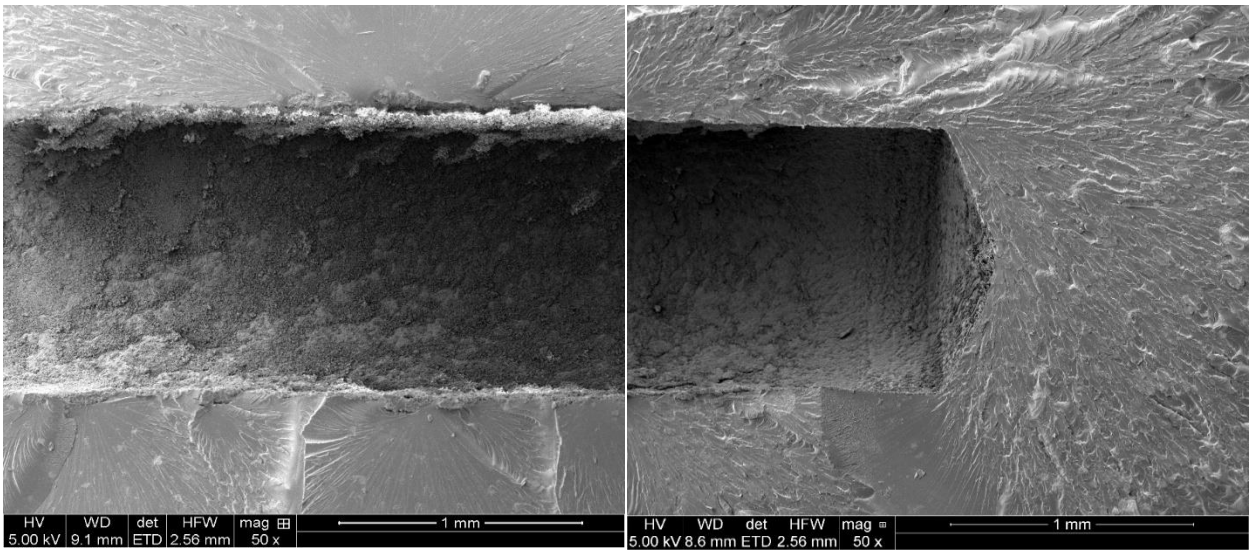


**Figure 4.11:** Fractured Surface of 1.0 wt. % MWCNT - epoxy at 3000 Thermal Cycles

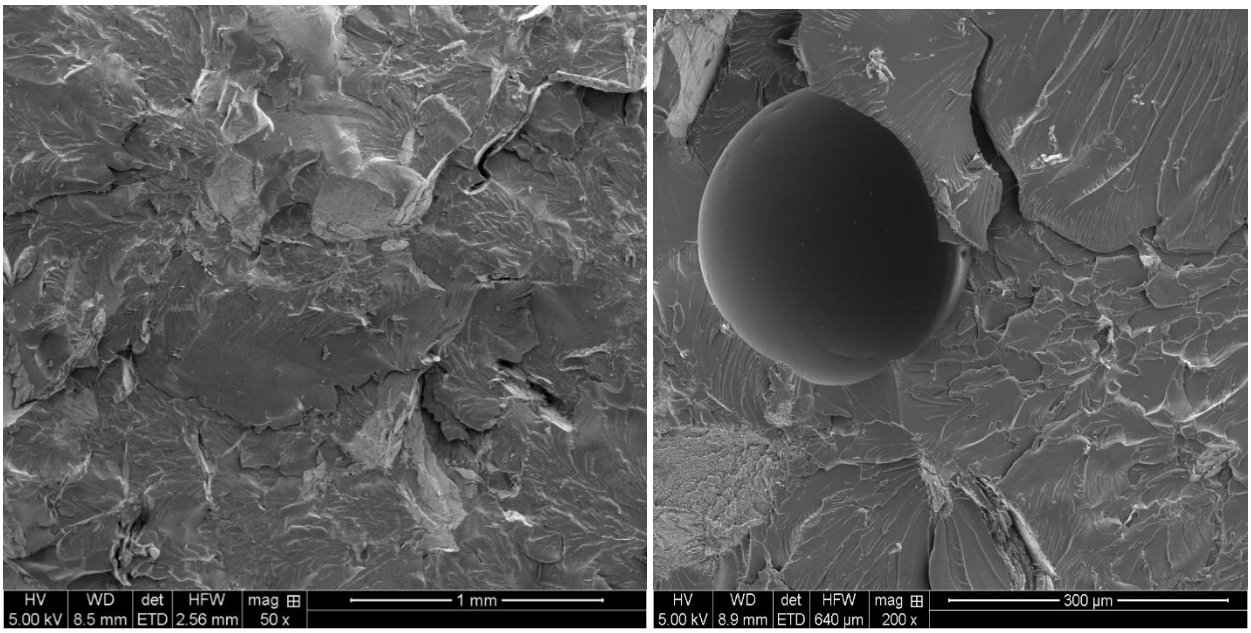


**Figure 4.12:** Fractured Surface of 1.0 wt. % SWCNT - epoxy at 3000 Thermal Cycles

# Chapter 5

## Conclusions

Epoxy polymers are used in a large number of applications where thermal cycling is a part of the working environment in addition to mechanical loading. Often the polymer matrix is reinforced with reinforcements that are in the form of fibers or particles. In this study, carbon nanotubes (CNT) have been used as a reinforcement to produce reinforced epoxy composite plates. The plates were subjected to 1500 and 3000 thermal cycles and these thermally cycled plates along with as cured plates at room temperature were tested for their tensile properties and transverse shear properties.

The modulus of elasticity of epoxy and the tensile strength increased with increasing thermal cycles due to greater crosslinking between the polymer chains. Addition of multiwall (MW) CNTs reduced the elastic modulus and the tensile strength for all three CNT concentrations studied as compared to unreinforced epoxy. It was observed that the 1.0 wt. % MWCNT – epoxy composite subjected to 1500 thermal cycles had the best tensile properties. The addition of single wall (SW) CNTs as reinforcement to epoxy matrix resulted in composites with mechanical properties inferior to both the monolithic epoxy and the MWCNT-epoxy materials.

The shearing properties of the two CNT reinforced composites are inferior to the unreinforced epoxy with the SWCNT composite displaying the lowest properties. As in the case of tensile behavior, the 1.0 wt. % MWCNT composite subjected to 1500 thermal cycles resulted in the best composite material properties.

Based on the results of this study it can be summarized that the addition of MWCNT produces better mechanical properties compared to the use of SWCNT reinforcement. However, unreinforced epoxy showed the highest mechanical properties. The scanning electron microscope images show the damage mechanisms in the three materials studied and the various trends have been discussed in the body of the paper. The fracture surfaces in SWCNT specimens show greater damage than in MWCNT composites, which signifies the lower mechanical properties of the SWCNT-epoxy composites. In this research the fracture toughness and fracture characteristics were not investigated and would be studies in a future paper. It is postulated that the CNT reinforced composites could show fracture toughness that is higher than the unreinforced epoxy and hence the former would be more resilient materials.

## REFERENCES

[1] Lijima, S., 1991, “Helical microtubules of graphic carbon,” Nature vol 354 no. 6348, 56-58.

[2] Fromy, T R., Hanson, F K, Olsen, T., 2012, “The optimum Dispersion of Carbon Nanotubes for Epoxy Nanocomposites: Evolution of the Particle Size Distribution by Ultrasonic Treatment,” Journal of Nanotechnology volume 2012 article ID. 545930, 14 pages.

[3] Rai, A., Subramanian, N., Chattopadhyay, A., 2017, “Investigation of damage mechanisms in CNT nanocomposites using multiscale analysis,” International Journal of Solids and Structures 120, 115-124.

[4] Ramana, G V., Padya, B., Kumar, R N., Prabhakar, K V P., Jain, P K., 2010, “Mechanical Properties of Multi-walled Carbon Nanotube Reinforced Polymer Nanocomposites,” Indian Journal of Engineering & Materials Science Vol. 17 October 2010, 331-337.

[5] Jayathilaka,[1] J R I., Dehigaspitiya, D D P D., [2]Pathirana, S T., Herath, K R B., 2016, “Failure Mechanisms of Carbon Nanotube Reinforced Composites,” [1]Swinburne University of Technology [2]Washington State University, Conference paper, January 2016.

[6] Abliz, D., Ziegmann, G., Duan, Y G., Li, D C., Meiners, D., 2014, “Effect of CNT Concentration on Mechanical Properties of Composites Manufactured by Compression Resin Transfer Molding (CRTM),” ECCM16-16th European Conference on Composite Materials, Seville, Spain, 22-26 June 2014.

[7] Chakraborty, A K., Plyhm, T., Barbezat, M., Necola, A., Terrasi, G P., 2011, “Carbon nanotube (CNT)-epoxy nanocomposites: a systematic investigation of CNT dispersion,” Journal of Nanoparticles Research December 2011. 

[8] Zhou, Y X., Wu, P X., Cheng, Z Y., Ingram, J., Jeelani, S., 2008, "Improvement in Electrical, Thermal and Mechanical Properties of Epoxy by Filling Carbon Nanotube," Express Polymer Letters Vol. 2 No. 1, 40-48.

[9] Allaoui, A., Bai, S., Cheng, H M., Bai, J B., 2002, "Mechanical and electrical properties of a MWNT/epoxy composite," Composites Science and Technology 62, 1993-1998.

[10] Rai, A., Subramanian, N., Koo, B., Chattopadhyay, A., 2017, "Multiscale damage analysis of carbon nanotube nanocomposite using a continuum damage mechanics approach," Journal of Composite Materials Vol. 51 No. 6, 847-858.

[11] Laurenzi, S., Botti, S., Rufoloni, A., Santonicola, M G., 2014, "Fracture mechanics in epoxy composites reinforced with carbon nanotubes," Procedia Engineering 88, 157-164.

[12] Martone, A., Formicola, C., Piscitelli, F., Lavorgna, M., Zarrelli, M., Antonucci, V., Giordano, M., 2012, "Thermo-mechanical characterization of epoxy nanocomposites with different carbon nanotube distributions obtained by solvent aided and direct mixing," Express Polymer Letters Vol. 6 No. 7, 520-531.

[13] Pilawka, R., Paszkiewics, S., Roslaniec, Z., "Epoxy composites with carbon nanotubes," Advances in manufacturing science and technology Vol. 36 No. 3, 67-79.

[14] Subramanian, N., Koo, B., Rai, A., Chattopadhyay, A., 2015, "A multiscale damage initiation model for CNT-enhanced epoxy polymers," 20th International Conference on Composite Materials, Copenhagen, 19-24th July 2015.

[15] Guadagnoa, L., Raimondoa, M., Vertuccioa, L., Naddeoa, C., Barraa, G., Longob, P., Lambertic, P., Spinellic, G., Nobile, M.R., 2018, "Morphological, rheological and electrical properties of composites filled with carbon nanotubes functionalized with 1-pyrenebutyric acid," Composites part B 147, 12-21.

[16] Yip, M.C., Chien, T.C., Wang, K.S., 2007, "Mechanical and Electrical Properties of MWNT/Phenolic Composites under Moisture-Temperature Effects," Key Engineering Materials Vols. 334-335, 765-768.

[17] Yang, J., 2012, "Carbon nanotubes reinforced composites for wind turbine blades," Master of Science Thesis, Department of Macromolecular Science and Engineering, Case Western Reserve University, January 2012.

[18] Du, J-H., Bai, J., Cheng H-M., 2007, "The present status and key problems of carbon nanotubebased polymer composites," eXPRESS Polymer letters Vol.1 No. 5, 253-273.

[19] Song, K., Zhang, Y., Meng, J., Green, E. C., Tajaddod, N., Li, H., and Minus, M. L., 2013, "Structural Polymer Based Carbon Nanotube Composite Fibers: Understanding the Processing Structure-Performance Relationship," Materials, 6, pp. 2543-2577.

[20] Anvari, A., 2017, "Thermal fatigue life of carbon nanotube wire and unidirectional carbon fiber/epoxy composite (UCFEC) in earth orbit," Journal of Chemical Engineering and Materials Science, Vol. 8(8), 101-111.

[21] Park, S. Y., Choi H. S., Choi W. J., Kwon, H., 2012, "Effect of vacuum thermal cyclic exposures on unidirectional carbon fiber/epoxy composites for low earth orbit space applications," Composites: Part B, 43, (2012), pp. 726–738.

[22] Ma, A W K., Yearsley, K M., Chinesta, F., and Mackley, M R., 2009, "A review of the microstructure and rheology of carbon nanotube suspensions," Proc. IMechE Vol.222 Part N: J. Nanoengineering and Nanosystems, 71-94.

[23] Nicholas, A., Fasanella and Veera Sundararaghavan, 2015, "Molecular dynamics of SWNT/epoxy nanocomposites," AIAA Sci Tech Forum, University of Michigan.

[24] Song, K., Zhang, Y., Meng, J., Green, E. C., Tajaddod, N., Li, H., and Minus, M. L., 2013, "Structural Polymer Based Carbon Nanotube Composite Fibers: Understanding the Processing Structure-Performance Relationship," Materials, 6, pp. 2543-2577.

[25] Saleh, T. A., 2016, "Nanomaterials and polymer membranes: Synthesis, characterization, and applications," 1st edition.

[26] Saleh, T. A., 2017, "Advanced nanomaterials for water engineering, treatment, and hydraulics," DOI: 10.4018/978-1-5225-2136-5.

[27] Saleh, T. A., 2018, "Nanotechnology in oil and gas industries: Principles and applications (Topics in mining, metallurgy and minerals engineering)," 1st edition.

[28] Saleh, T. A., Alshaheri, A. H., Tahir, M. I. M., Rahman, M. B. A., and Ravoof, T. B. S. A., 2017, "Catalytic oxidation of cyclohexane using transition metal complexes of dithiocarbazate Schiff base," Chem. Eng. J., 327, pp. 423-430.

[29] Gaddafi, I. D., and Saleh, T. A., 2017, "Effects of bimetallic Ce/Fe nanoparticles on the desulfurization of thiophenes using activated carbon," Chem. Eng. J., 307, pp. 914-927.

[30] Wilkerson, J., Daniel, A., and Daniel, D., 2007, "Fatigue Characterization of Functionalized Carbon Nanotube Reinforced Carbon Fiber Composites," Texas A & M University, College Station, Texas 77844-3012.

[31] Voicu, R., 2012, “Structural Characterization and Mechanical Behaviour of Carbon Fiber/epoxy Composite for Aeronautical Field,” Materiale Plastice, 49(1), pp. 34-40.

[32] Chow, W. S., Leu, Y. Y., and Ishak, Z. A. M., 2016, “Mechanical, Thermal and Morphological Properties of Injection Molded Poly (Lactic acid)/Calcium Carbonate Nanocomposites,” Periodica Polytechnica, Mech. Eng., 60(1), pp. 15-20.

[33] Meszaros, L., and Turcsan, T., 2014, “Development and mechanical properties of carbon fibre reinforced EP/VE hybrid composite systems,” Periodica Polytechnica, Mech. Eng., 58(2), pp. 127-133.

[34] Jo, H. S., and Lee, G. W., 2014, “Thermal Expansion Coefficient and Young’s Modulus of Silica Reinforced Epoxy Composite,” Int. J. Chem. Mol. Nuclear Mater. Metallurg. Eng., 8(11), pp. 1188-1191.

[35] Savkin, A., Andronik, A., and Abhilash, R., 2015, “Crack Closure Detection Using Photometrical Analysis,” Periodica Polytechnica Mech. Eng., 59(3), pp. 114-119.

[36] Ray, B. C., and Rathore, D., 2014, “Durability and integrity studies of environmentally conditioned interfaces in fibrous polymeric composites: Critical concepts and comments. Department of Metallurgical and Materials Engineering,” National Institute of Technology, Rourkela-769008, India.

[37] Qian, D., Liu, W. K., and Ruoff, R. S., 2003, “Load transfer mechanism in carbon nanotube ropes,” Compos. Sci. Technol., 63, pp. 1561-1569.

[38] Mirik, M., Ekinci, S., and Tasyurek, M., 2016, “Charpy impact resistances of carbon nanotubes reinforced high density polyethylene nanocomposite materials,” Int. J. Mater. Mech. Manuf., 4(4), pp. 247-250.

[39] Andrews, R., and Weisenberger, M. C., 2004, “Carbon nanotube polymer composites,” J. Solid State Mater. Sci., 8, pp. 31-37.

[40] Abhijeet, R. D., Swami, M. C., and Patil, P., 2015, “A review on study of composite materials in presence of cracks,” Int. J. Res. Eng. Technol., 4(2), pp. 43-45.

[41] Moufari, M. E. L., and Bakkali, L. E. L., 2015, “Interaction of thermal loading on the damage evolution of composite materials,” 22nd Congres Francais de Mecanique, University, Faculty of Sciences, Tetouan, Morocco.

[42] Anvari, A., 2017, “Crack growth as a function of temperature variation in carbon fiber/epoxy,” J. Chem. Eng. Mater. Sci., 8(3), pp. 17-30.

[43] Saleh, T. A., 2013, “The role of carbon nanotubes in enhancement of photocatalysis,” Syntheses and Applications of Carbon Nanotubes and their Composites, In Tech.

[44] Machado, F. M., Bergman, C. P., Lima, E. C., Adebayo, M. A., and Fagan, S. B., 2014, “Adsoption of a textile Dye from Aqueous Solutions by Carbon Nanotubes,” Materials Research, 17(1), pp. 153-160.

[45] Vallet, G. M., Dunand, M., and Silvain, J. F., 2015, “Influence of carbon nanotubes dispersion on thermal prperties of copper-carbon nanotubes (CNTs) composite materials,” Univers. J. Mater. Sci., 3(4), pp. 55-61.

[46] Gomez, S., Rendtorff, N. M., and Esteban, F., 2016, “Surface modification of multiwall carbon nanotubes by sulfonitric treatment,” Appl. Surf. Sci., 257(17), pp.7746-7751.

[47] Alswat, A. A., Ahmad, M. B., Hussein, M. Z., Ibrahim, N. A., and Saleh, T. A., 2016, “Copper oxide nano particles-loaded zeolite and its characteristics and antibactery activities,” J. Mater. Sci. Technol., http://dx.doi.org/10.1016/j.jmst.2017.03.015.

[48] Wang, Q., Wang, Y., Duan, B., and Zhang, M. M., 2016, "Modified Sol-Gel Synthesis of carbon nanotubes supported Titania composites with enhanced visible light induced photocatalytic activity," J. Nanomater., 6.

[49] Saleh, T. A., 2016, "Nanocomposite of carbon nanotubes/silica nanoparticles and their use for adsorption of Pb (II): from surface properties to sorption mechanism," Desalin. Water Treat., 57, pp. 10730-10744.

[50] Moyo, M., Chikazaza, L., Nyamunda, B. C., and Guyo, U., 2013, "Adsorption Batch Studies on the Removal of Pb(II) using Maize Tassel Based Activated Carbon," J. Chem. http://dx.doi.org/10.1155/2013/508934

[51] J. G. Funk and G. F. Sykes, "%e effects of simulated spacemenvironmental parameters on six commercially available composite materials," Langley Research Center Hampton, Hampton, Virginia, USA, NASA Technical Paper 2906, 1989.

[52] K.-B. Shin, C.-G. Kim, C.-S. Hong, and H.-H. Lee, "Prediction of failure thermal cycles in graphite/epoxy composite materials under simulated low earth orbit environments," *Composites Part B: Engineering*, vol. 31, no. 3, pp. 223–235, 2000.

[53] Y. B. Unigovski, A. Grinberg, and E. M. Gutman, "Low-cycle fatigue of the light advanced materials," *Procedia Engineering*, vol. 66, pp. 713–722, 2013.

[54] S. Y. Park, H. S. Choi, W. J. Choi, and H. Kwon, "Effect of vacuum thermal cyclic exposures on unidirectional carbon fiber/epoxy composites for low earth orbit space applications," *Composites Part B: Engineering*, vol. 43, no. 2, pp. 726–738, 2012.

[55] A. Anvari, "Thermal life of carbon structures: from the Earth to after the Titan," *International Journal of Aerospace Engineering*, vol. 2018, Article ID 7628614, 6 pages, 2018.

[56] Z. H. Karadeniz, “A numerical study on the thermal expansion coefficients of fiber reinforced composite materials,” Thesis, Graduate School of Natural and Applied Sciences, Dokuz Eylul University, Izmir, Turkey, 2005.

[57] T. H. Nam, G. Requena, and H. P. Degischer, “Modeling and numerical computation of thermal expansion of aluminum matrix composite with densely packed SiC particles,” *Technische Mechanik*, vol. 28, no. 3-4, pp. 259–267, 2008.

[58] T. Wenlang, Q. I. Lehua, C. Su, and J. Zhou, “Mean-field homogenization based approach to evaluate macroscopic coefficients of thermal expansion of composite materials,” *International Journal of Heat and Mass Transfer*, vol. 102, pp. 1321–1333, 2016.

[59] A. Kelly, “Composite materials for thermal expansivity matching and high heat flux thermal management,” *Advances in Composite Materials and Structures*, vol. 334-335, pp. 1017–1020, 2007.

[60] M. GeiBendorfer and C. Proppe, *Multiscale Modeling of the Fatigue Behaviour of Real Open-Cell Aluminum Foams*, vol. 10, Kaiserstr, Karlsruhe, Germany.

[61] M. Nosko, F. Simancik, and R. Florek, “%e fatigue behaviour of aluminum foam,” *Materials and Technology*, vol. 47, no. 3, pp. 295–298, 2013.

[62] D. K. Rajak, L. A. Kumaraswamidhas, and S. Das, “Technical overview of aluminum alloy foam,” *Reviews on Advanced Materials Science*, vol. 48, pp. 68–86, 2017.

[63] K. Shirasu, A. Nakamura, G. Yamamoto et al., “Potential use of CNTs for production of zero thermal expansion coefficient composite materials: an experimental evaluation of axial thermal expansion coefficient of CNTs using a combination of thermal expansion and uniaxial tensile tests,” *Composites Part A: Applied Science and Manufacturing*, vol. 95, pp. 152–160, 2017.

[64] H. G. Chae and S. Kumar, “Polymer/carbon nanotube composites-an overview,” *Indian Journal of Fibre & Textile Research*, vol. 31, pp. 29–40, 2006.

[65] Geng G, Ma X, Geng H, Wu Y (2018). Effect of Load on the Thermal Expansion Behavior of T700 Carbon Fiber Bundles. Polymers 10(152), 1-14.

[66] Vilatela J J, Khare R, Windle A H (2012). The hierarchical structure and properties of multifunctional carbon nanotube fibre composites. CARBON 50, 1227-1234.

[67] Shirasu K, Nakamura A, Yamamoto G, Ogasawara T, Shimamura Y, Inoue Y, Hashida T (2017). Potential use of CNTs for production of zero thermal expansion coefficient composite materials: An experimental evaluation of axial thermal expansion coefficient of CNTs using a combination of thermal expansion and uniaxial tensile tests. Composites: Part A 95, 152-160.

[68] Chae H G, Kumar S (2006). Polymer/carbon nanotube composites-An overview. Indian Journal of Fibre & Textile Research 31, 29-40.

[69] Anvari A (2018). Thermal Life of Carbon Structures: From the Earth to after the Titan. International Journal of Aerospace Engineering Volume 2018, Article ID 7628614, 6 pages. https://doi.org/10.1155/2018/7628614

[70] Maheswari T S U, Prasad P H (2013). Reliability of Thermal strain and stresses in simple bars. IOSR J. Math. 5(2), 05-09.

[71] Park S Y, Choi H S, Choi W J, Kwon H (2012). Effect of vacuum thermal cyclic exposures on unidirectional carbon fiber/epoxy composites for low earth orbit space applications. Composites: Part B. 43, 726-738.

[72] Yang S, Qu J (2012). Computing thermomechanical properties of crosslinked epoxy by molecular dynamics simulations. Polymer 53, 4806-4817.

[73] Deng L, Young R J, Kinloch I A, Sun R, Zhang G, Noe L, Monthioux M (2018). Coefficient of thermal expansion of carbon nanotubes measured by Raman spectroscopy. Applied Physics Letters, American Institute of Physics 104(5) 051907, 1-4.

[74] Karadeniz Z H (2005). A numerical study on the thermal expansion coefficient of fiber reinforced composite materials. Thesis, Graduate school of natural and applied sciences, Dokuz Eylul University, Izmir.

[75] Mori H, Hirai Y, Ogata S, Akita S, Nakayama Y (2005). Chirality Dependence of Mechanical Properties of Single-Walled Carbon Nanotubes Under Axial Tensile Strain. Japanese Journal of Applied Physics Vol. 44, No. 42, L1307-L1309.

[76] Lu Q, Bhattacharya B (2006). Fracture Resistance of Zigzag Single Walled Carbon Nanotubes. Nano technology, Institute of physics vol. 17, 1323-1332.

[77] Wang J, Gutierrez M (2007). Stress-Strain Behaviour of Carbon Nanotubes under Cyclic Loading. Micro & Nano Letters 2 (4), 111-114.

[78] Kahaly M U, Waghmare U V (2008). Effect of Curvature on Structures and Vibrations of Zigzag Carbon Nanotubes: A first-principles study. Bull. Mater. Sci. vol. 31, no. 3, 335-341.

[79] Gowri Sankar P A, Udhaya Kumar K (2011). Mechanical and Electrical Properties of Single Walled Carbon Nanotubes: A Computational Study. European Journal of Scientific Research vol. 60, no. 3, 342-358.

[80] Zakeri M, Shayanmehr M (2013). On the Mechanical Properties of Chiral Carbon Nanotubes. Journal of Ultrafine Grained and Nanostructured Materials vol. 46, no. 1, 01-09.

[81] Yarlagadda G, Solasa G, Boanapalli R, Paladugu P, Babu G S (2013). Three-Dimensional Finite Element (FE) Model for Armchair and Zigzag Type Single-Walled Carbon Nanotubes. International Journal of Scientific and Research Publications vol. 3, Issue 5, May 2013, 1-9.

[82] Ganesh E N (2013). Single Walled and Multi Walled Carbon Nanotube Structure, Synthesis and Applications. International Journal of Innovative Technology and Exploring Engineering (IJITEE) vol. 2, Issue 4, March 2013, 311-320.

[83] Annual Book of ASTM Standards 2000, "Standard Test Method for Short-Beam Strength of Polymer Matrix Composite Materials and Their Laminates," D 2344/D 2344M.

[84] Thakre, P.R., 2009, "Processing and characterization of carbon nanotubes reinforced epoxy resin based multi-scale multi-functional composites," PhD Thesis, Texas A & M University.

[85] ASTM International, 2004, "Introduction to Tensile Testing," Second Edition (#05106G).

[86] ASTM International, Designation: D638 – 14, 2014, "Standard Test Method for Tensile Properties of Plastics.

[87] Liu, S., and Nairn, J. A., 1990, "Fracture Mechanics Analysis of Composite Microcracking: Experimental Results in Fatigue," Proceedings of the 5th Technical Conference on Composite Materials, American Society of Composites, East Lansing, Michigan, June 11-14, 1990.

[89] Anvari, A., 2014, "Fatigue Life Prediction of Unidirectional Carbon Fiber/Epoxy Composite in Earth Orbit. Int. J. of Appl. Math and Mech., 10(5), pp. 58-85.

# Vita

My name is Ali Anvari and I am now a PhD at University of Missouri - Columbia. I am graduating with a PhD degree in mechanical engineering with a minor in materials science. I have a bachelor's degree in civil engineering, and master's degree in aerospace engineering with the minor in Aerospace Structural Design. I have passed the fluid mechanics, materials science, and mathematics in my PhD qualifier exam. In Iran, I ranked 4$^{th}$ nationally in Aerospace Engineering. I have more than 3 years' experience in conducting research and performing engineering tasks. Cumulatively, I have been either a Research or Teaching assistant at University of Missouri - Columbia in the Department of Mechanical and Aerospace Engineering in U.S.A. for about 3 years. I am honored that I have published 23 independent and collaborative manuscripts and have presented 2 national conferences in the fields of materials science, contact mechanics, aerospace, mechanical, and biomedical engineering, bio-mechanics, thermal and/or mechanical fatigue, plasma technology, and other related areas. Additionally, I have been a lead student of Industrial Assessment Center (IAC) in the University of Missouri - Columbia for over a year. I have had the honor and responsibility of preparing energy efficiency reports for manufacturing facilities with my team, after conducting required energy efficiency audits for such facilities.

My PhD Thesis topic is The Effect of Temperature on the Mechanical Behavior of the Carbon Nanotube Reinforced Epoxy. I have been a teaching assistant for the "Mechanical Engineering Design" course, as well as a teaching assistant for the 'Thermal Fluids Lab" course, which is a practical (experimental) course in the lab. I have more than 3 years' experience working in 4 labs: 1. Industrial Assessment Center lab; 2. Materials Fabrication Lab; 3. Materials Testing Lab; and 4. Thermal Fluids Laboratory.

I enjoy being part of a team and am proficient in leading projects, report and technical writing (with an emphasis on scientific articles), analyzing and designing structures, and teaching. I have the most experience in fabricating nanocomposite materials such as single-walled carbon nanotubes, reinforced epoxy and multi-walled carbon nanotubes; but I am also skilled at teaching different mechanical engineering courses -- with special focus on solids and materials. I have comfortability with Sap, Ansys, SolidWorks, Microsoft Word, Excel and Power - Point, and Auto - cad.